Flexural Response of Flat Plate Edge Slab-Column Connections

Author
Ryan Tack

Supervisor
Dr. Denis Mitchell

McGill University

A Thesis Submitted to the Faculty of Graduate Studies in Partial Fulfilment of the Requirements of the Degree of Master of Engineering

November 28, 2019

Abstract

The CSA A23.3-14 Standard and ACI 318-14 Code require that the slab reinforcement for the negative moment at edge connections be placed in a band width, b_b, extending a distance 1.5 times the slab thickness past the sides of the column. To investigate the effectiveness of the top slab reinforcement in width b_b, four full-scale edge slab-column specimens with varying column dimensions and top slab reinforcement arrangements were designed, constructed, and tested. The experimental results of this program revealed that not all reinforcing bars in width b_b were effective, especially when the distance from the inner column face to the free edge was less than 1.5 times the slab thickness. A method for determining the effectiveness of top slab reinforcing bars was developed based on the formation of torsional yield lines in the slab. Compared to the CSA A23.3-14 and ACI 318-14 approach, better agreement between the predicted and experimental results was achieved with this proposed method.

Résumé

Les normes CSA A23.3-14 et ACI 318-14 exigent que l'armature de dalle pour le moment négatif aux connexions de rive soit placée dans une bande de largeur, b_b, égale à 1.5 fois l'épaisseur de la dalle de chaque côté du poteau. Pour examiner l'efficacité de l'armature supérieure dans la bande de largeur, b_b, quatre spécimens de connexion dalle-poteau de rive à grande échelle dont les dimensions du poteau et la disposition de l'armature variaient ont été conçus, construits et testés. Les résultats de ce programme expérimental ont révélé que les barres d'armature dans la bande de largeur, b_b, n'étaient pas toutes éfficaces, surtout quand il s'agissait des spécimens dont la distance entre la face intérieur du poteau et le bord libre était moins de 1.5 fois l'épaisseur de la dalle. Une méthode pour déterminer l'efficacité de l'armature supérieur a été développée basée sur la formation des lignes de rupture dans la dalle. Par rapport à la méthode de CSA A23.3-14 et ACI 318-14, les résults prédits par la méthode proposée convenaient mieux aux résultats expérimentaux.

Acknowledgements

This thesis would not have been possible without the guidance and wisdom of Professor Denis Mitchell and Dr. Bill Cook, the know-how of John Bartczak, and the many dedicated hands lent by Rico Massa, Chris Orcutt, Albert Charuckhchyan, Julia Bond, and Omar Shemy. I would also like to thank my parents David and Judith Tack and my dear friends Mark Corrigan, Jeremy Usbourne, Kyle Muir, Dylan Gimpelj, Andy Lythe, Robert Gleisinger and Guillaume Duteaud for their support.

Table of Contents

List of Figures

List of Tables

Nomenclature

α_s	Column type coefficient
β_c	Ratio of long column dimension to short column dimension
γ_v	Ratio of applied moment transferred in shear
λ	Concrete density factor
ϕ	ACI strength reduction factor
ϕ_c	Concrete material resistance factor
ϕ_s	Steel material resistance factor
ρ_1	Percentage of steel perpendicular to free edge in moment tranfer band width
ρ_2	Percentage of steel parallel to free edge in moment transfer band
ε_y	Steel yield strain
a	Depth of compression block
a_{max}	Maximum aggregate size
A_{s1}	Area of steel perpendicular to the free edge in moment transfer band width
A_{s2}	Area of steel parallel to the free edge in moment transfer band width
b_b	band width of reinforced concrete slab
b_o	Perimeter of critical punching shear section
c_1	Column dimension perpendicular to the free edge
c_2	Column dimension parallel to the free edge
d	Average depth to top tension reinforcement
e_1	Distance from centroid of critical section to free edge
e_2	Distance from centroid of critical section to inner edge of critical section
E_c	Concrete modulus of elasticity
E_s	Steel modulus of elasticity

f'_c Concrete compressive strength

f_r Concrete modulus of rupture

f_{sp} Concrete splitting tensile strength

f_u Steel ultimate strength

f_y Steel yield strength

h Slab thickness

J_1 Polar moment of inertia of critical shear section about axis parallel to free edge

J_2 Polar moment of inertia of critical shear section about axis perpendicular to free edge

l_1 Length of span in direction that moments are being determined, measured center-to-center of supports

l_2 Length of span transverse to l_1, measured center-to-center of supports

l_n Length of span in direction that moments are being determined, measured face-to-face of supports

M Applied moment

M_{cg} Applied moment at centroid of critical section

M_{face} Applied moment at the face of the column

M_{flex} Moment transferred in flexure

M_n Nominal flexural strength

M_o Nominal moment resistance when shear not present

M_r Factored flexural strength

M_{shear} Moment transferred in shear

$M_{torsion}$ Moment transferred in torsion

M_u Moment at failure

V Applied shear

v Applied shear stress

v_c Shear strength contribution from concrete

V_n Nominal shear strength

v_n Nominal shear stress

V_o Nominal shear resistance when moment not present

V_r Factored shear strength

v_r Factored shear stress

V_u Shear at failure

v_u Maximum shear stress at failure

1 Introduction and Literature Survey

1.1 Introduction

Reinforced concrete flat plates provide numerous advantages over alternative, more complex reinforced concrete floor systems. Most notably, the cost and duration of construction are reduced by the uniform thickness of the slab and the absence of column capitals or beams (see Figure 1.1). This simple geometry reduces formwork requirements substantially, often accounting for nearly one half of the cost of the floor system, and permits the use of time-efficient flying forms. Moreover, the flat soffit facilitates the installation of services and eliminates the need for a false ceiling. Without beams, storey heights are minimized, leading to lower overall cladding and mechanical systems costs. For the spans and live loads common to mid to high-rise residential buildings, flat plates are on average 21 % less expensive than other floor systems (Taranath, 2010).

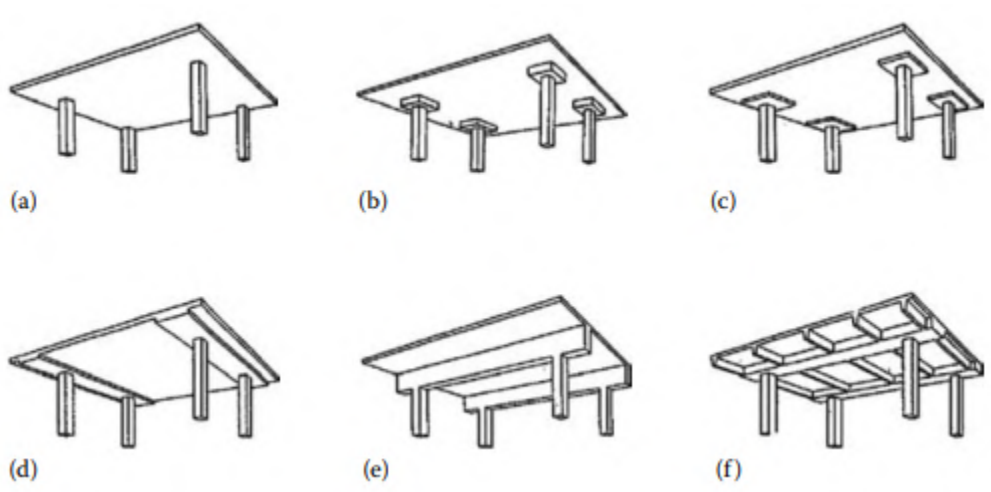

Figure 1.1: Common RC floor systems: a) Flat plate b) Flat slab with column capitals c) Flat slab with drop panels d) Flat slab with slab bands e) Flat slab with one-way beam f) Skip joist slab (Taranath, 2010)

Despite these benefits, a significant disadvantage to the flat plate is its susceptibility to failure in punching shear. Failures in this mode are sudden and brittle, involving the separation of the column from the surrounding slab. With the removal of one of the supports, the loads supported by neighbouring columns increase, potentially producing a cascading series of punching shear failures and the collapse of the entire structure. The flat plate is prone to punching shear failures because of the concentrated transfer of large shearing forces over the relatively thin depth of the slab. These stress conditions are further complicated when the connection is subjected to unbalanced moments, unavoidable at edge and corner columns where spans are discontinuous. Given the catastrophic nature of punching shear failures in flat plates, designers

must ensure a ductile failure mode that protects the integrity of the storey and the structure as a whole.

Research on moment-shear transfer in slab-column connections has mainly focused on interior slab-column connections. There are only a few experimental programs that have investigated the behaviour of exterior slab-column connections, where significant unbalanced moments are present. In this thesis, the response of isolated edge slab-column connections in flat plate reinforced concrete floor systems to gravity loads are examined. Of primary interest are the effect of column geometry and the arrangement of top flexural reinforcement on the ultimate strength of the connection. Additionally, the assumption made in the CSA A23.3-14 standard (2014) and ACI 318-14 code (2014) that 100% of top mat reinforcement is yields in the band width $c_2 + 3h$ in edge slab-column connections was investigated.

1.2 Research Objectives and Methodology

The objectives of this research program are as follows:

1. Observe the flexural behaviour of edge slab-column connections of varying column geometries (that is,, column dimensions and presence of overhang) and top bar arrangements.

2. Investigate the validity of the assumption that 100 % of reinforcing bars are effective and yield in a band width $c_2 + 3h$.

3. Confirm the accuracy of the punching shear provisions of the CSA A23.3-14 standard (2014) and ACI 318-14 code (2014).

4. Develop a revised procedure for determining the effectiveness of the top reinforcement, and hence the moment resistance of an edge slab-column connection.

To achieve these objectives, four reinforced concrete flat plate slab-column connections featuring varying column geometries and top mat steel reinforcement ratios were designed and tested under identical loading and support conditions. Top mat reinforcement strain gauge data in addition to deflection measurements of the slab and column during testing provided an accurate means of evaluating the effectiveness of individual reinforcing bars inside of the band width $c_2 + 3h$. Furthermore, the specimens were loaded until punching shear failure occurred, permitting an assessment of the punching shear strength models of the CSA A23.3-14 standard (2014) and ACI 318-14 (2014) code.

2 Literature Review

Studies on the failure of flat plate edge slab-column connections have yielded numerous models for estimating strength. These models differ principally in how they define the failure mechanisms of the connection and how they account for the interaction of moment and shear. In general, strength models for edge slab-column connections fall into three distinct approaches:

Limiting Shear Stress Approach In this approach, an edge slab-column connection may fail in punching shear, flexure, or punching-flexure. In the first mode, punching shear failure occurs when a limiting shear stress is reached on a control perimeter at or close to the faces of the column. Models based on the limiting shear stress approach assume that some portion of the unbalanced moment is transferred to the column in shear at the side faces. These additional shear stresses are assumed to have a linear shear stress distribution along the control perimeter that is maximum at the front face and decreases linearly to the free edge. This approach forms the basis for the CSA and ACI code punching shear strength models, which use elements adopted from the work of Di Stasio and Van Buren (1960) and Moe (1961). In the second mode, failure in flexure, the connection is idealized as a beam section embedded in the slab whose depth is the thickness of the slab and whose width is assumed to be a defined band width, b_b. Similar to the flexural failure of one-way slabs, flexural failure of an edge connection occurs when the reinforcement in width b_b yields. Lastly, a combined, punching shear-flexural failure is possible, where the connection punches after partial or complete yielding of the reinforcement in width b_b.

Beam Analogy The connection is modelled as three idealized beam sections framing into the faces of the exterior. The failure of the connection occurs when either the shear, flexural, or torsional capacity of each idealized beam section is attained. In practice, 6 distinct failure modes are possible for edge column connections.

Truss Analogy The flow of forces into the connection is described in terms of compression struts and tension ties. The strength of the connection depends strongly on the geometry of these elements. Truss models typically differ in terms of how this geometry is described.

2.1 Limiting Shear Stress Approach

2.1.1 Elstner and Hognestad (1956)

The experimental program carried out by Elstner and Hognestad was the first to investigate punching shear failure in reinforced concrete flat plates. They tested 34 isolated interior slab-column specimens, varying the concrete strength, percentage of tension and compression reinforcement, column dimensions,

and load eccentricity. All specimens failed in punching shear with significant flexural cracking occurring in the slab around the column. Before failure, yielding of the tension reinforcement passing through the column occurred in specimens with low top reinforcement ratios, whereas specimens with high top reinforcement ratios exhibited no yielding. In both cases, strains were the largest in the bars passing through the column and decreased linearly with distance from the column faces.

The researchers proposed that punching shear failure is characteristically a combined shear and flexure phenomenon. Failure of the connection occurs when the shear stress at the perimeter of the column exceeds a value dependent on the shear and flexural capacities of the connection:

$$\left(333 + 0.046\frac{f'_c}{\phi_o}\right) \leq \frac{V}{7/8 b_b d} \qquad (psi) \tag{2.1}$$

Where ϕ_o is the ratio of the unfactored shear strength to the pure unfactored flexural capacity of the connection determined through yield-line analysis.

2.1.2 Di Stasio and Van Buren (1960)

The model developed by Di Stasio and Van Buren adapted the work of Elstner and Hognestad for edge slab-column connections, where unbalanced moments are present. They assumed that, once the flexural capacity of the connection has been attained, any further unbalanced moment is transferred by torsion in the slab on both sides of the column. This torsion generates additional shear stresses in the connection, producing a linear shear stress distribution along a control perimeter taken at a distance t-$\frac{1}{2}$" from the column faces, where t is the slab thickness (see Figure 2.1). The degree to which the unbalanced moment is transferred in torsion depends on the ultimate flexural capacity of the slab bound by the control perimeter.

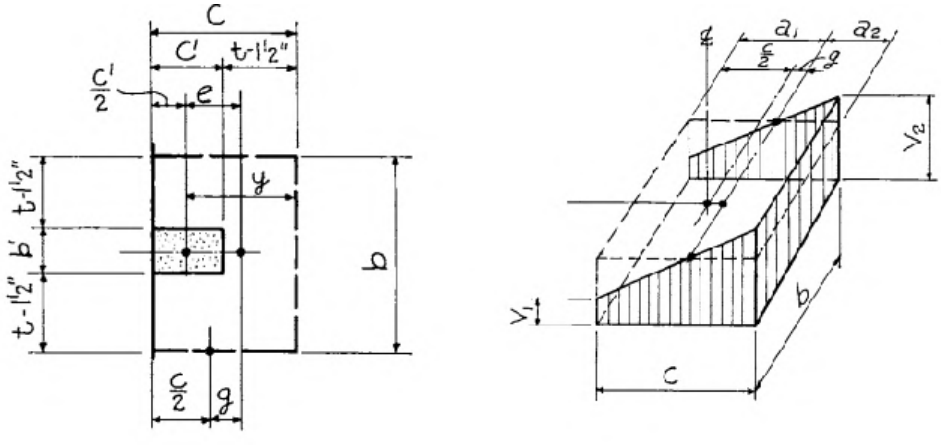

Figure 2.1: Critical section and distribution of shear stresses (Di Stasio and Van Buren, 1960)

The minimum and maximum shear stresses are then:

$$v_1 = \frac{8t}{7d}\left[\frac{V}{b_0 d} - \frac{(V_{col}H - M_{face} - Ve)a_1}{J_1}\right] \quad (ksi) \tag{2.2}$$

$$v_2 = \frac{8t}{7d}\left[\frac{V}{b_0 d} + \frac{(V_{col}H - M_{face} - Ve)a_2}{J_1}\right] \quad (ksi) \tag{2.3}$$

Where V_{col} represents the horizontal shear in the column, H is the storey height, and M_{face} is the moment at the front column face. The connection fails when a recommended limiting shear stress of $0.0625f'_c$ is reached on the control perimeter. Di Stasio and Van Buren's model was later validated with the testing of edge slab-column connections conducted by Beresford (1967), who found good agreement between the predicted and experimental results.

2.1.3 Andersson (1966)

The punching shear model developed by Andersson provides a similar description of the conditions necessary for failure in edge slab-column connections. Failure occurs when a limiting shear stress is reached in the slab along a critical section at a distance d/2 from the face of the column, where d is the average depth to the top reinforcement. This stress is composed of a uniform shear stress and torsional stresses produced in the presence of unbalanced moments. Using the results of four edge slab-column connections that were tested, Andersson proposed that a constant 40% of the unbalanced moment is transferred in torsion. The maximum shear stress at the critical section is then:

$$v = \frac{V}{d^2}\left[1 + \frac{0.4e}{2(c_1 - d/3)}\right] \Big/ \left[\frac{c_2}{d} + \frac{c_1}{d}\left(1 + \frac{c_1}{6e}\right) + \frac{\pi}{2}\right] \quad (ksi) \tag{2.4}$$

2.1.4 Hanson and Hanson (1968)

Hanson and Hanson tested 13 isolated interior slab-column connections and 1 isolated edge slab-column connection in order to evaluate the accuracy of different models for predicting punching shear strength. They found that Di Stasio and Van Buren's method for determining the amount of unbalanced moment transferred in torsion was inconsistent with their experimental results. The researchers proposed that 40% of the unbalanced moment is transferred in torsion in edge slab-column connections, extending Moe's (1961) model for describing unbalanced moment transfer in interior slab-column connections. The effect of reinforcement on punching shear strength is incorporated in the strength equation with the inclusion of the flexural strength of the connection. The maximum permissable shear stress along the critical perimeter is given as:

$$v_1 = \frac{V}{b_0 d} + \frac{0.4 M_{cg} c_1}{J_1} \leq 4\sqrt{f'_c} \qquad (ksi) \tag{2.5}$$

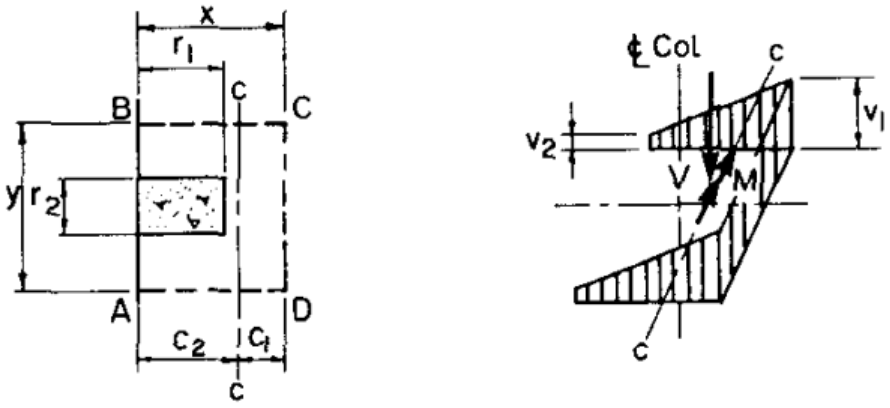

Figure 2.2: Critical secton and distribution of shear stresses around an edge slab-column connection (Hanson and Hanson, 1968)

2.1.5 Kinnunen (1971)

Kinnunen tested 6 specimens consisting of a slab supported on two opposing edge columns. The objective of this experimental program was to evaluate the effect of the ratio and arrangement of flexural steel on the pure moment capacity of the connection. In the course of testing, only edge column connections with low steel ratios demonstrated complete yielding of the tension reinforcement. Additionally, as Elstner and Hognestad (1956) had observed in their tests, the bar strains in the tensile reinforcement declined linearly with increasing distance from the column side faces. The rate at which bar strains decreased with distance was inversely proportional to the amount of tension reinforcement parallel to the free edge and passing through the column faces. Using a yield-line analysis of the slab, Kinnunen proposed that only bars perpendicular to the free edge and passing through diagonal yield lines branching off of the front column face can reach yield. For all of the tension reinforcement perpendicular to the free edge to yield, then, the connection must have an adequate amount of tension reinforcement parallel to the free edge and passing through the column to resist the vertical torsional stresses generated along a critical section around the column bounded by a condition of zero moment.

2.1.6 Regan (1981)

Regan applied Kinnunen's yield-line approach for the pure flexural capacity of edge connections in a model for punching shear strength. Using test data from 18 isolated edge slab-column specimens, they

developed a punching shear strength model with two possible failure modes: flexure dominant and shear dominant.

In a flexure dominant failure, diagonal yield lines originating at the face of the column and concluding at the free edge form. Assuming that shears are not transferred across yield lines, the critical section of the connection is shortened, terminating at the yield lines (Figure 2.4). The failure of the connection then occurs when the maximum shear stress on this perimeter reaches a limiting value. In the shear dominant case, yielding of the perpendicular tension reinforcement is limited to those bars passing through the column and no diagonal yield lines form. The critical section of the connection is thus greater than that of the first failure mode and the connection can handle a higher shear demand before failure (Figure 2.4).

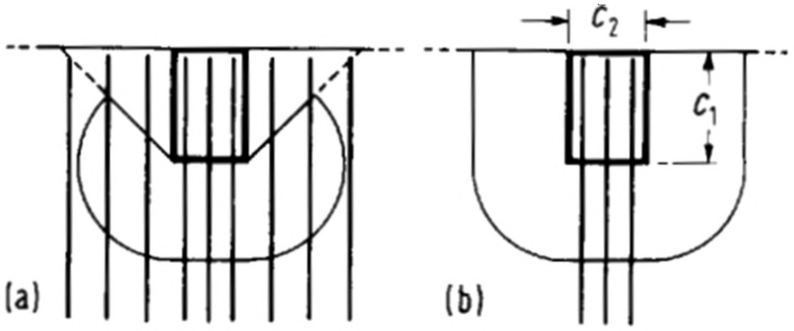

Figure 2.3: a) Flexure dominant critical section b) Shear dominant critical section (Regan, 1981)

The researchers suggested a revised tension reinforcement band width of $c_2 + 2c_1$ for edge columns, see Figure 2.4. If this band width is determined to be too small, a wider band width of $c_2 + 3.33c_1$ is also recommended. However, as per yield line theory, adequate transverse steel passing through the column or the addition of stirrups with spacings parallel to the reinforcement and crossing the yield lines is needed. Importantly, any torsional resistance is assumed to be lost after the formation of torsion cracks, thus resistance to pure bending is limited to the bars in these band widths.

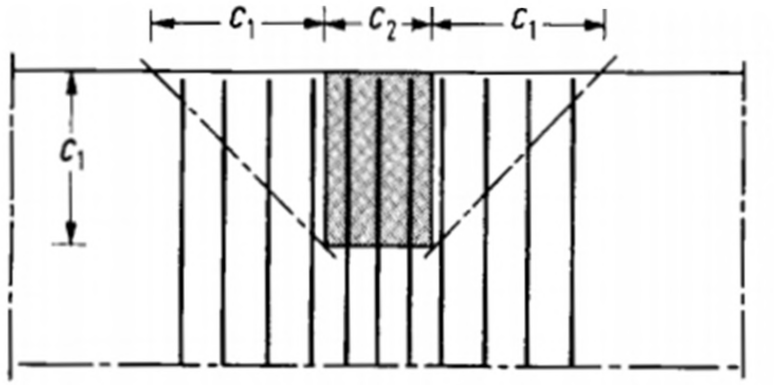

Figure 2.4: Moment transfer width (Regan, 1981)

2.1.7 Neth et al. (1981)

Neth et al. tested four continuous slab specimens at $\frac{1}{2}$, $\frac{1}{4}$, $\frac{1}{6}$, and $\frac{1}{8}$ scale, respectively. The researchers described the failure of their specimens in terms of the formation and progression of cracks in the slab. Initially, diagonal flexural cracks appear at 10-15% of the failure load. These cracks form on the top surface of the slab adjacent to the column and terminate along the side of the free edge. As the load increases, the primary flexural failure crack forms. With subsequent increases in load, the slab behaves like a rigid body rotating about the primary flexural failure crack. At punching shear failure, the secondary failure crack forms, intersecting the primary flexural failure crack at a 90 degree angle.

The researchers observed that the elastic analysis employed by the ACI 318-77 code (1977) underestimates the shear-moment transfer ratio, γ_v, after cracking occurs. Additionally, the top tension reinforcement placed in a strip bounded by predicted lines of contraflexure did not yield all at once. Rather, all of the top reinforcement passing through the primary flexural failure crack yielded first, with yielding of adjacent bars at significantly larger rotations. The authors recommended that an analytical model centred on the development and post-cracking behaviour of the primary flexural failure crack be investigated.

2.1.8 Rughani (1983)

Rughani tested isolated four edge slab-column specimens at McGill University. The specimens consisted of a 300 x 300 mm column whose front face position relative to the free edge varied from 300 mm for the first specimen, to 150 mm for the second specimen and 0 mm for the third and fourth specimens. The first specimen failed in punching shear, while the other specimens failed in flexure. Rughani found that the critical section for shear and the moment transfer band width ,b_b, should be defined as a function of the distance from the column front face to the free edge, c_3. That is to say, only the portion of the column connected to

the slab is effective in transferring shear and moment. Rughani developed the following expression for b_b, where this band width may not exceed $c_2 + 3h$ in width:

$$b_b = c_2 + \left(\frac{c_3}{c_2}\right)^2 1.5h \qquad (m) \tag{2.6}$$

2.1.9 Sherif and Dilger (2003)

Using test data from Zaghlool (1971), Regan (1981), Sherif (1996), Stamenkovic and Chapman (1972), Hanson and Hanson (1968), Hawkins et al. (1978), Mortin (1989), Scavuzzo (1978), and Kane (1978), Sherif and Dilger critiqued the CSA A23.3-94 (1994) provisions for edge slab-column connections. Sherif and Dilger found that the code overestimates the interaction of moment and shear. Thus, for higher eccentricities, the code underestimates the shear strength of the connection.

Regarding the influence of the reinforcement in $c_2 + 3h$ on the strength of the connection, Sherif and Dilger determined that the flexural capacity of the connection does not increase linearly with increasing reinforcement percentage. In fact, the ratio of moment at failure to predicted moment resistance of the connection decreases with an increasing reinforcement percentage. In this sense, the assumption made by Moehle (1988) and the ACI 318-14 that γ_v may be taken as zero may be incorrect.

2.1.10 Park and Choi (2006)

A nonlinear finite element study of edge slab-column connections was conducted by Park and Choi. A total of 21 specimens were analyzed, where c_1, c_2, ρ_l, ρ_b, and the ratio of nominal shear to the ACI 318-05 code (2005) predicted shear varied. From their FEM data, the researchers made two primary observations:

1. At failure, the eccentric shear strength at the side faces was higher compared to the front and back faces of the column. This reduction in the shear strength at the front face was attributed to the normal stresses generated by the moment transferred in flexure. The ACI 318-05 code (2005), in contrast, assumes that the maximum shear stress at the side faces is equal to the shear stress at the front face.

2. The flexural moment capacity of the connection was attained first, followed by the torsional capacity. Additionally, the unbalanced moment was resisted mostly in torsion, with$\gamma_v = 0.8$ approximately, as opposed to the ACI 318-05 code (2005), which typically provides $\gamma_v = 0.4$.

In response to the first finding, the authors developed a new equation for the front face shear strength:

$$v_{u1} = 0.33\sqrt{f'_c}\left[0.8 - 0.8\left(\frac{c_2}{d}\right)\right]\frac{a}{d} \qquad (MPa) \tag{2.7}$$

Where v_{u1} is the unfactored front face shear strength and a is the depth of the compression block. This formula takes into consideration the effect of dowel action in resisting shear, which also depends on the depth of the compression block.

Regarding the second finding, Park and Choi suggested that the band width $c_2 + 3h$ be shortened to the critical section defined by the ACI 318-05 code (2005) for eccentric shear, $c_2 + d$. The rationale for this decision was that, as $c_2 + d$ lies inside $c_2 + 3h$, the flexural capacity of the connection must be affected by the moment transferred in eccentric shear. By restricting the flexural transfer band width to $c_2 + d$, the unfactored moment strength of the connection may be defined in terms of independent components:

$$M_u = M_{flex} + M_t + M_v \tag{2.8}$$

Where M_{flex} is the portion of the moment resisted in flexure, M_t the portion of the moment resisted in torsion at the side faces, and M_v the portion of moment resisted in eccentric shear. Park and Choi define these components as such:

$$M_u = A_{s1} f_y \left(d - \frac{a}{2}\right) + \left[\left(0.83\sqrt{f'_c} + \frac{V}{b_o d}\right) \frac{J_1}{c_1 + d/2 - e_1}\right] + \left[\left(0.33\sqrt{f'_c} - \frac{V}{b_o d}\right)(c_2 + d)\, d\right] e_1 \tag{2.9}$$

2.1.11 Sudarsana and Gardner (2006)

Sudarsana and Gardner tested 8 isolated edge slab-column specimens and one continuous slab specimen with four edge columns. The primary variables in these tests were the load eccentricity and the percentage of top tension reinforcement in $c_2 + 3h$. The researchers found that, although the predicted moment resistance of the reinforcement in $c_2 + 3h$ was exceeded in specimens with low top reinforcement ratios, the connection did not fail in flexure. Furthermore, in all of their test specimens, only those reinforcing bars perpendicular to the free edge and inside the column yielded, including the isolated test specimen.

2.1.12 Rha et al. (2014)

Rha et al. constructed and tested five half-scale continuous flat plate specimens. The specimens consisted of four edge columns, four corner columns, and one interior column supporting a slab measuring two bays by two bays in plan. The top and bottom mat reinforcement in the column strip was the same for each column, that is, the detailing of the interior and edge column connections was identical. The researchers found that, for edge slab-column connections, the interaction between shear and moment was negligible, as Moehle (1988) had suggested. In other words, none of the unbalanced moment was transferred in eccentric

shear. Despite this observation, the authors witnessed a 25 % increase in punching shear strength with a 50 % increase in the top mat reinforcement perpendicular to the free edge.

2.2 Beam Analogy

2.2.1 Hawkins and Corley (1971)

Hawkins and Corley's approach to punching shear strength involves modelling an edge slab-column connection as idealized beam sections framing into the column (Figure 2.5). The shear, flexural, and torsional strength of these beam sections contribute to the total strength of the connection. Failure occurs in two possible modes: moment-torsion and shear-torsion. In a moment-torsion failure, the flexural capacity of the face, CB, and the torsional capacities of the side faces, AB and CD, are reached. Complete yielding of the tension reinforcement in CB occurs and large rotations of the slab are observed prior to failure. In a shear-torsion failure, the shear capacity of the front face, CB, is first exhausted. Any additional shear stresses are then transferred to the side faces until the torsional capacities of the side faces are reached at failure. Complete yielding of the tension reinforcement in CB does not occur and slab rotations are significantly smaller than those in a moment-torsion failure. The critical sections corresponding to these failure modes are shown in Figure 2.6.

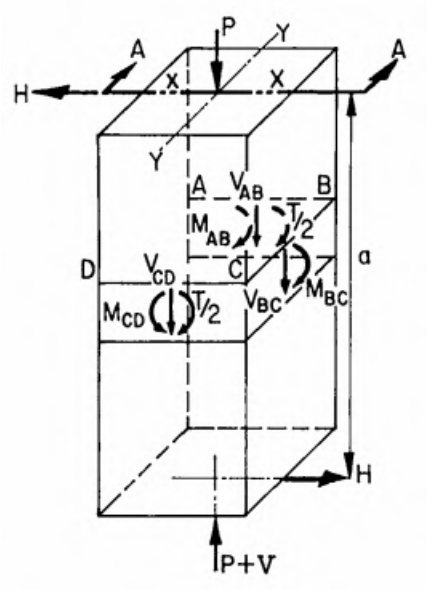

Figure 2.5: Idealized beams sections of Hawkins and Corley's model (1971)

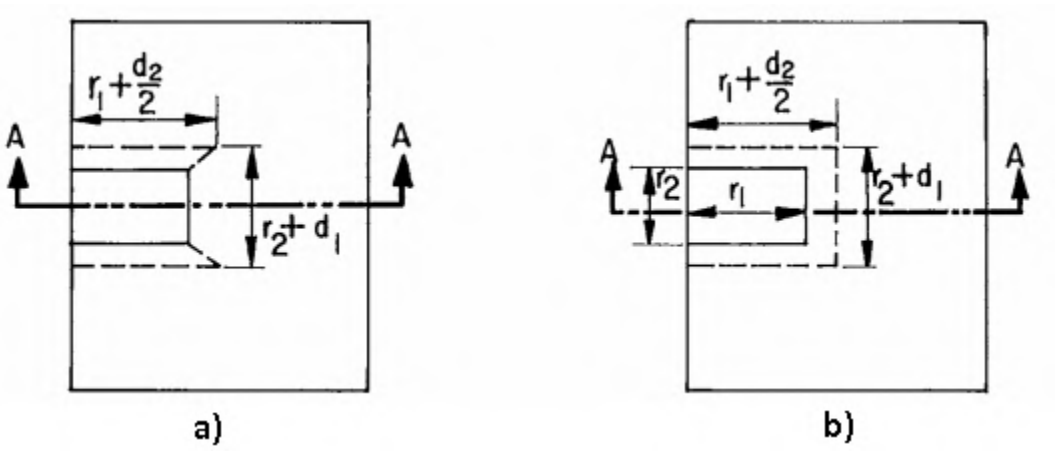

Figure 2.6: a) Critical section for moment-torsion failure b) Critical section for shear-torsion failure (Hawkins and Corley, 1971)

The researchers validated their model with test results from Hanson and Hanson (1968), Anderson (1966), and Beresford (1967). Good agreement between the model predictions and test results was observed; ratios of measured strength to predicted strength varied between 1.02-1.22.

2.2.2 Stamenkovic and Chapman (1974)

Stamenkovic and Chapman tested 5 edge slab-column connections with different applied moment to shear ratios and 1 edge column specimen with a slot in front of the column. Initially, Moe's (1961) model was used for the analysis; however, poor agreement was observed for specimens with high moment-to-shear ratios. Furthermore, the experimental results of the slotted specimen demonstrated that Moe's model does not accurately describe the percentage of moment transferred in torsion. By comparing the experimental results from the specimens without a slot to the specimen with a slot, Stamenkovic and Chapman determined that 44 % of the unbalanced moment is resisted in flexure and 56 % in torsion. These results were incorporated into their formula for the unfactored moment resistance of the connection as follows:

$$M_u = M_{flex} + 2M_t = 0.9A_{s1}f_y d_1 \left(1 - 0.59\frac{\rho_1 f_y}{f'_c}\right) + 0.7\frac{A_{s2}f_y}{bd}d^2\left(b - \frac{d}{3}\right) \tag{2.10}$$

In addition, the authors found that their test data was more accurately described using a a circular shear-moment interaction formula (Figure 2.7). The unfactored shear strength of the connection, V_u, includes the flexural strength of the slab, V_{flex}.

$$\left(\frac{V}{V_u}\right)^2 + \left(\frac{M}{M_u}\right)^2 = 1 \tag{2.11}$$

$$V_u = 0.9\frac{3c_1 + 4h}{4c_1 + 8h}4d\sqrt{f'_c}\frac{15\left(1 - 0.075c_1/d\right)}{1 + 5.25\left(3c_1 d\sqrt{f'_c}\right)/V_{flex}} \tag{2.12}$$

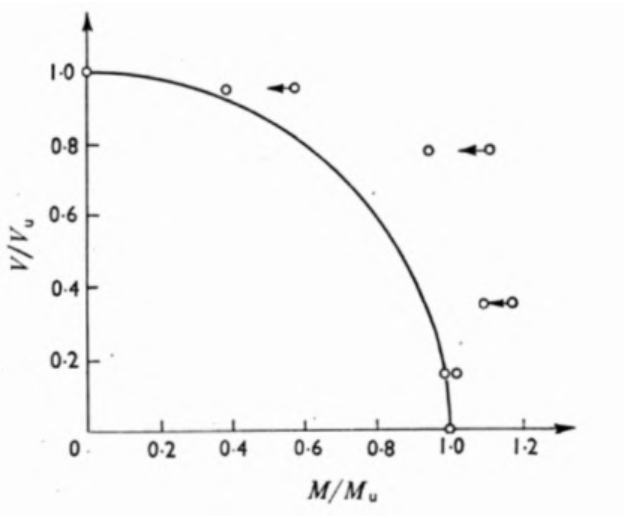

Figure 2.7: Circular M-V interaction diagram with test results (Stamenkovic, 1974)

2.2.3 Rangan and Hall (1983)

Rangan and Hall tested four continuous slab reinforced concrete flat plate specimens. Using the reinforcement strains and load cell data from the tests, they developed an empirical formula for the percentage of unbalanced moment transferred in flexure before and after cracking, where M_{BS} is the moment at the front face of the connection (see Figure 2.8):

$$\left(\frac{M_{BS}}{M}\right)_{pre-crack} = 0.34 - 0.32\frac{(c_2 + t)t}{(c_2 + t)t + 2c_1 h} + 1.42\left(\frac{(c_2 + t)t}{(c_2 + t)t + 2c_1 t}\right)^2 \tag{2.13}$$

$$\left(\frac{M_{BS}}{M}\right)_{post-crack} = 0.20 - 0.32\frac{(c_2 + t)t}{(c_2 + t)t + 2c_1 h} + 1.42\left(\frac{(c_2 + t)t}{(c_2 + t)t + 2c_1 t}\right)^2 \tag{2.14}$$

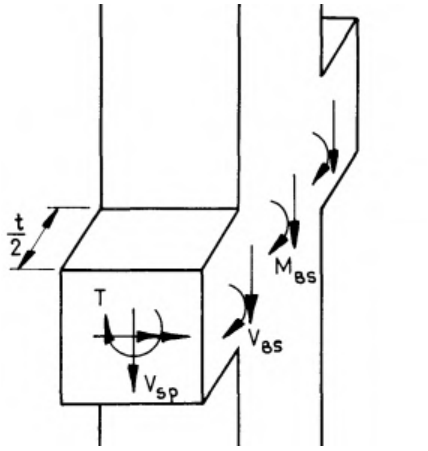

Figure 2.8: Beam model according to Rangan and Hall (1983)

They found that, contrary to the assumption made in limiting shear stress models, the majority of the unbalanced moment is transferred in torsion along the edge of the slab. Furthermore, a significant increase in the percentage of the unbalanced moment transferred in torsion was observed after the formation of flexure cracks along the top of the slab. The percentage of shear at the front face of the connection was then determined using the slope of the moment distribution calculated in Equation 2.14:

$$\left(\frac{V_{BS}}{V}\right)_{pre-crack} = 0.08 + 0.5\frac{(c_2+t)t}{(c_2+t)t+2c_1t} \tag{2.15}$$

$$\left(\frac{V_{BS}}{V}\right)_{post-crack} = 0.5\frac{(c_2+t)t}{(c_2+t)t+2c_1t} \tag{2.16}$$

With the shears and moments acting on the front and side faces found, a modified version of the beam model was used for the estimating punching shear strength. It was assumed that the slab provides some axial restraint to the idealized beam sections framing into the column, increasing their torsional capacity by a factor of 4-5 times. Rangan and Hall found that typical punching shear failures were characteristically torsion-shear failures of the spandrel sections, that is V_{sp} and M_{sp}.

2.2.4 Moehle (1988)

Moehle (1988) criticized the ACI 318-83 (1983) code for providing overly conservative estimations for the punching shear strength of edge slab-column connections. Using data obtained from 7 independent experimental programs he found that better agreement between predicted and actual shear strength could be attained if *zero* interaction between shear and moment is assumed. Instead, he proposed that the connection will fail when either its pure shear strength or pure flexural strength is exceeded . By extension, the top

tension reinforcement will resist 100% of the unbalanced moment, rather than the typical 60% suggested by the code.

Additionally, Moehle found that the code prescribed effective moment transfer width of $c_2 + 3h$ poorly reflected the test data. He recommended that the effective moment transfer width, b_b, be redefined according to yield line theory as:

$$b_b = c_2 + 2c_t = c_2 + 2c_1\sqrt{\rho_2/\rho_1} \tag{2.17}$$

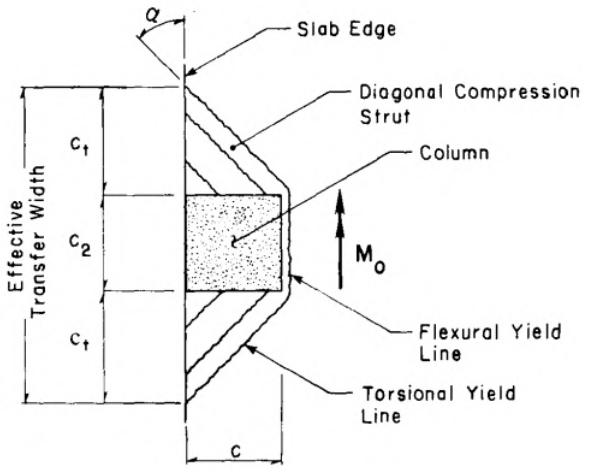

Figure 2.9: Torsional yield lines (Moehle, 1988)

2.3 Truss Analogy

2.3.1 Simmonds and Alexander (1987)

The punching shear strength model developed by Simmonds and Alexander employs a truss analogy to describe the flow of forces in edge slab-column connections. Three truss elements form the basis of their *Truss Model*:

1. Out-of-plane struts that transfer shears from the slab to the column.

2. In-plane struts that permit the involvement of top reinforcing bars outside of the column in the transfer of the unbalanced moment.

3. Steel tension ties that balance the compressive forces in the struts. The tension reinforcing bars entering the front face of the column may contribute both to balancing the out-of-plane struts and transferring the unbalanced moment to the column.

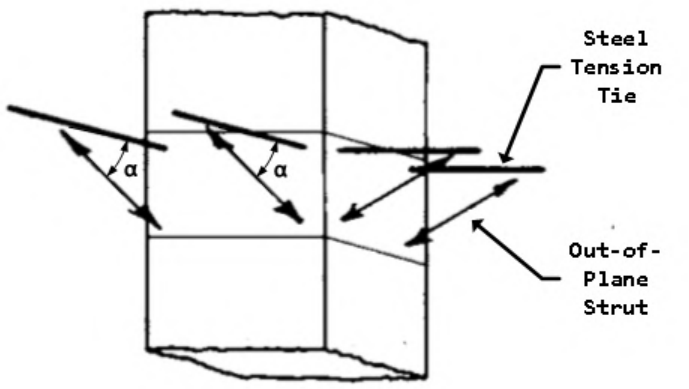

Figure 2.10: The Truss Model of Simmonds and Alexander (1987)

The geometry of the strut elements depends on the detailing of the connection, with the out-of-plane struts acting at an angle α. Assuming that the concrete compressive struts will not fail, the strength of the connection is determined by considering only the yielding of the steel tension ties. The interaction of shear and moment can be described by varying the contribution of the front face tension steel in equilibrating the out-of-plane struts.

In terms of the flexural contribution of top reinforcing bars adjacent to the column, the authors consider only those bars within a distance d from the column side faces. Note, however, that in-plane struts are needed for this contribution, reducing the shear strength of the connection.

2.3.2 Alexander and Simmonds (1991)

After a series of tests at the University of Alberta in 1990 demonstrated several flaws in their *Truss Model*, Alexander and Simmonds developed the *Bond Model*. Instead of straight line compressive struts, the authors propose that shear is transferred to the column through curved, arching compressive struts entering each face (Figure 2.11).

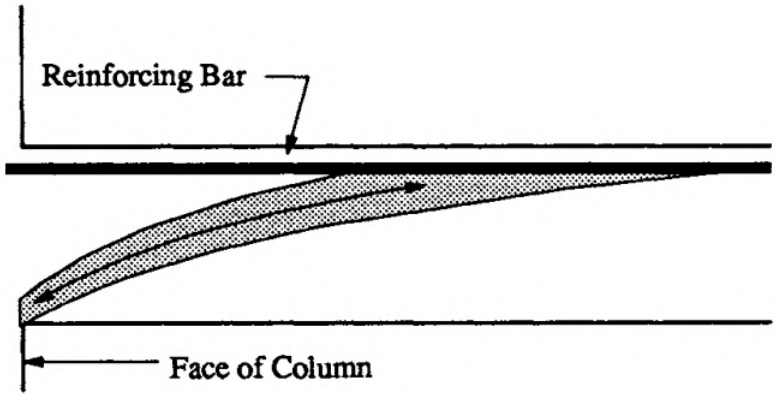

Figure 2.11: Arching compression struts (Alexander and Simmonds, 1991)

The connection is modelled as three struts, or "radial strips," that frame into the column and support two adjacent slab quadrants, all bounded by lines of zero shear, see Figure 2.12. The strips are equilibrated at their point of origin by top mat tension steel and terminate at the soffit of the slab and the column. The force in the strut is assumed to be constant, with its vertical component maximum at the face of the column and its horizontal component maximum at its point of origin.

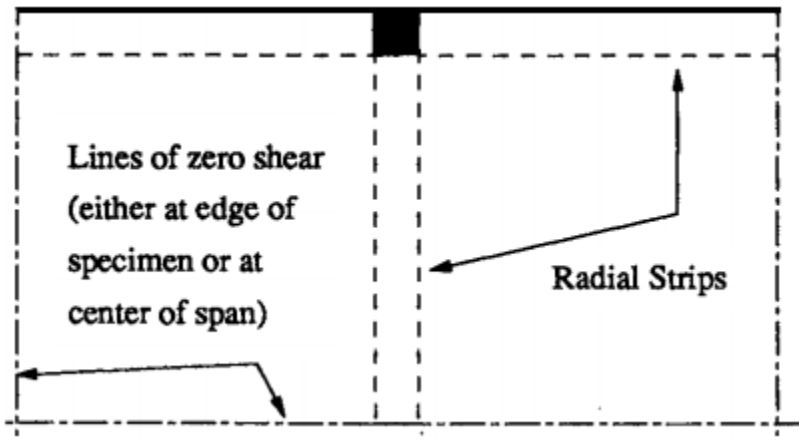

Figure 2.12: Geometry of radial strips and slab quadrants (Alexander and Simmonds, 1991)

Punching shear failure of the connections occurs when the moment gradient necessary to transfer shears between the radial strips and adjacent slab quadrants exceeds the bond strength of the top mat reinforcement. Ductile failure of the connection is also possible through the formation of a yield mechanism. These two failure modes are mutually exclusive.

2.3.3 Sherif (1996)

Sherif tested four isolated edge slab-column specimens and two continuous slab specimens consisting of one edge column and one interior column. The author observed that the CSA A23.3-94 (1994) significantly overestimates the interaction of shear and moment in edge slab-column connections. Sherif developed a new formula for the fraction of the unbalanced moment transferred in shear based on a truss analogy, see Figure 2.13. The moment resisted in flexure is determined by evaluating the force in the tension ties, corresponding to the bars inside and adjacent to the column:

$$M_{flex} = \sum \left(T_i - C_i cos\theta_i\right) 0.9d \tag{2.18}$$

The force in the ties is a function of the angle θ_i and the capacity of the compressive struts C_i. Furthermore, only those bars within a band width of $c_2 + 2c_1\sqrt{\frac{\rho_t}{\rho_l}}$ are effective in resisting the unbalanced moment. The portion of moment transferred in shear is then:

$$\gamma_v = 1 - \frac{M_{flex}}{M_{cg}} = 1 - \frac{\sum \left(T_i - C_i cos\theta_i\right) 0.9d}{M_u + V\left(e_1 - d/2\right)} \tag{2.19}$$

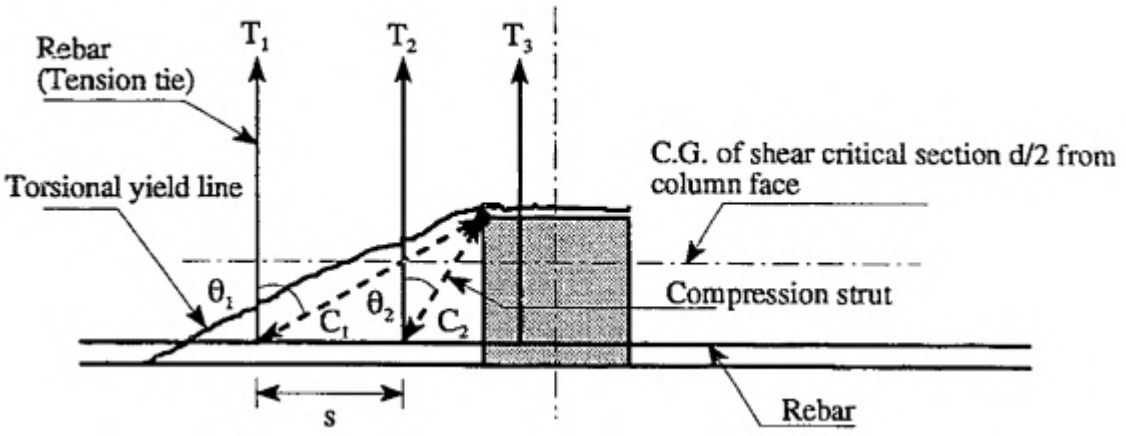

Figure 2.13: Sherif's Strut and Tie Model (1996)

2.3.4 Muttoni (2008)

Muttoni developed a mechanical model describing the strength and failure mechanism of flat plate slab-column connections. His model simplifies for design purposes the *Critical Shear Crack Theory* of Kinnunen and Nylander (1960), who proposed that punching shear failure of the connection occurs when some critical rotation of the slab is reached, Figure 2.14. As the critical shear crack opens with increasing rotation of the slab, the capacity of the concrete compressive struts carrying shear to the column decreases until failure.

The angle of rotation at which failure occurs is primarily a function of the slab thickness, the maximum aggregate size, and the reinforcement ratio.

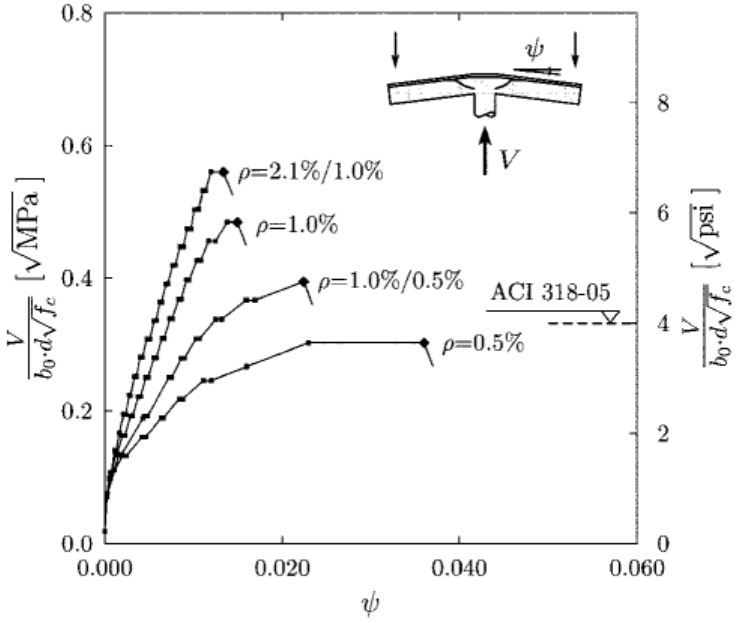

Figure 2.14: Load-rotation Relationship (Muttoni, 2008)

To determine the punching shear strength of the connection, the rotation for a given shear and the shear capacity at that rotation must be known. For the former, Muttoni describes the load-rotation of the connection in terms of a simplified elasto-plastic moment-curvature relationship, dependent on the span and pure moment capacity of the connection:

$$\psi = 0.33 \frac{l_1}{d} \frac{f_y}{E_s} \left(\frac{V}{8 M_{r,flex}} \right)^{3/2} \tag{2.20}$$

The shear capacity of the connection at a given rotation is a function of the perimeter of the critical section, the average flexural depth of the slab, and the maximum aggregate size:

$$\frac{V_r}{b_0 d \sqrt{f'_c}} \geq \frac{3/4}{1 + 15 \frac{\psi d}{16 + a_{max}}} \tag{2.21}$$

2.3.5 Alexander (2017)

Based on the *Bond Model* (Alexander and Simmonds, 1991), Alexander developed a new model, entitled the *Strip Model*, to describe the behaviour of slab-column connections. As with the *Bond Model*, the connection consists of three radial strips sideed by two slab quadrants; however, unlike the *Bond Model*, the

front radial strip in edge connections has the potential to progress to a "super strip." In this case, the width of the radial strip increases to $c_2 + 3h$, encompassing a greater portion of the reinforcement perpendicular to the free edge. The efficacy of this reinforcement in resisting the unbalanced moment in this band width is determined by evaluating the anchorage of individual bars relative to boundaries of the critical flexure section shown in Figure 2.15. Alexander recognizes that bars without at least l_{dh}, taken from the free edge to the point of intersection with the boundaries of the critical flexure section, will not yield.

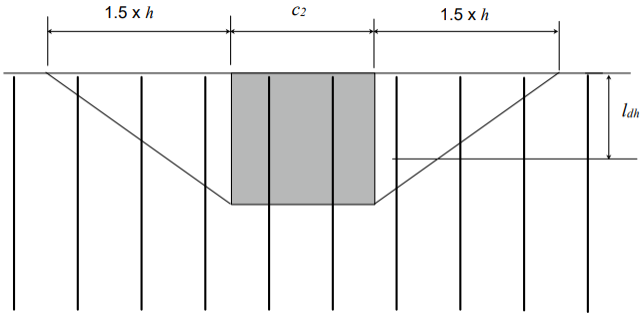

Figure 2.15: Yield mechanism according to Alexander (2017)

2.4 North American Codes

2.4.1 CSA A23.3-14 Standard (2014)

In the CSA A23.3-14 standard (2014), failure of an edge slab-column connection occurs when either the punching shear strength or flexural capacity is exceeded. In the case of punching shear, the connection fails when a limiting shear stress, shown in Equation 2.22, is reached on a critical perimeter $d/2$ from the faces of the column. The interaction of the unbalanced moment and shear is taken into account with the assumption that a portion of the unbalanced moment is transferred by eccentric shear stresses. This portion, γ_v, depends solely on the connection geometry, see Equation 2.23. The maximum shear stress, v_u, is limited to v_c and is given by Equation 2.24, where V_g is the uniform shear acting on the critical section and M_{cg} is the applied moment at the centroid of the critical section.

$$v_c = min \begin{bmatrix} a. & \left(1 + \frac{2}{\beta_c}\right) 0.19\lambda\phi_c\sqrt{f'_c} \\ b. & \left(\frac{\alpha_s d}{b_0} + 0.19\right) \lambda\phi_c\sqrt{f'_c} \\ c. & 0.38\lambda\phi_c\sqrt{f'_c} \end{bmatrix} \tag{2.22}$$

$$\gamma_v = 1 - \frac{1}{1 + 2/3\sqrt{\frac{c_1+d/2}{c_2+d/2}}} \tag{2.23}$$

$$v_u = \frac{V_g}{b_0 d} + \frac{\gamma_v M_{cg} e_1}{J_1} \tag{2.24}$$

In the case of failure in flexure, while a portion of the unbalanced moment is assumed to be transferred in shear, the code requires that an edge connection be designed to resist 100 % of the moment at the front face of the column. This moment is to be transferred to the column by the reinforcement inside a band width, $b_b = c_2 + 3h$. The code assumes that all reinforcement in $c_2 + 3h$ is effective and will yield.

2.4.2 ACI 318-14 Code (2014)

The punching shear design provisions in the CSA A23.3-14 (2014) standard are based on the provisions of the ACI 318-14 code (2014) and hence are nearly identical. As with CSA A23.3-14 standard (2014), the critical section for punching shear is taken at a distance $d/2$ from the faces of the column and a portion of the unbalanced moment acting on the connection is assumed to be transferred in eccentric shear. However, a significant difference between the ACI 318-14 (2014) and CSA A23.3-14 (2014) is the provision that, if $\frac{V_g}{b_0 d} < 0.75\phi v_c$, a modified γ_v may be used that reduces the percentage of the unbalanced moment transferred by eccentric shear. The ACI 318-14 code (2014) requirements for v_c are given by:

$$v_c = min \begin{bmatrix} a. & 0.17\phi \left(2 + \frac{4}{\beta_c}\right) \sqrt{f'_c} \\ b. & 0.083\phi \left(\frac{\alpha_s d}{b_0} + 2\right) \sqrt{f'_c} \\ c. & 0.33\phi \sqrt{f'_c} \end{bmatrix} \tag{2.25}$$

Where ϕ is a strength reduction factor equal to 0.75 for shear, β_c is the ratio of the long column dimension to short column dimension, and α_s is 30 for edge slab-column connections.

3 Experimental Program

3.1 Prototype Structure

A flat plate prototype structure was designed in order to determine the load conditions, that is, the ratio of shear and moment, present in a typical edge slab-column connection. The structure was designed with clear spans of 5000 mm in each principal direction and storey heights of 3 m. A thickness of 200 mm was chosen for the slab and a clear cover of 25 mm specified. Using the Direct Design Method of the CSA A23.3-14, the first point of zero moment in the span was determined to be approximately 400 mm from the inner face of the edge column. This eccentricity was used to determine the loading for each isolated slab-column test specimen.

3.2 Design of Test Specimens

Four full-scale isolated edge slab-column connections of different typical column configurations, that is, column dimensions and presence of an overhang, were designed according to the CSA A23.3-14 standard. The configurations of Specimen 1, 2, 3, and 4 were as follows: a 250 x 500 mm column, a 250 x 500 mm column with a 150 mm overhang, a 400 x 400 mm column, and finally a 500 x 250 mm column. This scheme was chosen as it provided a range of column depths and breadths with varying predicted strain distributions in $c_2 + 3h$.

The general specimen layout consisted of an edge column cast in the middle of a 2000 mm wide, 200 mm thick slab that extended an additional 1225 mm from the front face of the columns as shown in Figures 3.1, 3.2, 3.3, and 3.4. The columns measured 1400 mm above and below the slabs, corresponding to the assumed points of inflection in the columns of the prototype structure. The top and bottom mat reinforcing bars were composed of 15M and 10M bars, respectively. In terms of material strengths used in design, 28-day concrete compressive strength of 35 MPa and a steel yield strength of 400 MPa were chosen. A clear cover of 25 mm for the slab and a 30 mm cover for the column was specified.

The slab reinforcement was designed such that failure occurred in negative bending along an axis parallel to the free edge and not in punching shear. This entailed ensuring that the top tension reinforcement perpendicular to the free edge within the band width $c_2 + 3h$ reached yield before punching. In order to provide the most detailed picture of the distribution of bar strains in this band width, a number of 15M bars were placed in the band width b_b while still ensuring that flexural yielding would occur. Bars outside of this band width were then spaced at 250 mm. In each specimen, 2-15M bars were concentrated inside the column. As per the CSA A23.3-14, all bars in the $c_2 + 3h$ band width were assumed to reach yield before

failure.

The top mat reinforcement parallel to the free edge and the bottom mat reinforcement were designed to resist the moments in the prototype structure at yielding of the bars in b_b. Additionally, 4-10M bars were used to maintain structural integrity if punching failure occurred. To ensure proper anchorage of reinforcing bars, the top and bottom mat bars perpendicular to the free edge were bent with 180 degree hooks at the free edge. Hooks were not provided at the other edges; however, the distance between the end of the bar and the point of maximum moment exceeded the development length of the bars in all cases.

The column was designed with 20M longitudinal bars and 10M ties at a spacing of 250 mm, that is, the maximum spacing permitted by CSA A23.3-14. An adequate number of longitudinal bars was provided given the interaction of axial load and moment present in testing.

3.2.1 Details of Specimen 1

The first specimen was designed with slab dimensions 2000 x 1475 x 200 mm and column dimensions 500 x 250 mm, with the column oriented such that c_1 was 250 mm and c_2 was 500 mm. For the top mat reinforcement perpendicular to the free edge, the effective reinforcement transfer band width b_b was 1100 mm. As shown in Figure 3.5, 6-15M bars were placed in this band width at a spacing of 175 mm, corresponding to a predicted moment resistance of 80.9 kNm. The bottom mat reinforcement is shown in Figure 3.6.

3.2.2 Details of Specimen 2

The second specimen was designed with slab dimensions 2000 x 1625 x 200 mm and column dimensions 500 x 250 mm, with the column oriented such that c_1 was 250 mm and c_2 was 500 mm. The column was offset from the free edge by an overhang of 150 mm. The effective reinforcement transfer band width b_b was identical to the first specimen, at 1100 mm. As shown in Figure 3.7, 8-15M bars were placed in this band width at a variable spacing. This configuration possessed an estimated moment resistance of 106.8 kNm. The bottom mat reinforcement details may be found in Figure 3.8.

3.2.3 Details of Specimen 3

The third specimen was designed with slab dimensions 2000 x 1625 x 200 mm and square column dimensions 400 x 400 mm. The effective reinforcement transfer band width b_b for this specimen was 1000 mm. A total of 8-15M bars were placed in this band width at a spacing of 120 mm, as seen in Figure 3.9, with an estimated moment resistance of 106.2 kNm. The layout of the bottom mat reinforcement is shown in Figure 3.10.

3.2.4 Details of Specimen 4

The fourth specimen was designed with slab dimensions 2000 x 1725 x 200 mm and column dimensions 250 x 500 mm, with the column oriented such that c_1 was 500 mm and c_2 was 250 mm. The effective reinforcement transfer band width of this specimen was 850 mm. As with specimens 2 and 3, 8-15M bars were placed within this band width, spaced at 120 mm, see Figure 3.11. The predicted moment resistance of the connection was 105.0 kNm. The details of the bottom mat reinforcement are displayed in Figure 3.12.

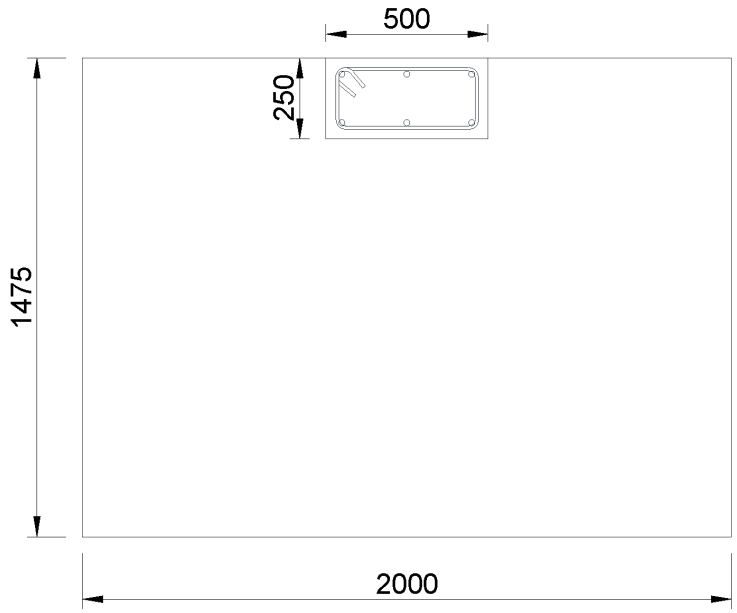

Figure 3.1: Layout of Specimen 1 (units in mm)

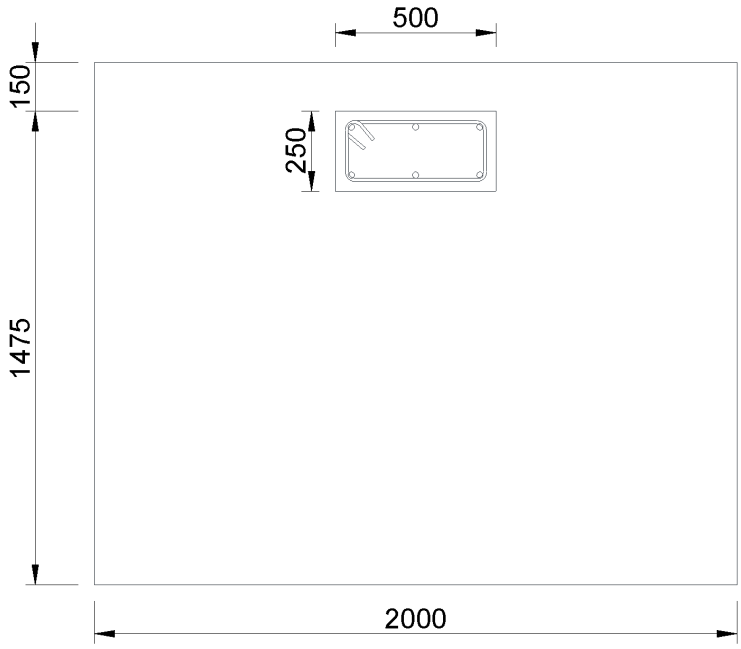

Figure 3.2: Layout of Specimen 2 (units in mm)

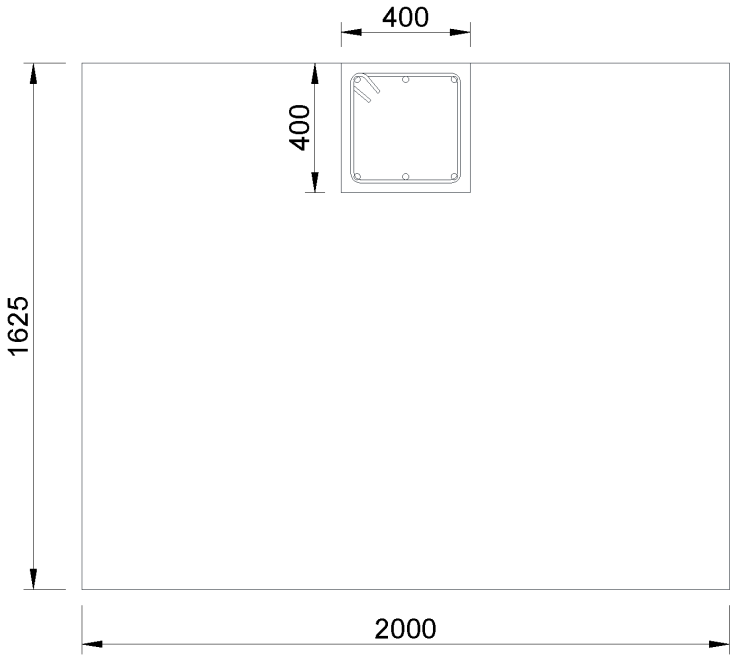

Figure 3.3: Layout of Specimen 3 (units in mm)

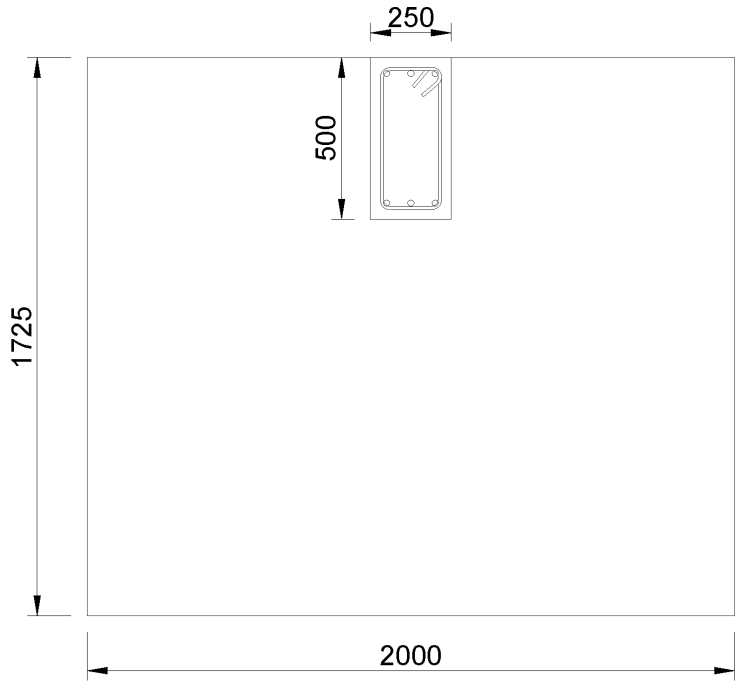

Figure 3.4: Layout of Specimen 4 (units in mm)

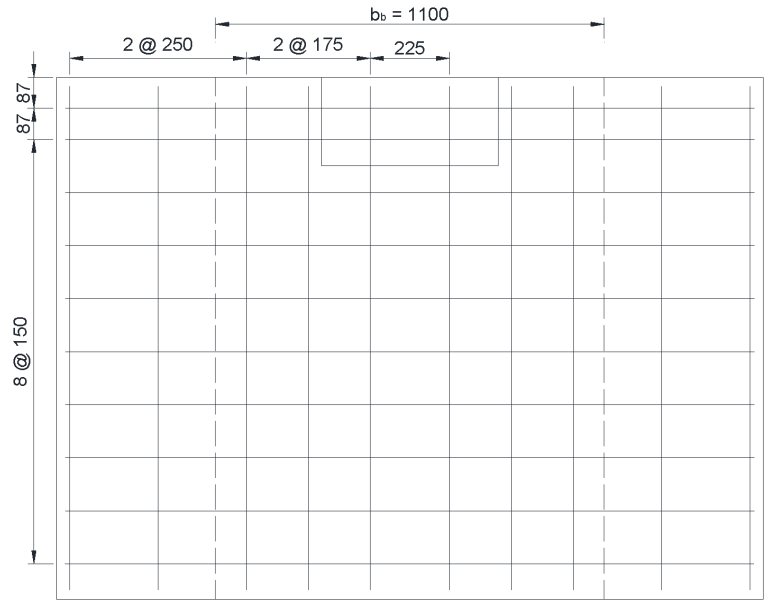

Figure 3.5: Top mat reinforcement details for Specimen 1 (15M bars) (units in mm)

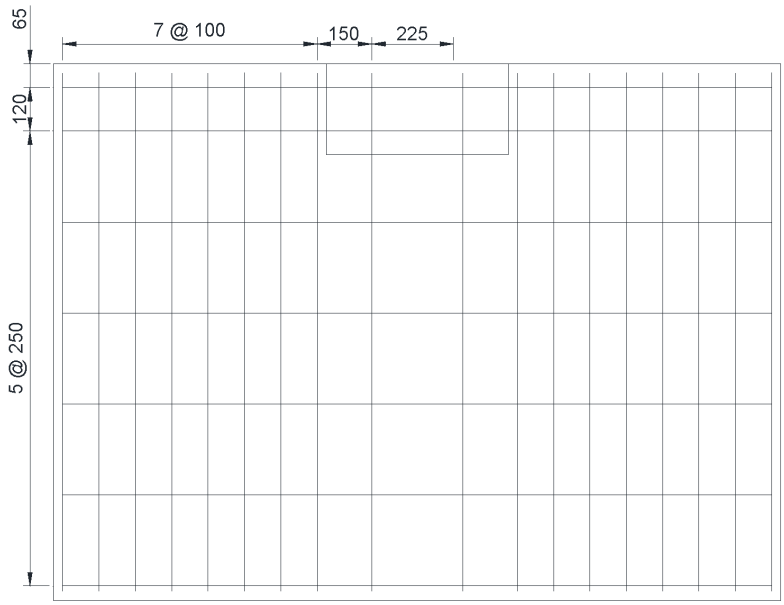

Figure 3.6: Bottom mat reinforcement details for Specimen 1 (10M bars) (units in mm)

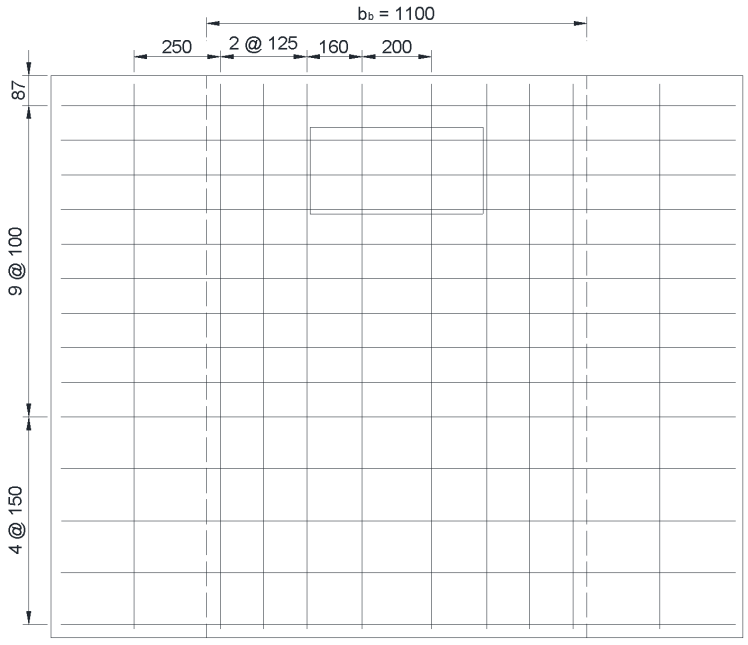

Figure 3.7: Top mat reinforcement details for Specimen 2 (15M bars) (units in mm)

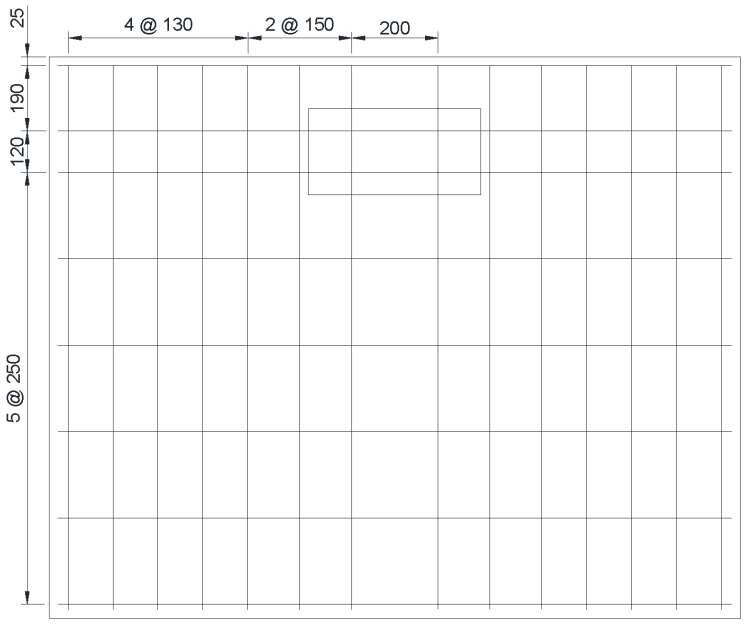

Figure 3.8: Bottom mat reinforcement details for Specimen 2 (10M bars) (units in mm)

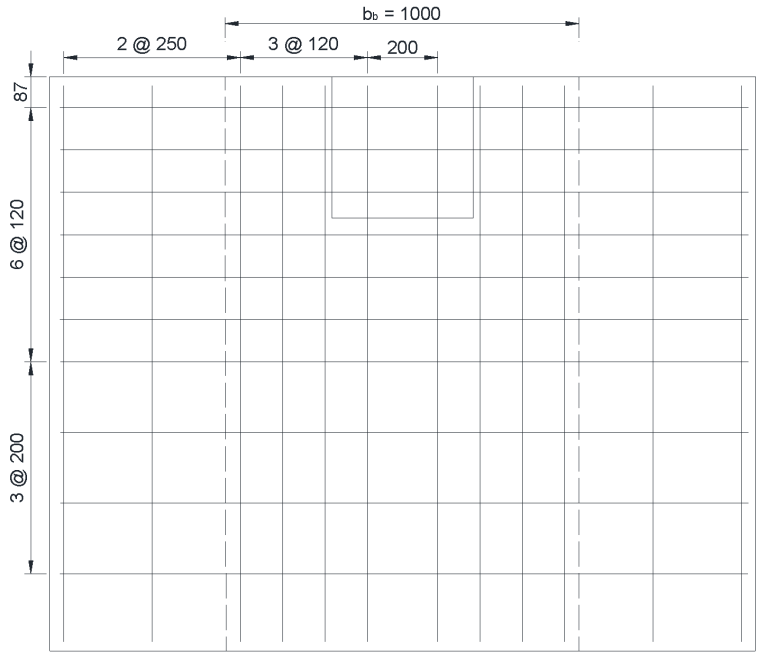

Figure 3.9: Top mat reinforcement details for Specimen 3 (15M bars) (units in mm)

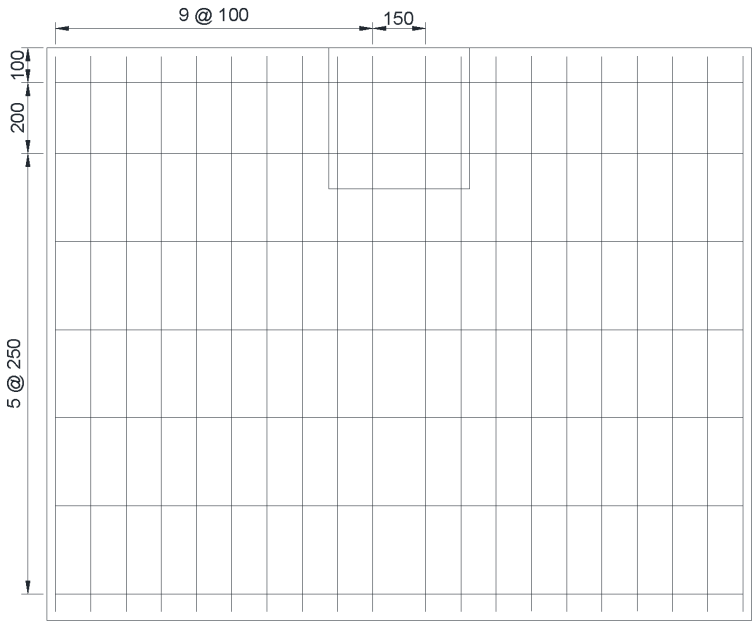

Figure 3.10: Bottom mat reinforcement details for Specimen 3 (10M bars) (units in mm)

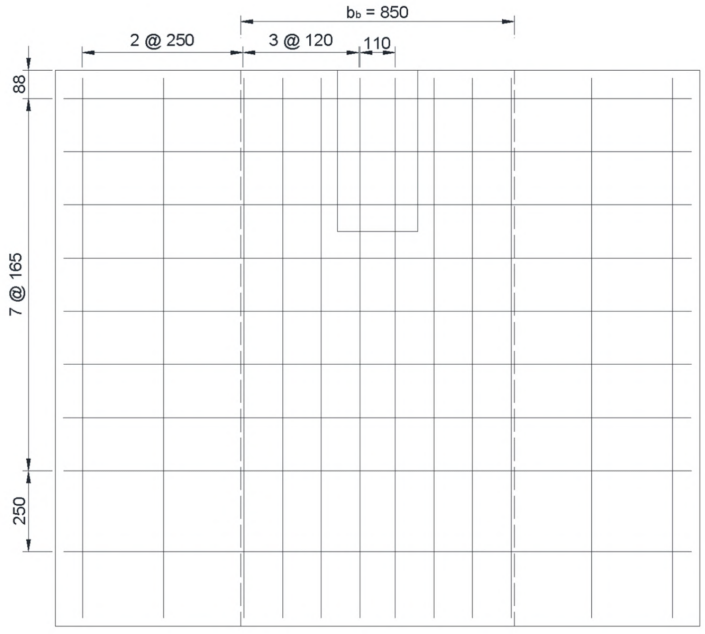

Figure 3.11: Top mat reinforcement details for Specimen 4 (15M bars) (units in mm)

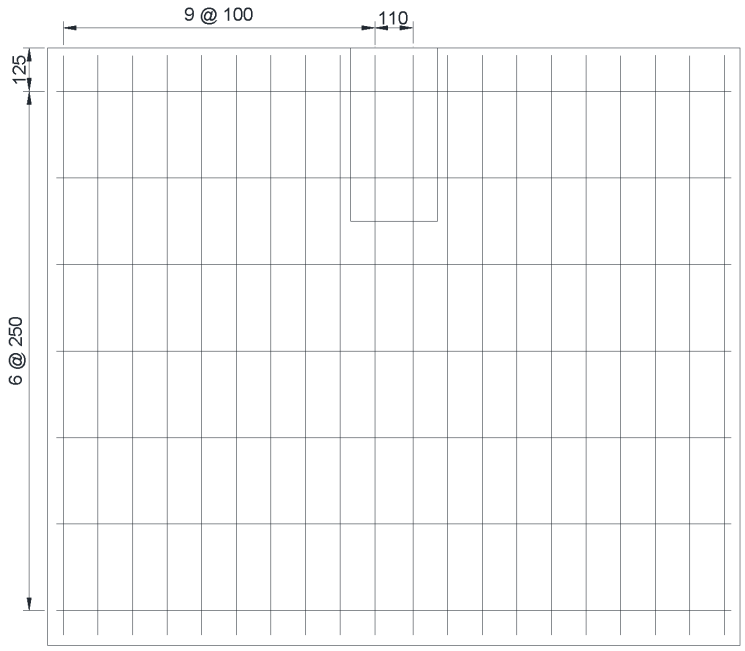

Figure 3.12: Bottom mat reinforcement details for Specimen 4 (10M bars) (units in mm)

3.3 Construction Process

The test specimens were all built simultaneously and in two phases. In the first phase, the formwork for the slab and lower storey column were built, and the slab and column reinforcement placed. The holes in the slab needed for the loading beams were "pre-drilled" using stainless steel tubes welded to a small frame and secured to the reinforcement. The lower storey column and slab were then cast together and the specimens left to cure for a week before starting the second phase.

In the second phase, the formwork for the upper storey column was constructed and a second batch of concrete placed 14 days after the first casting. The concrete mix design for both concrete placements were identical. A minimum of 28 days was allocated between the second casting and the testing of the specimens. Part of the construction sequence is shown in Figures 3.13 to 3.18.

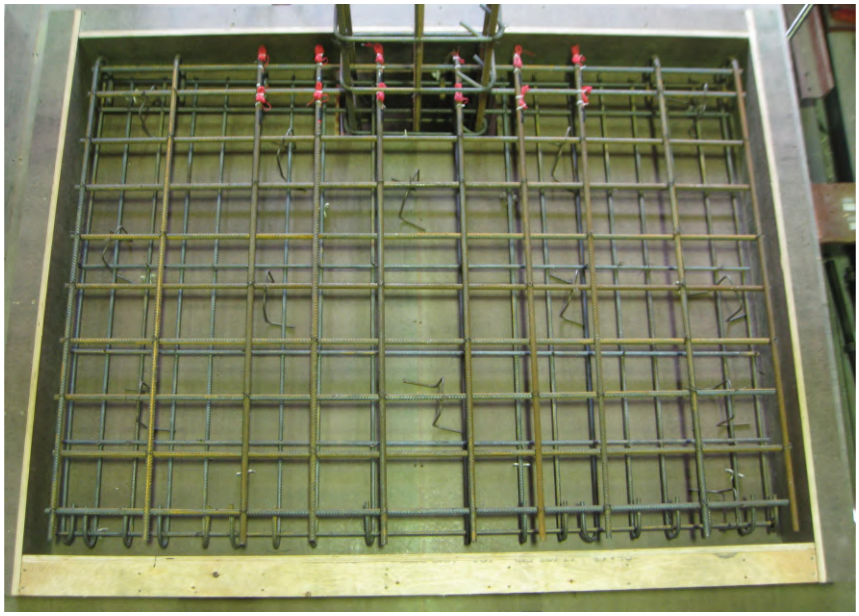

Figure 3.13: Assemblage of Specimen 1

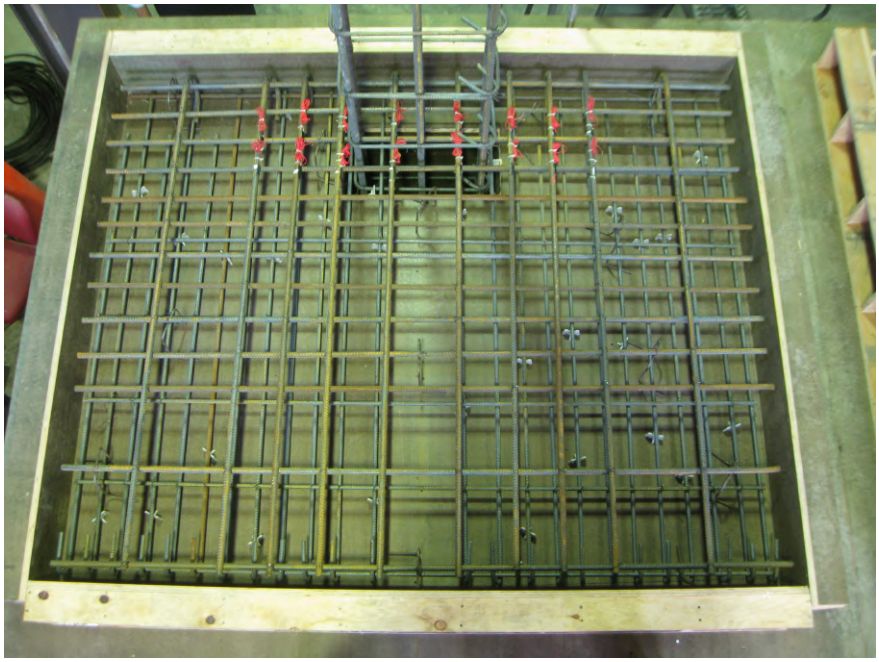

Figure 3.14: Assemblage of Specimen 2

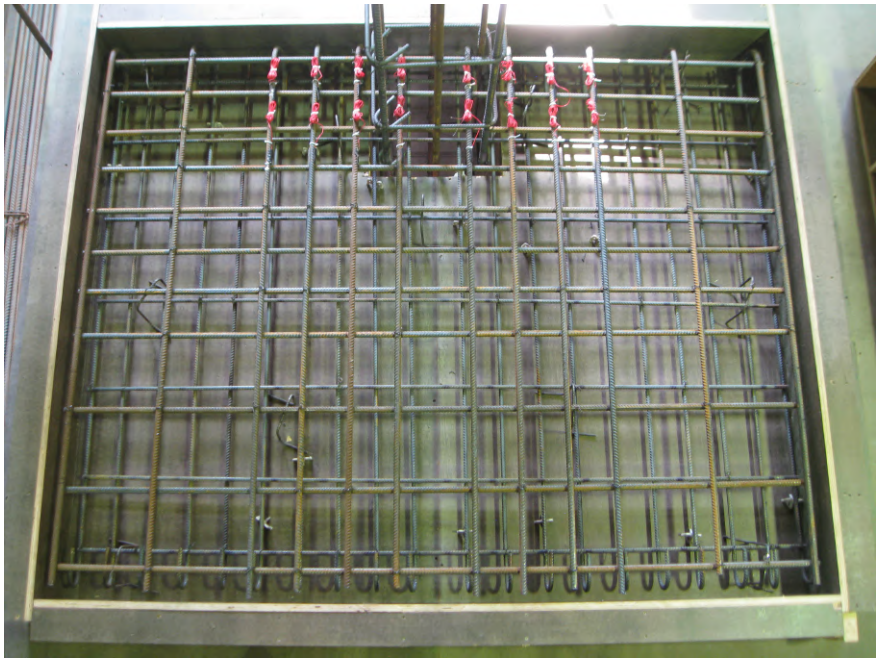

Figure 3.15: Assemblage of Specimen 3

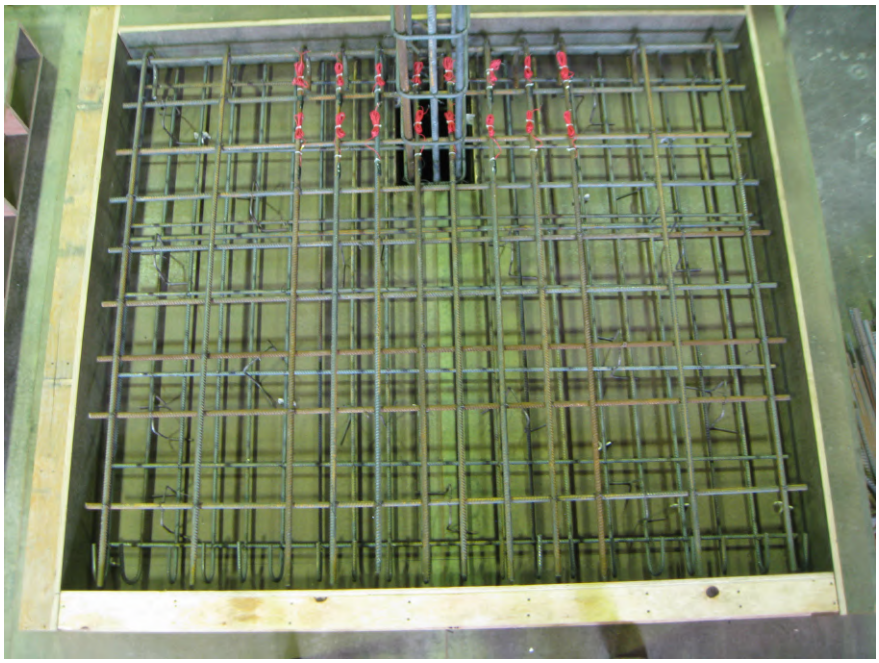

Figure 3.16: Assemblage of Specimen 4

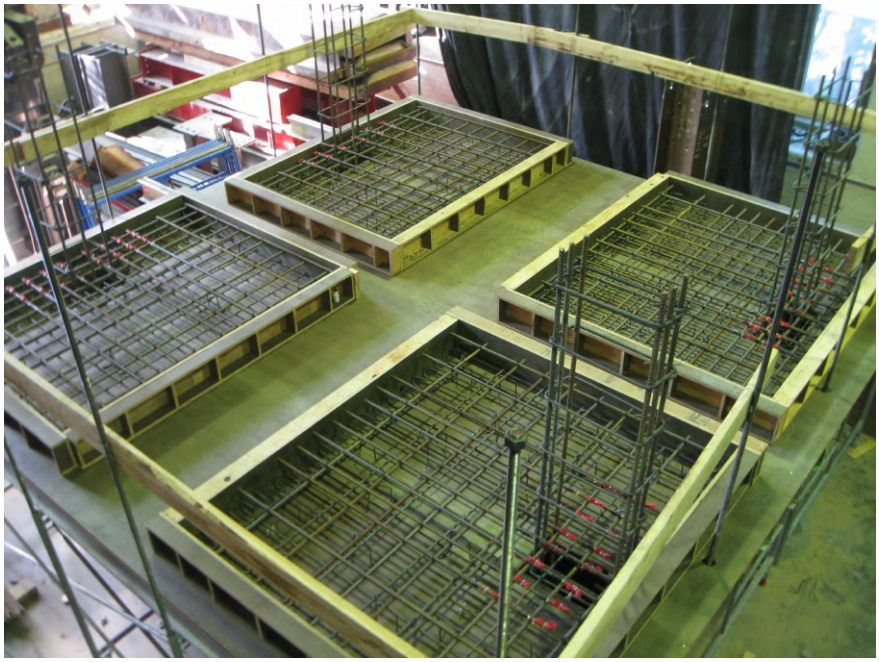

Figure 3.17: Assemblage of reinforcement before first concrete placement

Figure 3.18: Specimens after first concrete placement

3.4 Material Properties

3.4.1 Concrete Properties

The lower column and slab were cast together and the upper column cast afterwards. The mix design of these two concrete placements was identical and described in Table 3.1. The specified concrete compressive strength at 28-days was 35 MPa for the column and the slab. Normal density concrete was used and the maximum aggregate size was 20 mm.

Table 3.1: Concrete Mix Design

Component	Quantity
Cement (kg/m^3)	370
Fine Aggregates (kg/m^3)	850
Coarse Aggregates (kg/m^3)	964
Water Content	0.40
Air Content (%)	6.5
Superplasticizer ($ml/100\,kg$)	159
Air Entrainer ($ml/100\,kg$)	16
Water Reducer ($ml/100\,kg$)	199

For each concrete placement, 24-150 mm diameter, 300 mm long test cylinders were collected, corresponding to 6 test cylinders per specimen. Half of these cylinders were used to measure the compressive strength, f'_c, and the other half used to measure the splitting tensile strength, f_{sp}, of the concrete. In addition, 12-100 mm x 100 mm x 350 mm concrete test beams were prepared to be used to measure the modulus of rupture, f_r.

In compliance with the CSA A23.2-9C (2014) test procedure, the concrete compressive strength of the slab was determined ± 4 days from the day of testing, see Table 3.2.

Table 3.2: Concrete Properties

Specimen #	f'_c (MPa) (Std. Dev.)	f_{sp} (MPa) (Std. Dev.)	f_r (MPa) (Std. Dev.)
1	42.20 (2.65)	-	-
2	42.20 (1.32)	-	-
3	43.91 (1.32)	-	-
4	43.91 (0.68)	4.22 (0.24)	4.79 (0.34)

3.4.2 Steel Properties

The steel reinforcement consisted of 10M, 15M, and 20M Grade 400 deformed, weldable hot-rolled bars conforming to the CSA G30.18-09 standard (2009). The yield strength, ultimate strength, and yield strain were determined in compliance with ASTM 615/A615M-16 (2016) and are shown in Figure 3.3.

Table 3.3: Steel Properties

Bar Size	f_y (MPa)	f_u (MPa)	ε_y (mm/mm)
10M	464.4 (12.8)	562.6 (9.2)	0.00232 (0.0000)
15M	420.1 (9.2)	535.5 (0.5)	0.00210 (0.0000)
20M	435.8 (13.7)	565.3 (12.2)	0.00268 (0.0000)

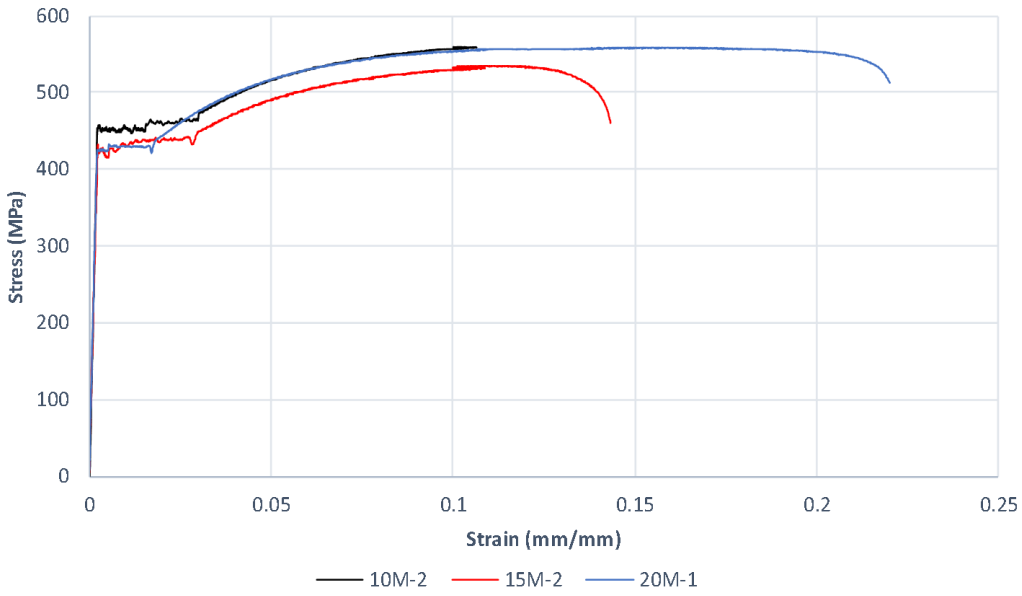

Figure 3.19: Stress-strain behaviour of 10M, 15M, and 20M reinforcing bars

3.5 Experimental Set-up

The experimental set-up was designed to simulate the loading present in a typical edge connection of the prototype structure. In order to recreate the mid-storey inflection points in the columns of the prototype structure, the upper and lower columns were pin connected at their ends to a rigid test frame (see Figure 3.22). The lower column was seated on a steel roller with an HSS "bumper" sandwiched between the column and the test frame. The upper column was tied back to the testing frame using HSS clamps and threaded rods that provided negligible rotational stiffness.

The distribution of shear and moment present in the edge span of the prototype structure was reproduced using two cantilevered built-up beams bolted to the underside of the slab (Figures 3.20 and 3.21). The beams consisted of two 152 x 152 x 11 mm hollow steel sections welded to each other in a cruciform configuration and secured to the slab with a 150 x 450 x 9.51 mm plate and threaded rods. The placement scheme of the beams was consistent for all specimens; the centroid of the bolt group was located 800 mm from the face of the column and the beams were spaced 1500 mm apart. Using this loading system, a negative shear and positive moment were generated in the slab with a point of inflection located 400 mm from the face of the column. To load the specimens, the beams were connected to hydraulic jacks beneath a strong floor via 1" threaded rods.

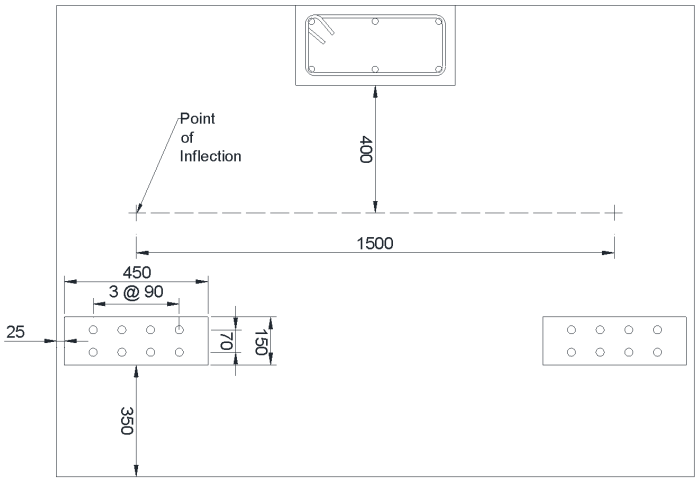

Figure 3.20: Typical plan view of loading beams (units in mm)

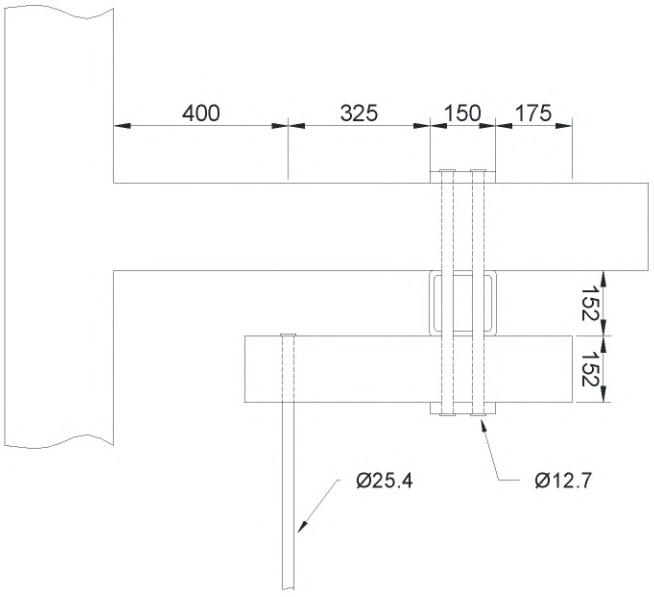

Figure 3.21: Typical elevation view of loading beams (units in mm)

Figure 3.22: Specimen 1 in test set-up

Figure 3.23: Elevation of Specimen 1 in test set-up

3.6 Instrumentation

Strain gauges, load cells, string potentiometers, linear variable differential transformers (LVDTs), and inclinometers were used to measure bar strains, displacements, and rotations respectively. The data from these instruments was collected using a data acquisition system, or DAQ, and recorded with computer software. Before testing, these instruments were calibrated and zeroed.

3.6.1 Strain Measurements

The longitudinal bar strains of the top mat reinforcing bars within b_b were measured using electrical resistance strain gauges with a 5 mm gauge length. The strains of these bars were measured along lines passing through the front face and midline of the column, as shown in Figures 3.24, 3.25, 3.26, and 3.27.

3.6.2 Deflection Measurements

String potentiometers, LVDTs, and inclinometers were used to measure the deflection of the slab. The string potentiometers were arranged in a 4 x 3 grid, as shown in Figure 3.28, and recorded the vertical displacement of the slab relative to the strong floor. The vertical lines of this grid corresponded to the centerline of the slab and the centerlines of the loading beams. The horizontal lines followed the midline of the column with the middle string pot placed 100 mm in front of the column, the point of inflection at 400 mm from the column face, the center of the bolt group of the loading beam, and 1150 mm from the face of the column.

Two sets of LVDTs measured the horizontal displacement of the column relative to the rigid test frame and the deflection of the slab relative to the lower column respectively. As shown in Figure 3.23, two LVDTs were secured to the rigid test frame $\pm$ h/2 from the middle of the slab; these displacements served to measure the rotation of the column. The second set of five LVDTs were attached to an aluminum cantilever beam clamped to the lower column at 150 mm from the middle of the slab, see Figure 3.22. These LVDTs measured the deflection of the slab along a line centered on and perpendicular to the column.

Finally, inclinometers were used to record the X and Y rotations of the free edge of the slab. As shown in Figure 3.29, the inclinometers were epoxied to the middle of the slab at three locations: the centerline of the slab and the centerlines of the loading beams.

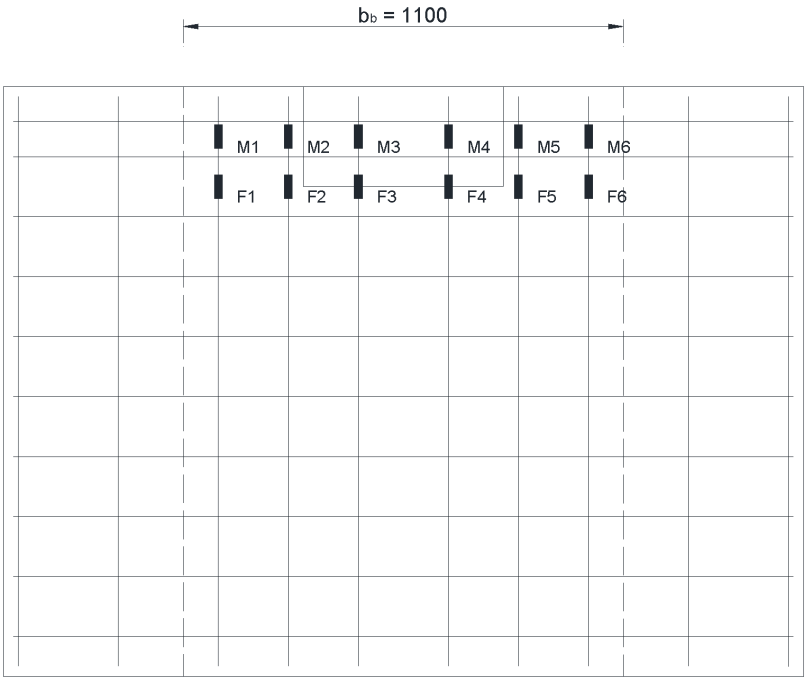

Figure 3.24: Strain gauge layout for Specimen 1 (units in mm)

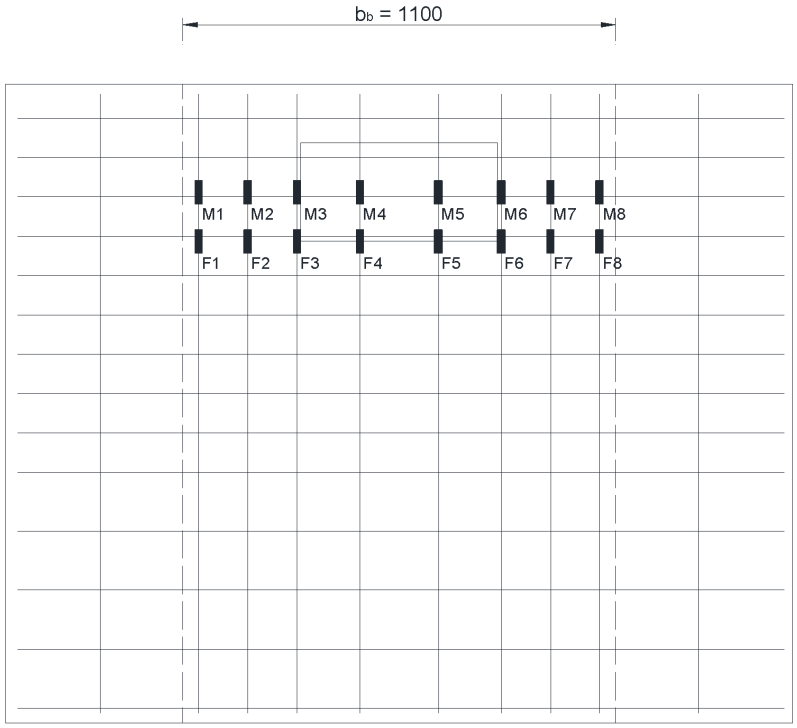

Figure 3.25: Strain gauge layout for Specimen 2 (units in mm)

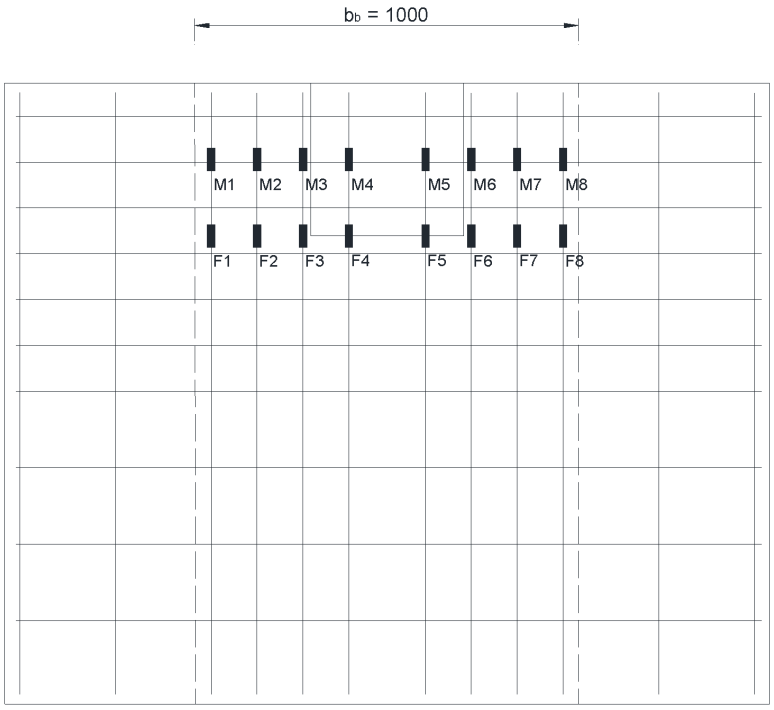

Figure 3.26: Strain gauge layout for Specimen 3 (units in mm)

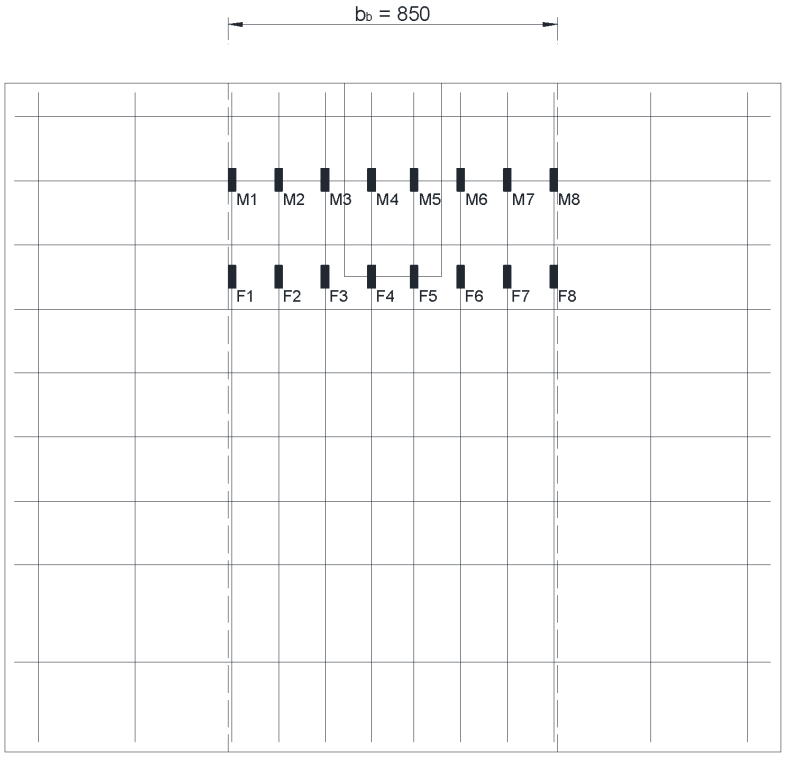

Figure 3.27: Strain gauge layout for Specimen 4 (units in mm)

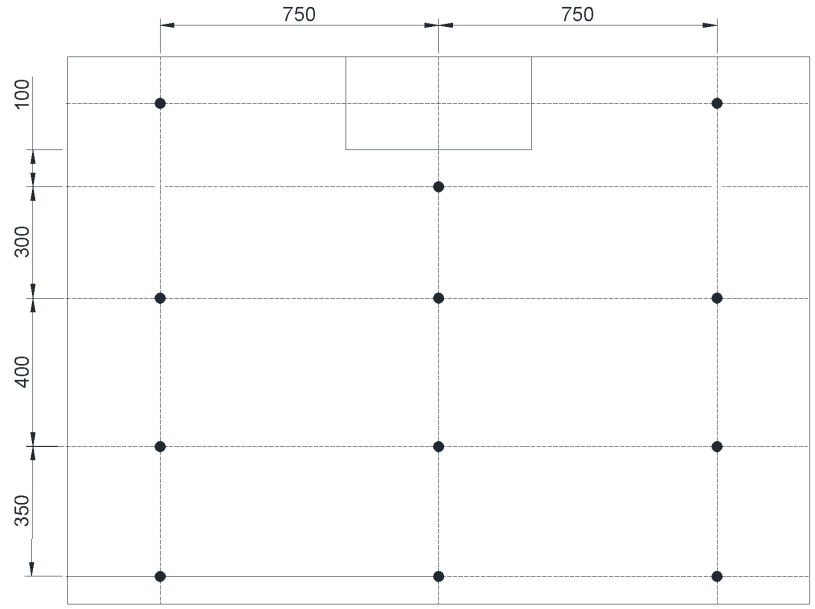

Figure 3.28: Typical grid of string pots (units in mm)

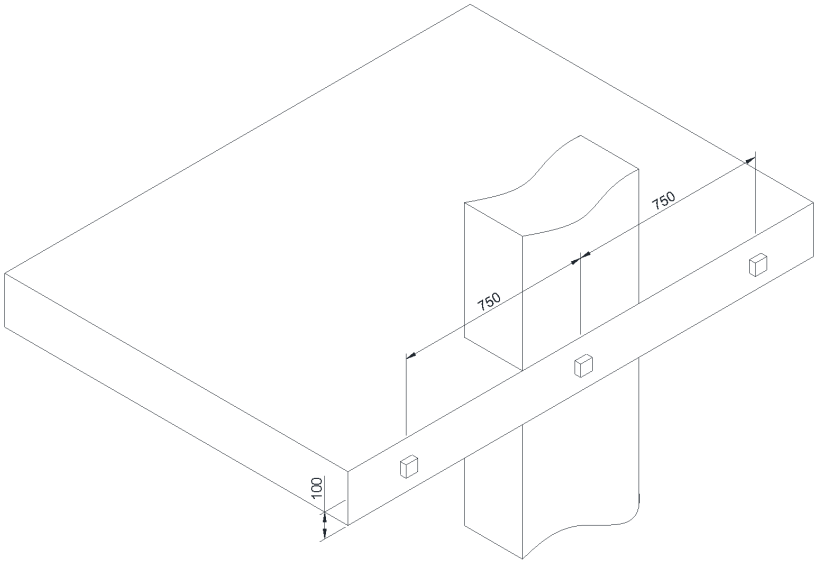

Figure 3.29: Typical layout of inclinometers (units in mm)

3.7 Testing Procedure

Testing of the specimens was carried out in the Jamieson Structural Laboratory at McGill University. The specimens were loaded at 10 kN increments using a single hand-operated pump connected to the hydraulic jacks beneath the strong floor. The total applied shear was measured with load cells. The difference in load cell readings was typically a maximum of 5 kN.

At each load stage, the hydraulic jacks were locked and the specimen inspected. The cracks in the slab and the upper column were then traced and their widths measured and labelled. Pictures were taken to record the progression of cracks until failure.

4 Experimental Results

The load-deflection, crack progression, reinforcement strains, slab deflection and load-rotation results of the specimens tested are presented in this section. The total shear for each load stage was computed as the sum of the dead weight of the slab and the two shear forces applied by the loading beams. The crack widths were marked and measured at the beginning of a load stage. Missing data points in the strain gauge results were due to broken gauges during casting or during testing. In these cases, the strain distribution was assumed to be symmetric about the 1-axis of the column. The slab deflection results were compiled using the LVDT displacements at 100 mm from the front column face, the point of inflection at 400 mm, the center of the loading beam bolt group at 800 mm, and at 1150 mm from the front column face. The load-rotation results consist of the column rotation and average of the east and west free edge rotations.

4.1 Specimen 1 Results

The load-deflection relationship of Specimen 1 is given in Figure 4.1. The specimen behaved elastically until a total shear of 63.6 kN and a deflection of 0.5 mm at the point of inflecton, or POI. Initial yielding of the reinforcement perpendicular to the free edge in width b_b was observed with bar F3 at 122.1 kN and a POI deflection of 3.7 mm (for bar numbers, see Figure 4.9). Further yielding of the reinforcing bars in width b_b occurred at 141.6 kN and a POI deflection of 5.4 mm with bar F4 and M2. The specimen failed in flexure at a total shear of 171.4 kN and a deflection of 16.7 mm at the POI. Continued loading of the specimen after this point resulted in the opening of cracks and notable decreases in the strength and stiffness of the connection.

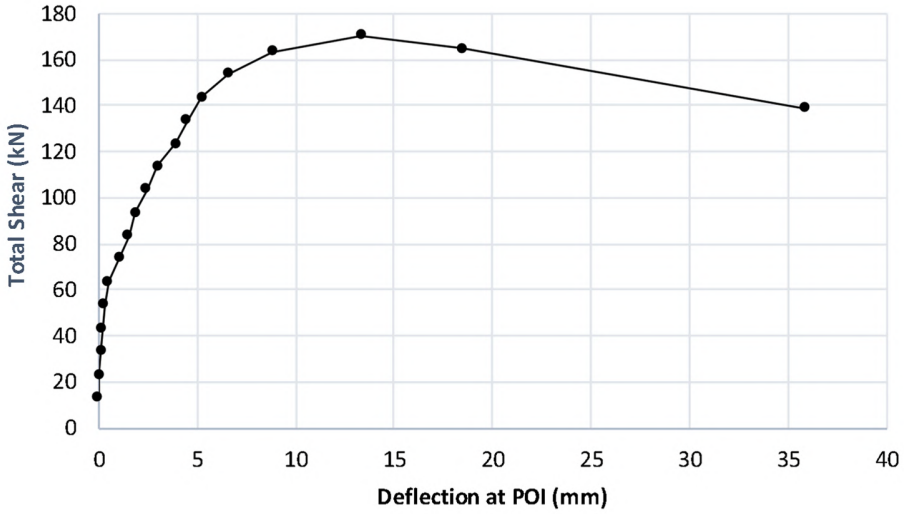

Figure 4.1: Load-deflection response of Specimen 1

4.1.1 Crack Progression

At a total shear of 63.6 kN, a hairline flexural crack developed across the front column face. Two hairline torsional cracks in the slab, or slab torsional cracks, also developed at this load stage, extending outwards to the free edge from the east and west column faces at 10 and 65 degree angles, respectively. At 73.6 kN, the flexural cracks widened on the top surface (Figure 4.2) and the first torsional cracks on the free edge face of the slab, or free edge torsional cracks, formed. These cracks originated at the corners of the rear column face and propagated downwards and outwards towards the soffit at 46 degrees (Figure 4.3). At a total shear of 113.6 kN, the slab torsional cracks widened to 0.20 mm, lengthened and intersected with the free edge of the slab, as shown in Figure 4.4. As well, cracks of width 0.10 mm perpendicular to the free edge and initiating at the front column face were also observed at this load stage. These perpendicular cracks were joined by a straight line crack parallel to the free edge, approximately 45 mm from the front face of the column. At this load stage, the free edge torsional cracks widened to 0.10 mm (Figure 4.5).

At failure, the front column face crack had opened to 6.00 mm and additional slab torsional cracks had developed off the side faces of the column, see Figure 4.6. Cracks perpendicular to the free edge had formed, with the original crack parallel to the front face of the column extending to intersect them. As shown in Figure 4.7, the free edge torsional cracks had opened signficantly to a width of 6.00 mm. The total shear-maximum crack width response for Specimen 1 is presented in Figure 4.8.

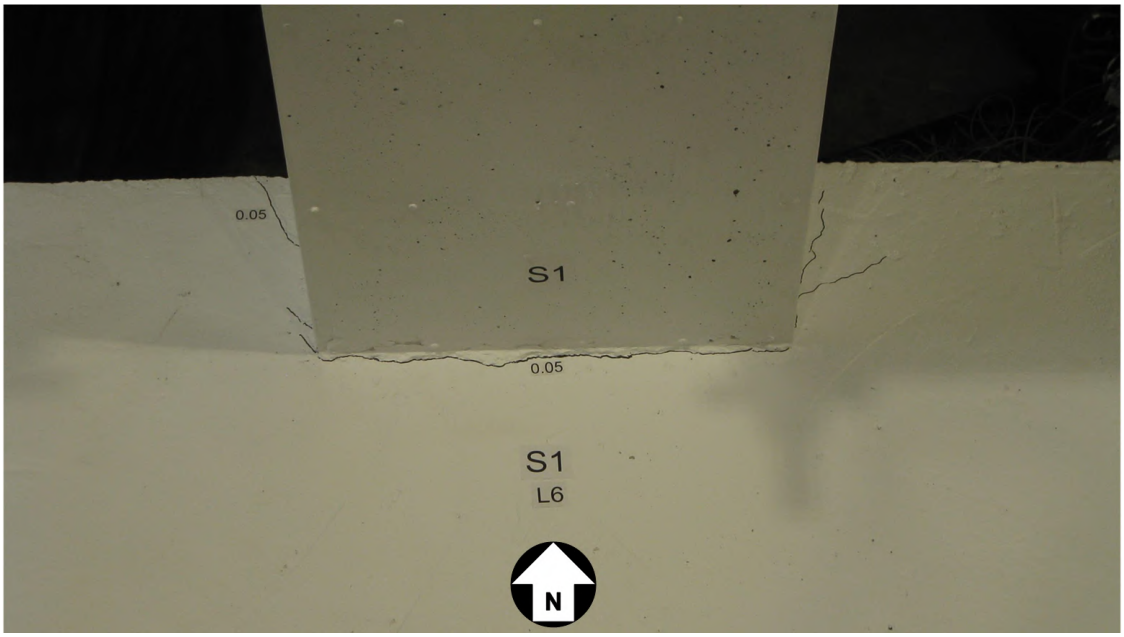

Figure 4.2: Specimen 1 slab cracks at V = 73.6 kN

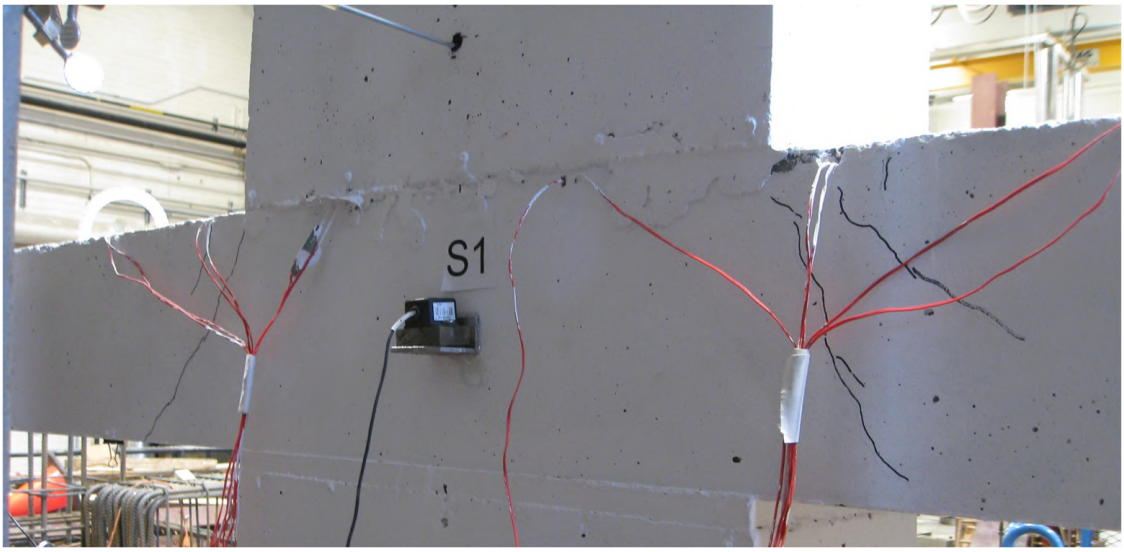

Figure 4.3: Specimen 1 free edge face cracks at V = 73.6 kN

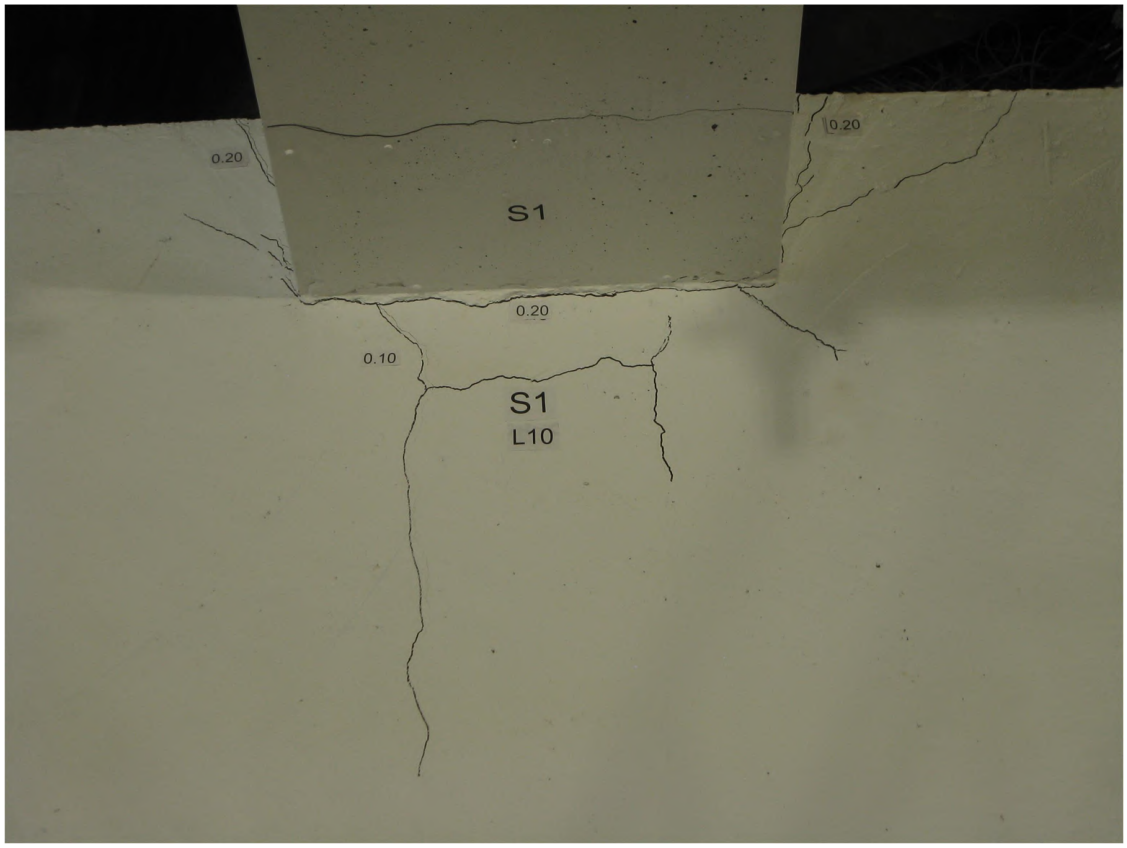

Figure 4.4: Specimen 1 slab cracks at V = 113.6 kN

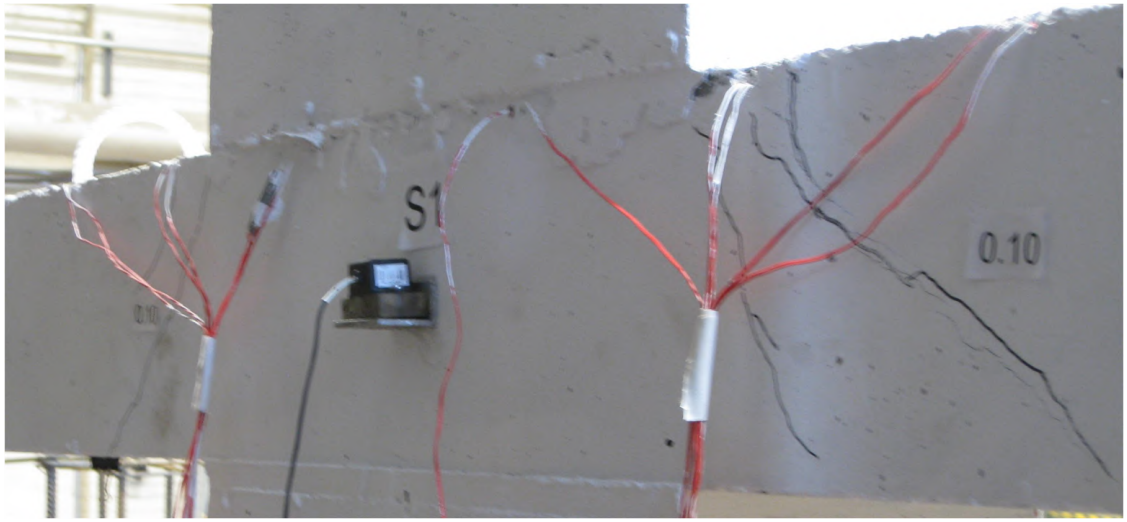

Figure 4.5: Specimen 1 free edge face cracks at V = 113.6 kN

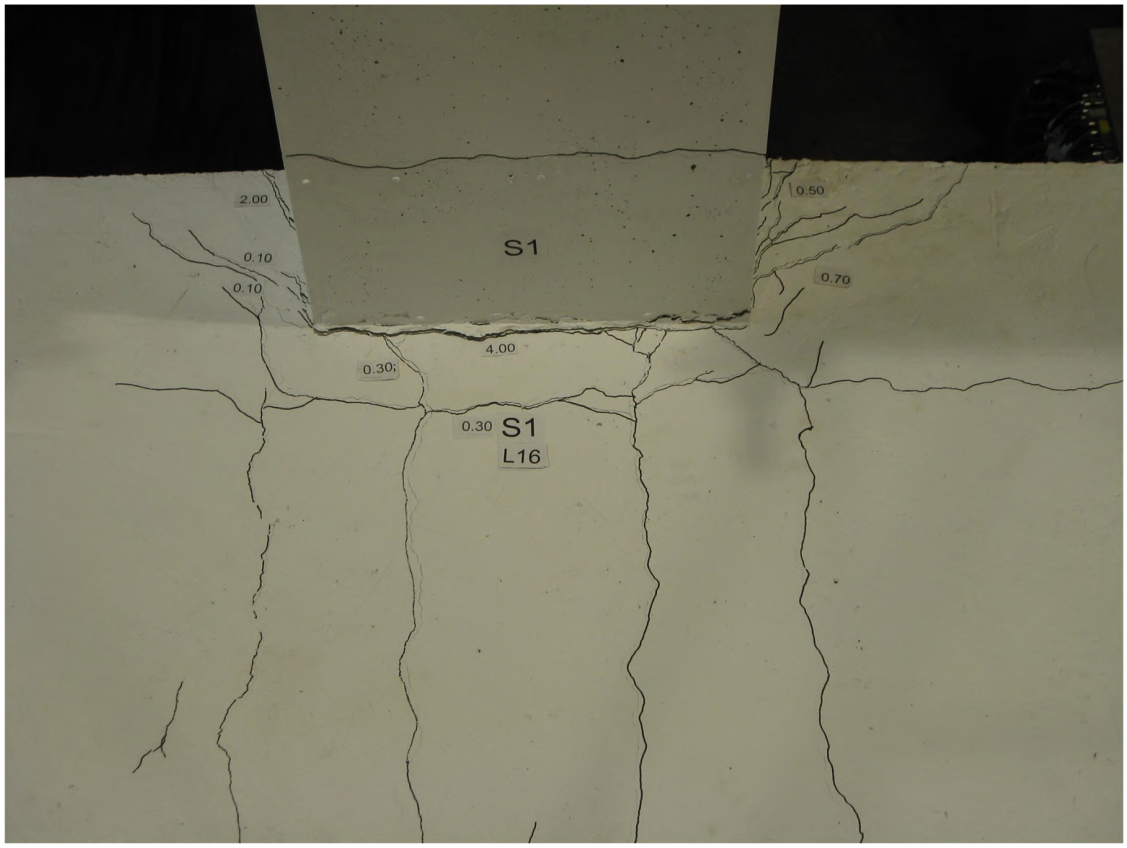

Figure 4.6: Specimen 1 slab cracks at failure

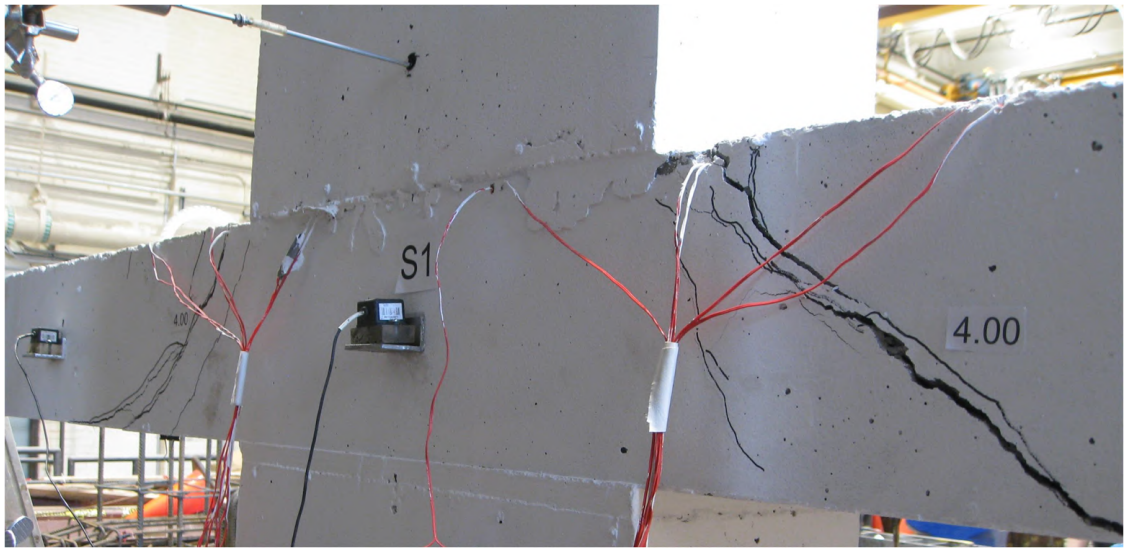

Figure 4.7: Specimen 1 free edge face cracks at failure

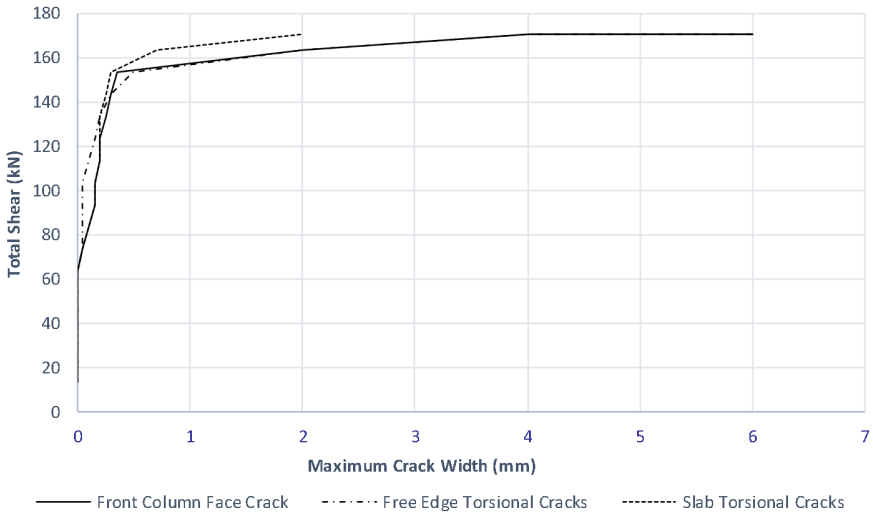

Figure 4.8: Load-maximum crack width response of Specimen 1

4.1.2 Reinforcement Strains

The reinforcement strains measured along a line parallel to and passing through the front column face are shown in Figure 4.9. The reinforcement strains measured along a line passing through the middle of the column are provided in Figure 4.10. The load stages represented in these figures correspond to the strains at the initial formation of cracks in the slab, at 63.6 kN; the first yielding of one of the bars in width b_b, F3, at 122.1 kN; the complete yielding of the bars inside the column, M2 and F4, at 141.6 kN; and the bar strains at failure at 171.4 kN.

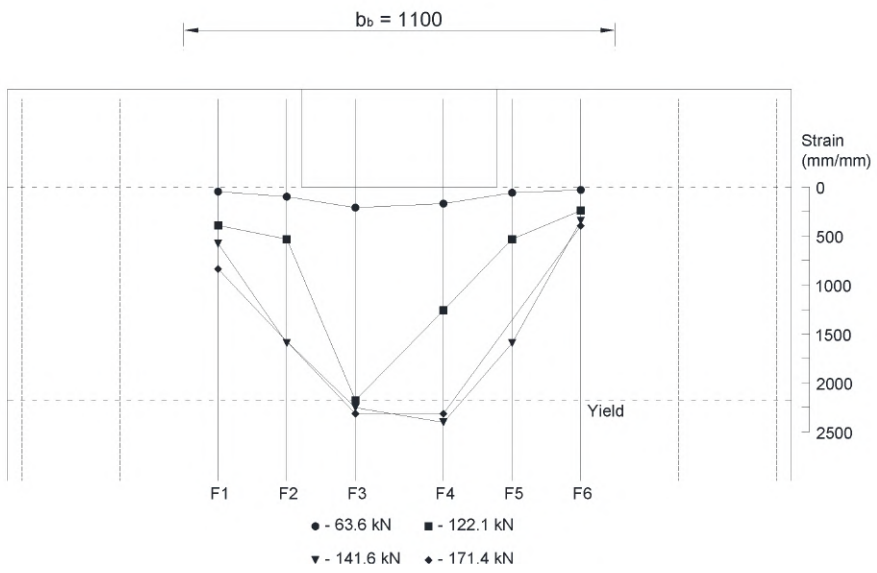

Figure 4.9: Reinforcement strains along the columne face for Specimen 1 (units in mm)

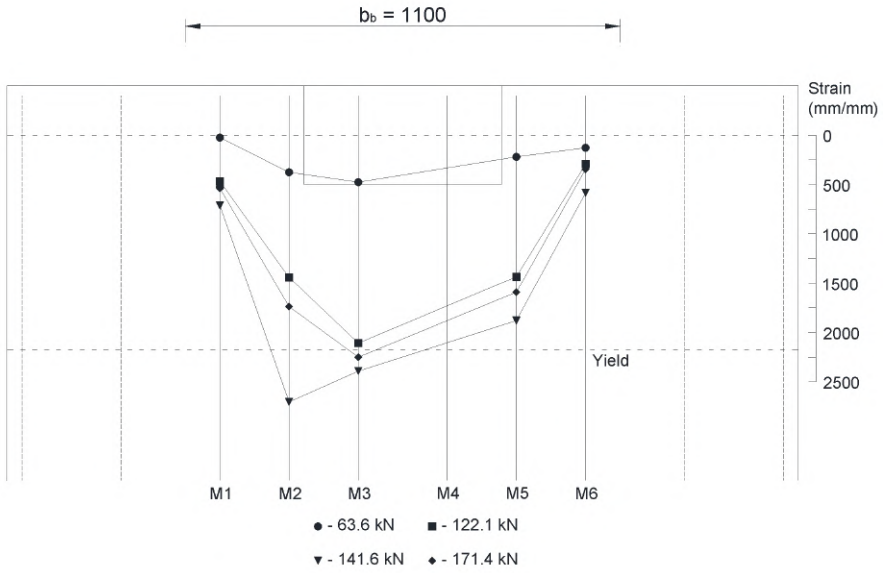

Figure 4.10: Reinforcement strains along the columne midline for Specimen 1 (units in mm)

4.1.3 Slab Deflections

Deflections along the centerline of the slab are given in Figure 4.11 and Table 4.1 for the load stages described in Section 4.3.2. The load-rotation responses of the column and the free edge of the slab are presented in Figure 4.12.

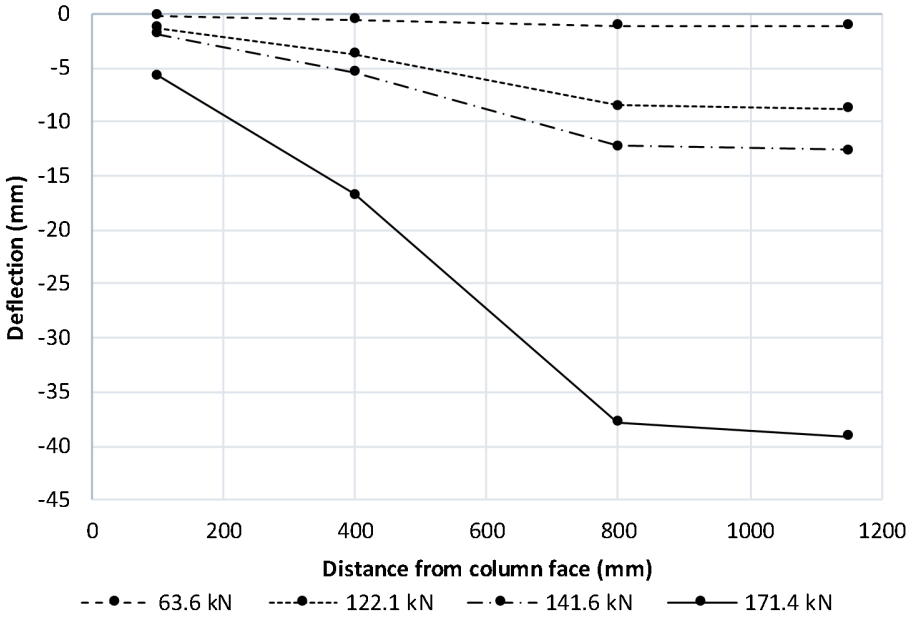

Figure 4.11: Slab deflections for Specimen 1

Table 4.1: Slab deflections for Specimen 1

	Deflection (mm)			
Distance from column face (mm)	V = 63.6 kN	V = 122.1 kN	V = 141.6 kN	V = 171.4 kN
100	0.2	1.3	1.8	5.7
400	0.5	3.7	5.4	16.7
800	1.1	8.5	12.3	37.7
1150	1.0	8.7	12.6	39.1

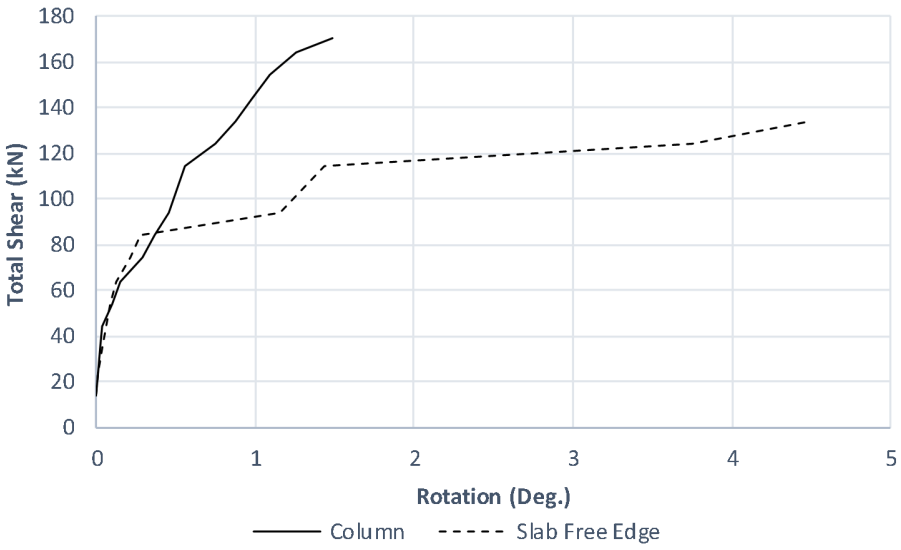

Figure 4.12: Column and slab free edge load-rotation responses for Specimen 1

4.2 Specimen 2 Results

The load-deflection response for Specimen 2 is shown in Figure 4.13. An elastic load-deflection relationship was observed until a total shear of 85.0 kN and a deflection of 0.43 mm at the POI. The first bar to yield was F4 at 165.0 kN and a POI deflection of 2.4 mm (see Figure 4.26 for bar numbers). By 235.0 kN and a POI deflection of 5.0 mm, bars F2, F5, and F7 had also yielded. The specimen failed in punching shear at 280.0 kN and a POI deflection of 10.8 mm.

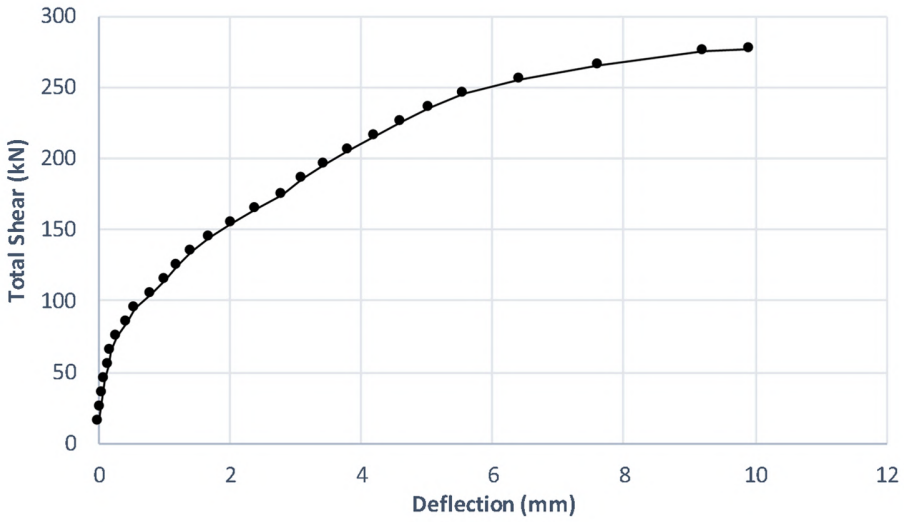

Figure 4.13: Load-deflection response of Specimen 2

4.2.1 Crack Progression

The first crack to form occurred along the front column face at 85.0 kN. Hairline slab torsional cracks then developed off the east and west faces of the column at 95.0 kN at 56 degree angles, see Figure 4.14. The first free edge torsional cracks were observed at 115.0 kN at a 52 degree angle from the soffit of the slab, as shown in Figure 4.15 and Figure 4.16. Cracks perpendicular to the free edge that originated at the front column face developed at 125.0 kN. Additionally, the front column face crack had widened to 0.10 mm, while the slab and free edge torsional cracks remained hairline at this load stage.

With yielding of bar F4 at 165.0 kN, the front column face crack had opened to 0.20 mm and the slab torsional cracks had opened to 0.15 and 0.10 mm on the west and east sides respectively, see Figure 4.17. A new hairline crack parallel to the front face crack was formed at a distance 100 mm from the column front face. No widening of the free edge torsional cracks was observed.

After bars F2, F5, and F7 had yielded, at 235.0 kN, the front column face crack had widened to 0.60 mm and the slab torsional cracks had opened to 0.35 mm, as shown in Figure 4.18. New free edge torsional cracks appeared with widths of 0.20 mm on the east side and 0.10 mm on the west side, see Figure 4.19 and Figure 4.20. The original free edge torsional cracks that had formed at 115.0 kN remained hairline.

Immediately before failure of the specimen in punching shear at 275.0 kN, the front column face crack had opened to 1.00 mm and the slab torsional cracks had opened to 0.80 and 0.60 mm, see Figure 4.21. An additional slab torsional crack on the west side had also formed and widened to 0.15 mm. New free

edge torsional cracks had developed, while earlier free edge torsional cracks became longer and wider, with a maximum crack width of 0.40 mm on both sides, as shown in Figure 4.22 and Figure 4.23. The failure of the connection in punching shear is shown in Figure 4.24. Finally, the load-maximum crack width response for Specimen 2 is shown in Figure 4.25.

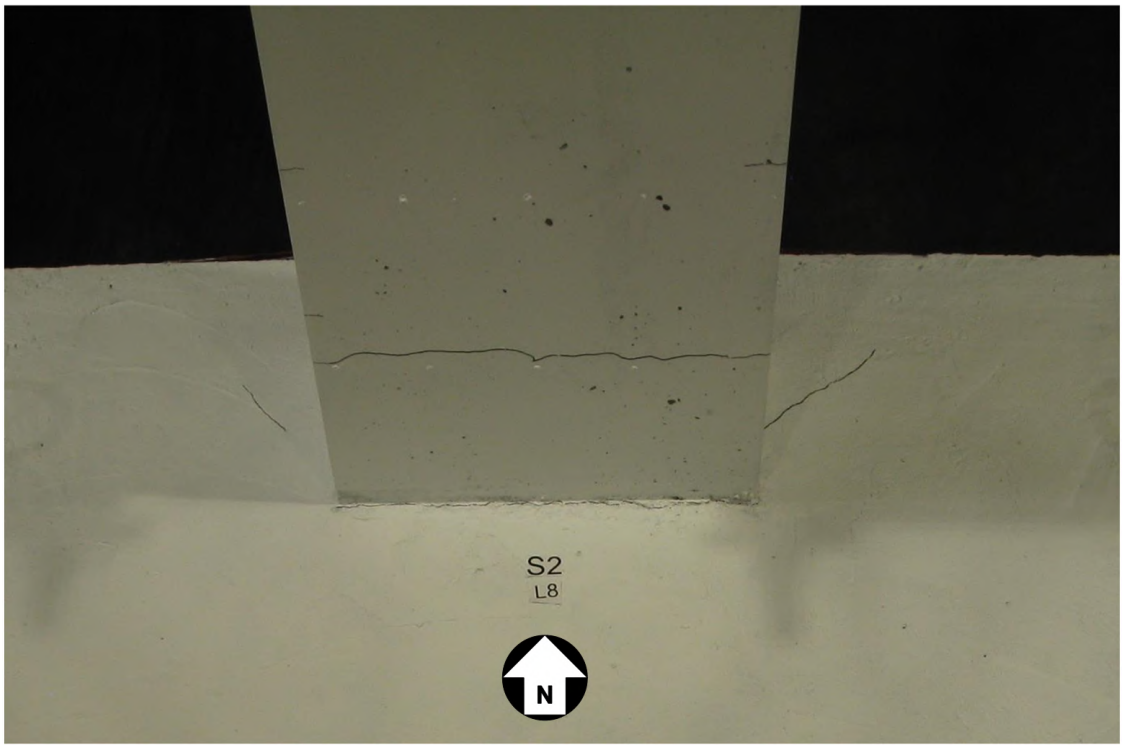

Figure 4.14: Specimen 2 slab cracks at V = 95.0 kN

Figure 4.15: Specimen 2 free edge face cracks at V = 115.0 kN (west side)

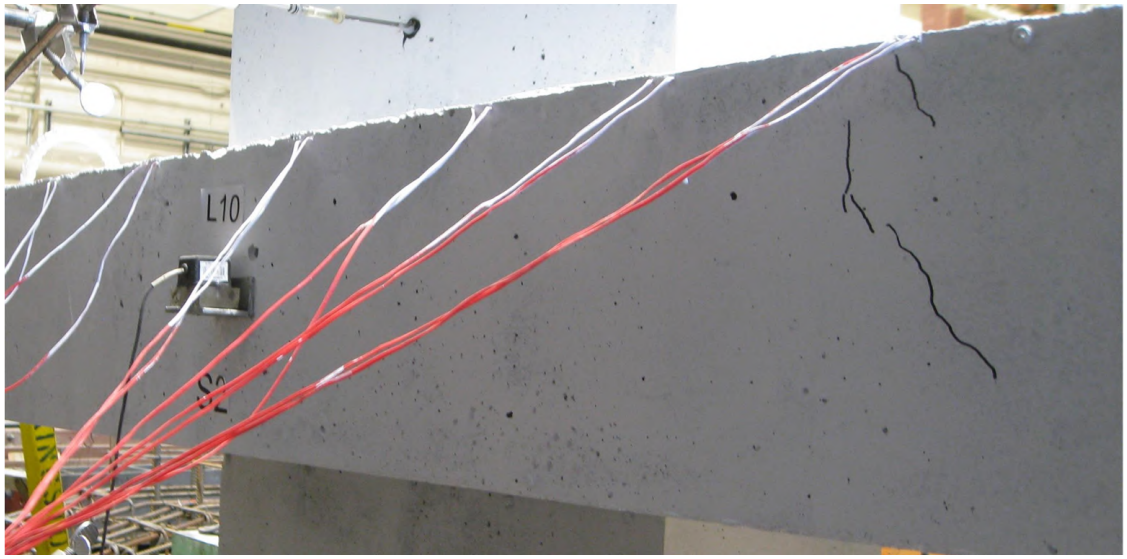

Figure 4.16: Specimen 2 free edge face cracks at V = 115.0 kN (east side)

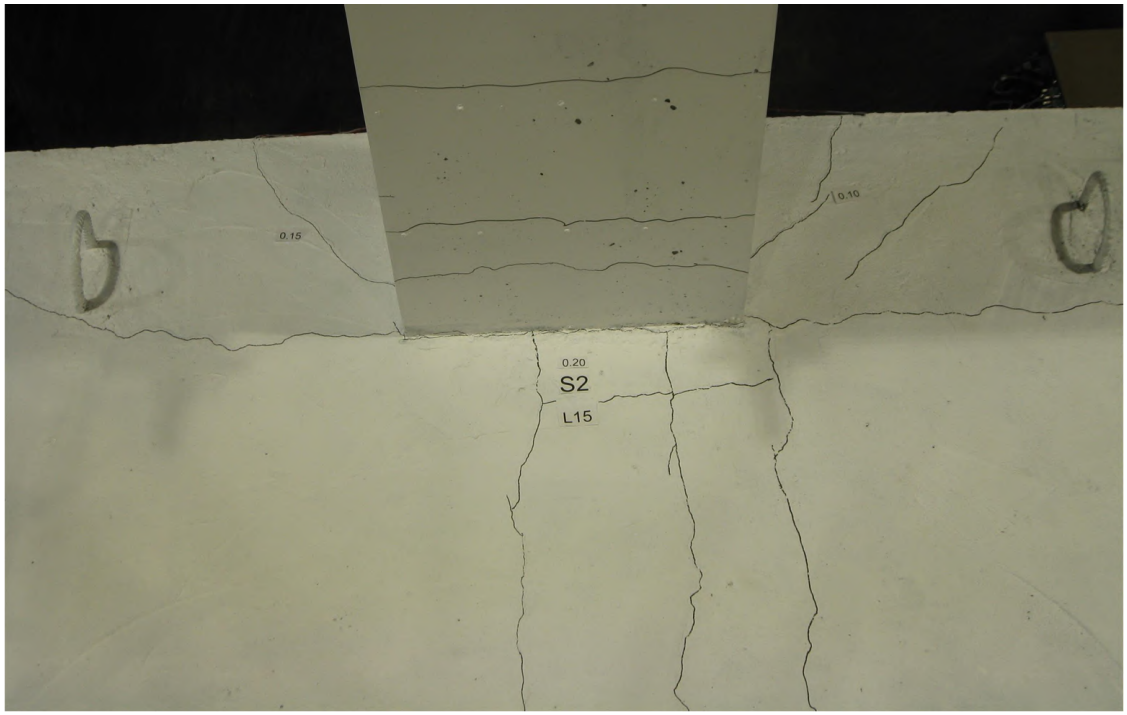

Figure 4.17: Specimen 2 slab cracks at V = 165.0 kN

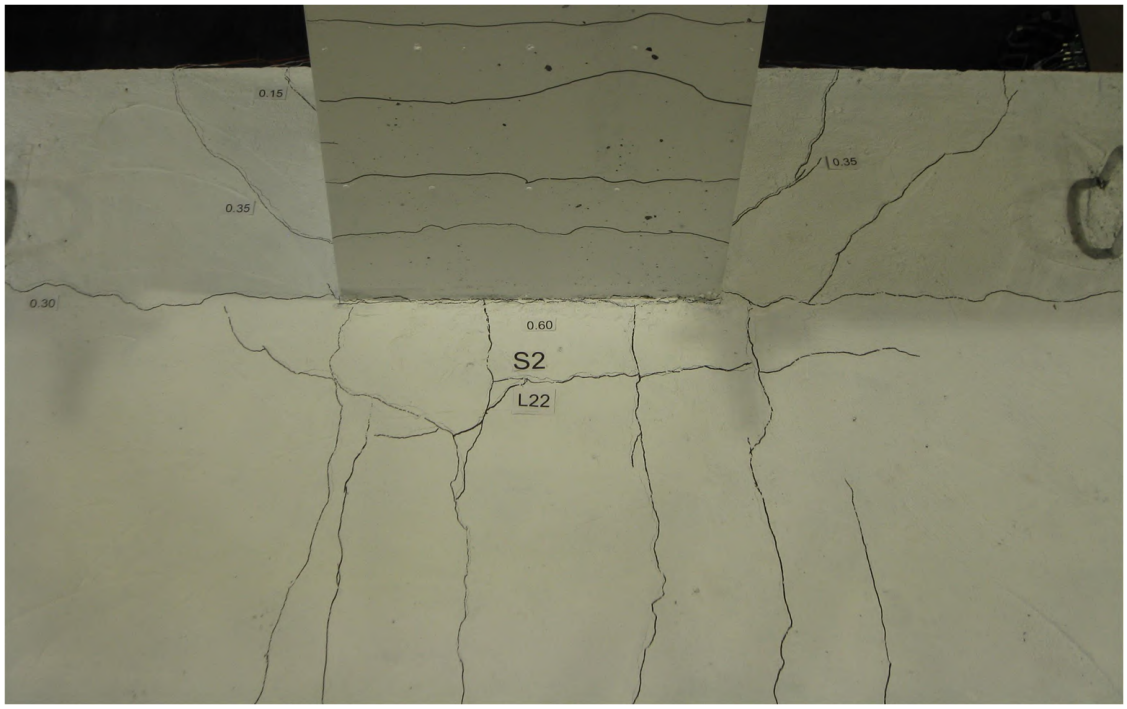

Figure 4.18: Specimen 2 slab cracks at V = 235.0 kN

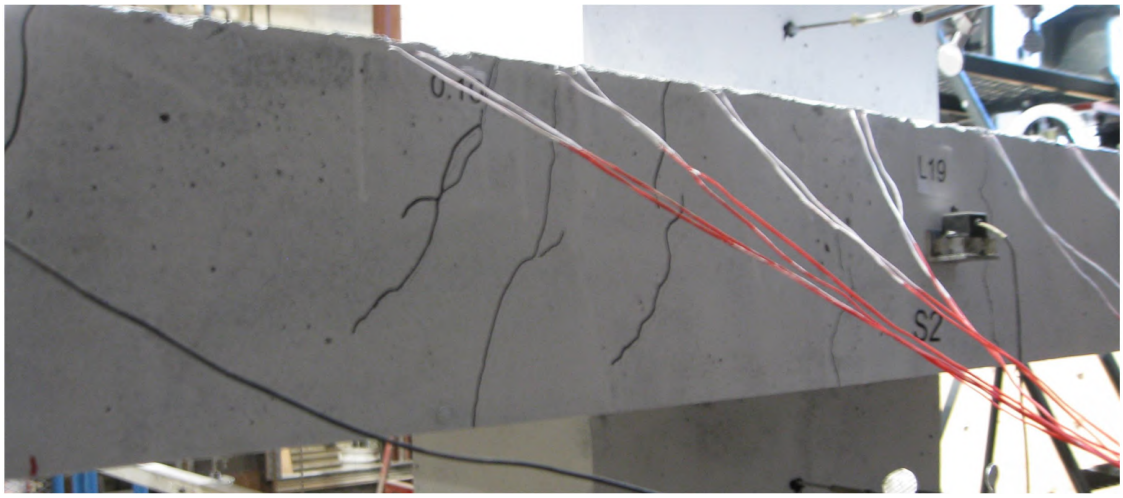

Figure 4.19: Specimen 2 free edge face cracks at V = 235.0 kN (west side)

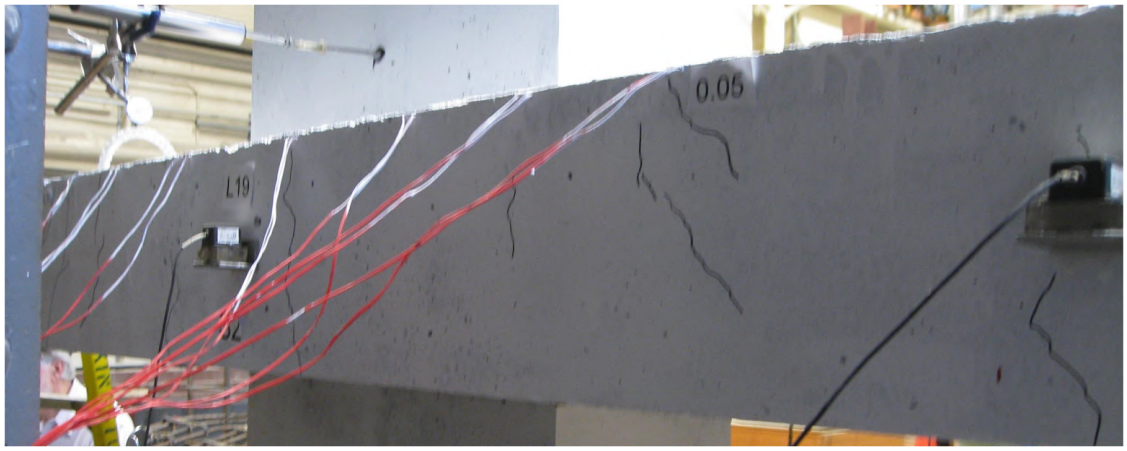

Figure 4.20: Specimen 2 free edge face cracks at V = 235.0 kN (east side)

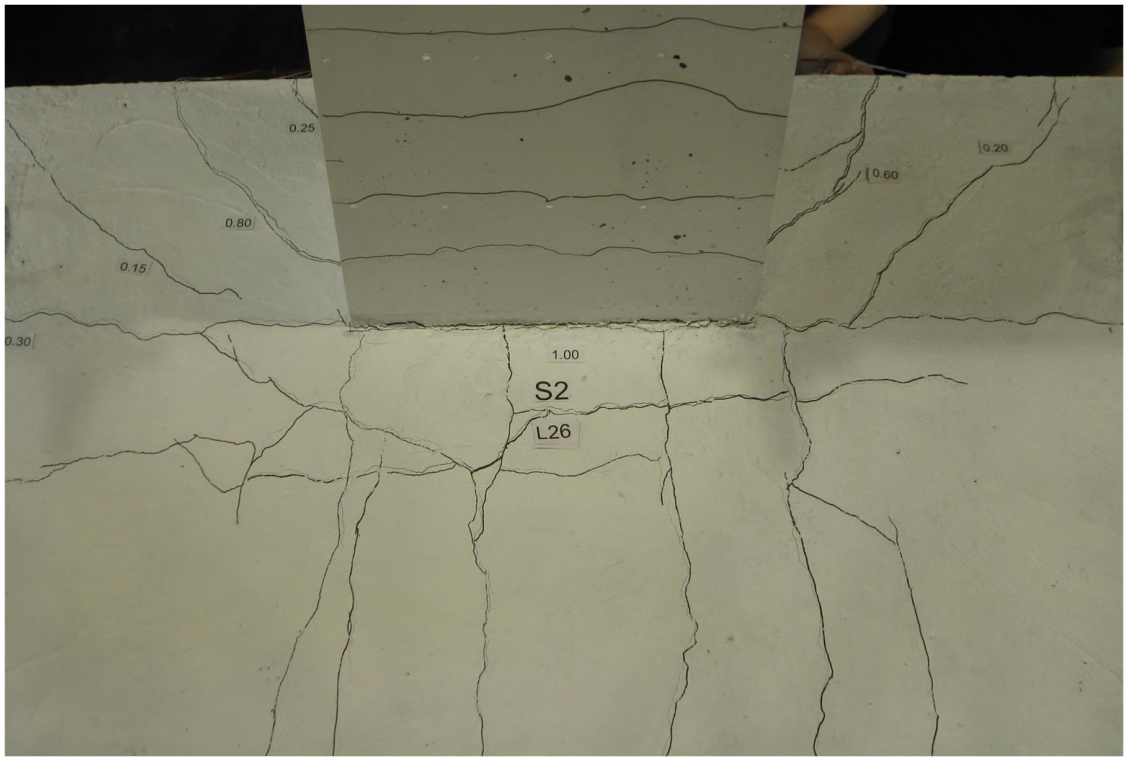

Figure 4.21: Specimen 2 slab cracks at V = 275.0 kN

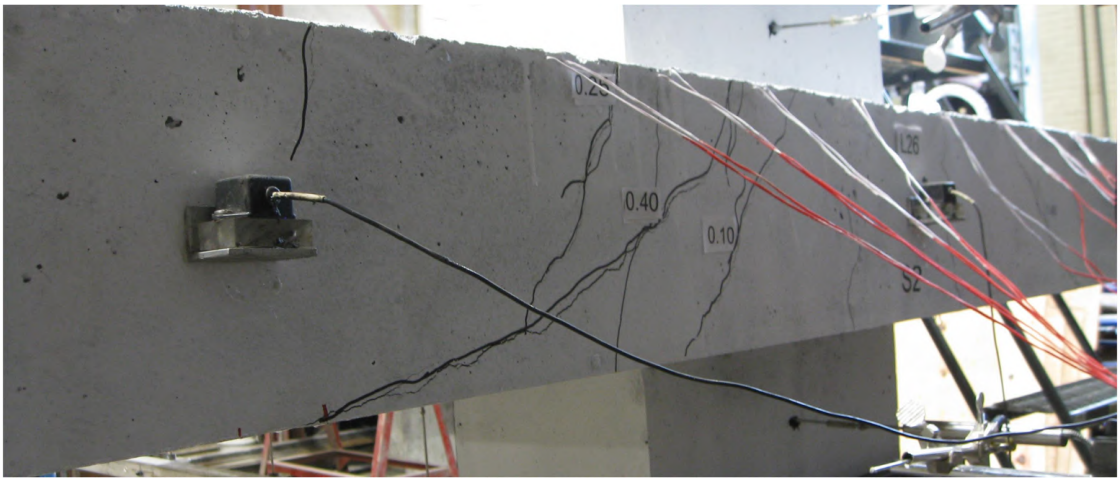

Figure 4.22: Specimen 2 free edge face cracks at V = 275.0 kN (west side)

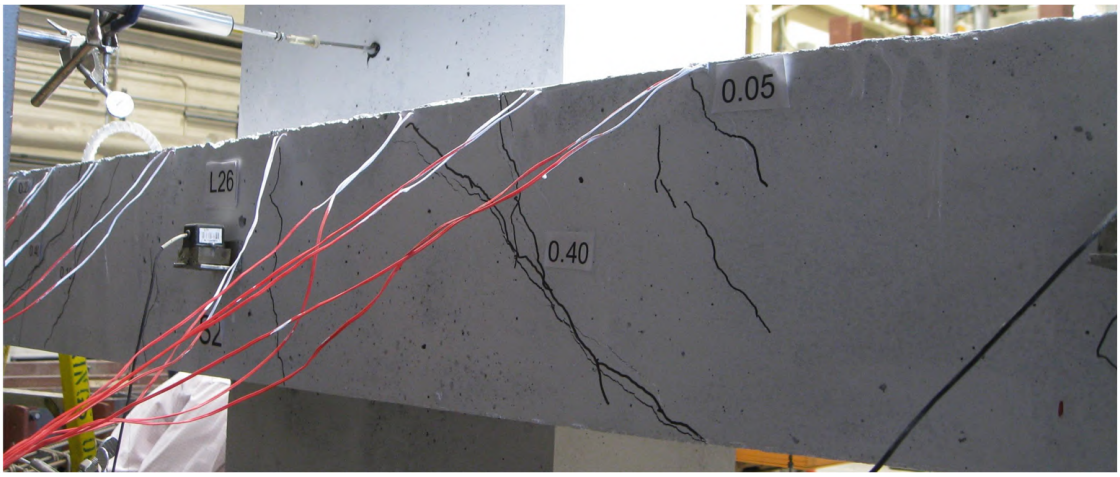

Figure 4.23: Specimen 2 free edge face cracks at V = 275.0 kN (east side)

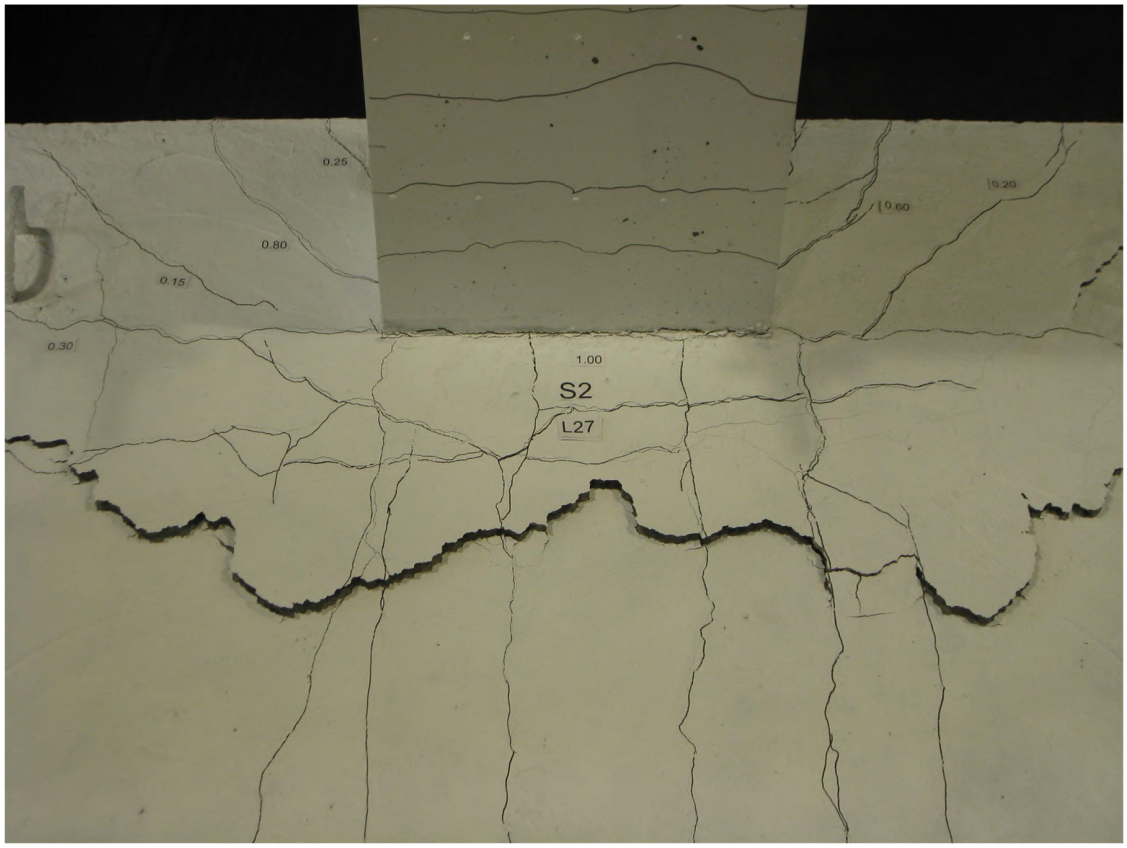

Figure 4.24: Specimen 2 at failure

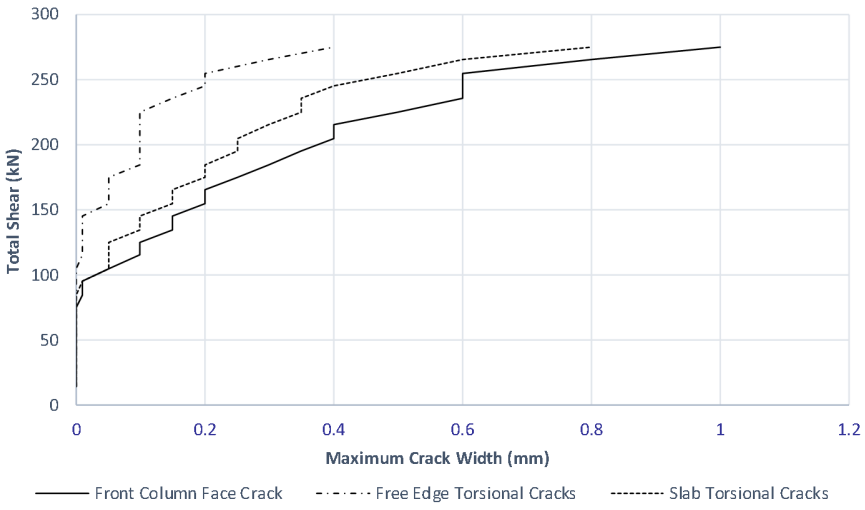

Figure 4.25: Load-maximum crack width response of Specimen 2

4.2.2 Reinforcement Strains

The reinforcement strains measured along a line parallel to and passing through the front column face are shown in Figure 4.26 for four load stages. The reinforcement strains measured along a line passing through the middle of the column are provided in Figure 4.27 for the same load stages. The first load stage corresponds to formation of the first crack along the front face of the column at a total shear of 85.0 kN. The second and third load stages, at 165.0 kN and 235.0 kN respectively, correspond to the first yielding of one of the reinforcing bars in width b_b and the second round of yielding of adjacent bars. Finally, the bar strains at failure are given. These load stages are also presented for the reinforcement strains measured at the midline of the column.

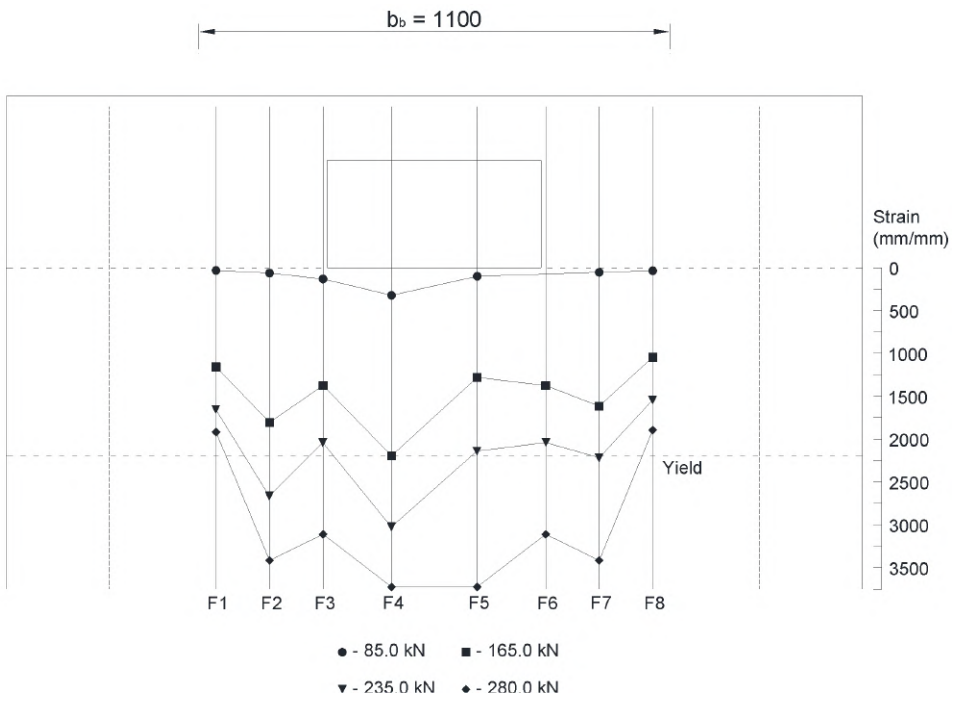

Figure 4.26: Reinforcement strains along the columne face for Specimen 2 (units in mm)

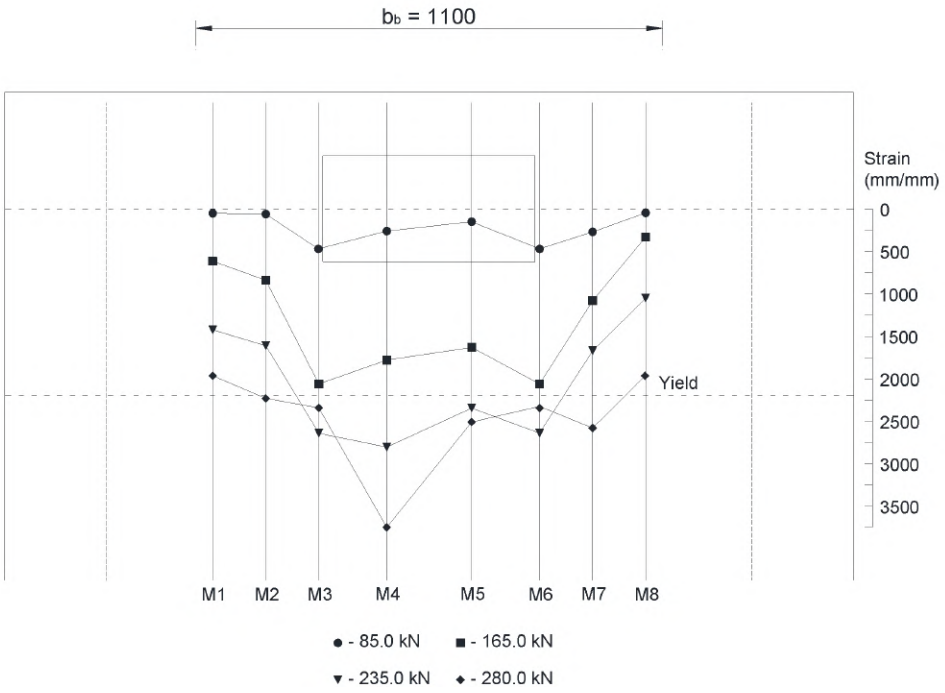

Figure 4.27: Reinforcement strains along the columne midline for Specimen 2 (units in mm)

4.2.3 Slab Deflections

The centerline deflections of the slab at load stages: 85.0 kN, 165.0 kN, 235.0 kN, and 280.0 kN, are shown in Figure 4.28 and Table 4.2. In addition, the load-rotation responses of the column and the free edge of the slab are provided in Figure 4.29.

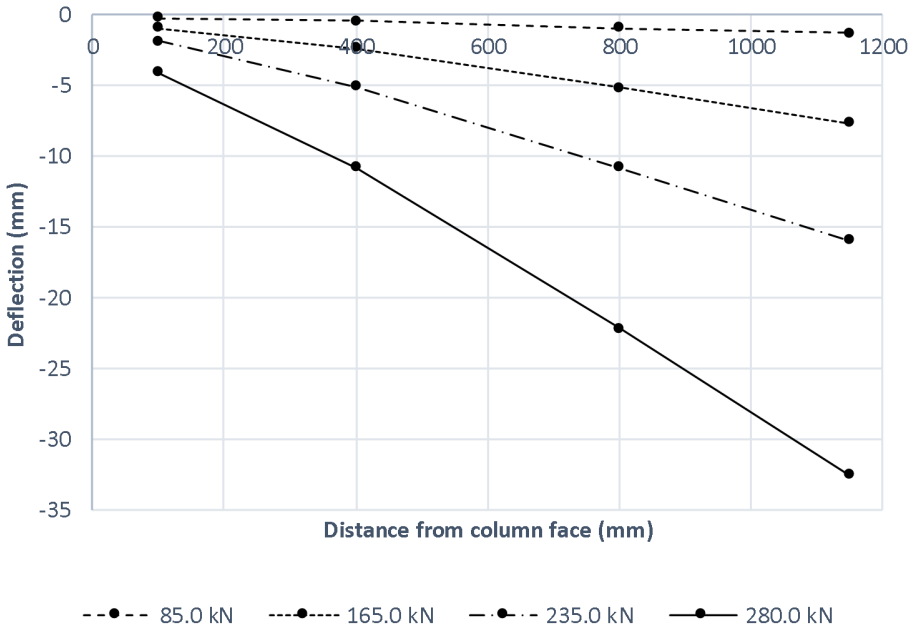

Figure 4.28: Slab deflections for Specimen 2

Table 4.2: Slab deflections for Specimen 2

	Deflection (mm)			
Distance from column face (mm)	V = 85.0 kN	V = 165.0 kN	V = 235.0 kN	V = 280.0 kN
100	0.2	0.9	1.9	4.1
400	0.4	2.3	5.0	10.8
800	0.9	5.1	10.8	22.1
1150	1.3	7.7	15.9	32.5

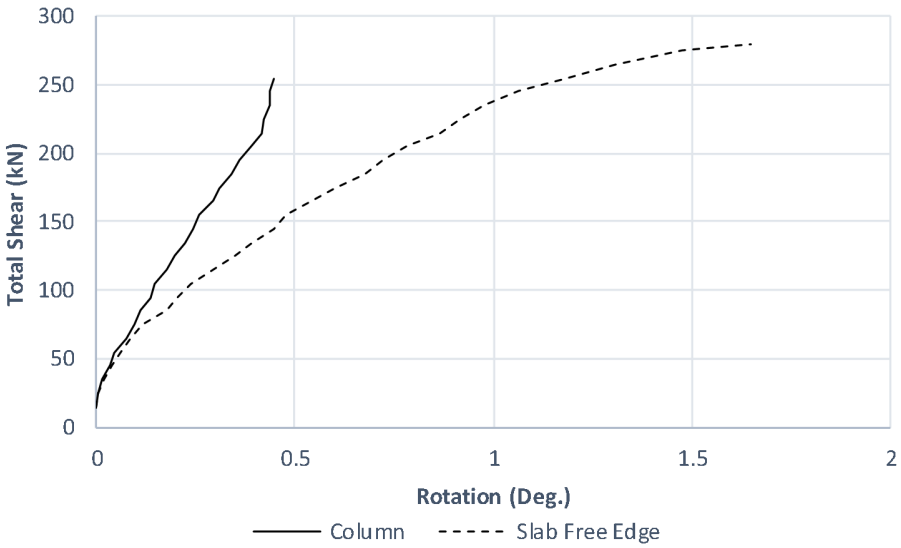

Figure 4.29: Column and slab free edge load-rotation responses for Specimen 2

4.3 Specimen 3 Results

The load-deflection response for Specimen 3 is given in Figure 4.30. The connection behaved elastically until the formation of the front column face crack at a total shear of 64.9 kN and a POI deflection of 0.24 mm. Initial yielding of the top slab reinforcement inside the column was observed at 154.9 kN and a POI deflection of 2.26 mm with bar F5 (see Figure 4.43 for bar labels). Additional yielding of bars F3 and F4 occurred at an approximate total shear of 184.9 kN and POI deflection of 3.24 mm. Subsequently, yielding of bar F7 was observed at 229.9 kN and a POI deflection of 5.08 mm. The last bar to yield before failure was bar F6 at 242.0 kN and a POI deflection of 5.71 mm. Failure occurred in punching shear at 240.8 kN and a POI deflection of 8.49 mm after a maximum recorded total shear of 252.0 kN and a POI deflection of 7.23 mm.

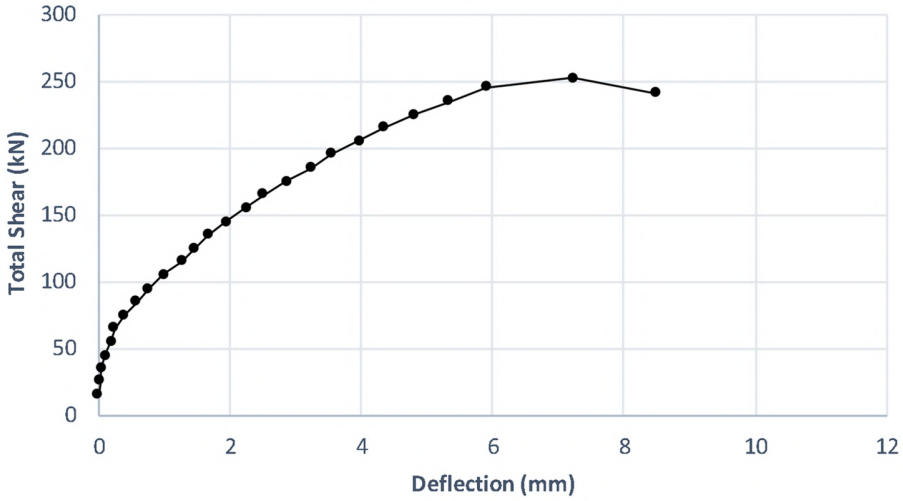

Figure 4.30: Load-deflection response of Specimen 3

4.3.1 Crack Progression

Initial cracking of the specimen was observed along the front face of the column at a total shear of 64.9 kN (Figure 4.31). At 74.9 kN, hairline slab torsional cracks formed originating at the side faces of the column that travelled towards the free edge of the slab at angles of 60 and 45 degrees for the west and east sides, respectively. In the next load stage, at 84.9 kN, hairline cracks perpendicular to the free edge originating from the front column face were observed, as shown in Figure 4.32. The first free edge torsional cracks occurred at this load stage, see Figures 4.33 and 4.34. At 94.9 kN, a hairline crack parallel to and offset from the column front face was formed.

With the yielding of bar F5 at a total shear of 154.9 kN, the front column face crack had opened to 0.20 mm, see Figure 4.35. Additional slab torsional cracks had formed by this load stage, with the original slab torsional cracks having widened to 0.15 mm and 0.20 mm for the west and east sides, respectively. As well, the crack parallel to and offset from the column front face had extended across the full width of column, turning towards the free edge of the slab. Finally, the free edge torsional cracks had widened to 0.15 mm for the west side and 0.10 mm for the east side (Figures 4.36 and 4.37).

With yielding of bars F3 and F4 at 229.9 kN, the front column face crack had widened to 0.35 mm and the maximum slab torsional crack widths for the west and east sides were 0.30 mm and 0.25 mm, respectively. The free edge torsional cracks had also opened to 0.30 mm for the east side and 0.25 mm for the west side. By this load stage, a second crack parallel to and offset from the column front face had formed.

In the load stage prior to failure, at 245.9 kN, no significant crack development had occurred. The crack

patterns after punching shear failure are shown in Figure 4.41. Finally, the load-maximum crack width response is given in Figure 4.42.

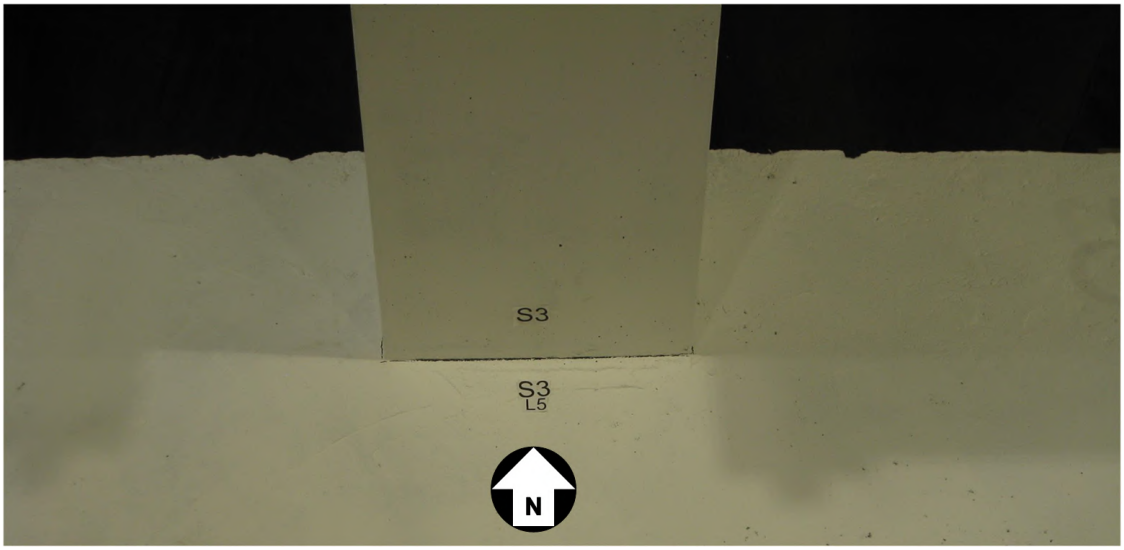

Figure 4.31: Specimen 3 slab cracks at V = 64.9 kN

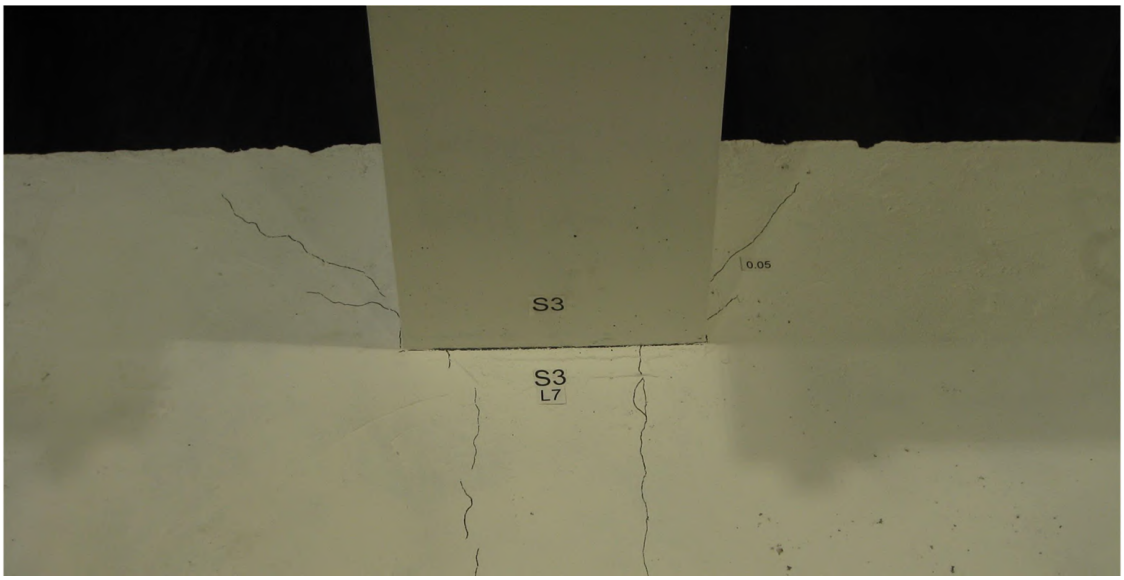

Figure 4.32: Specimen 3 slab cracks at V = 84.9 kN

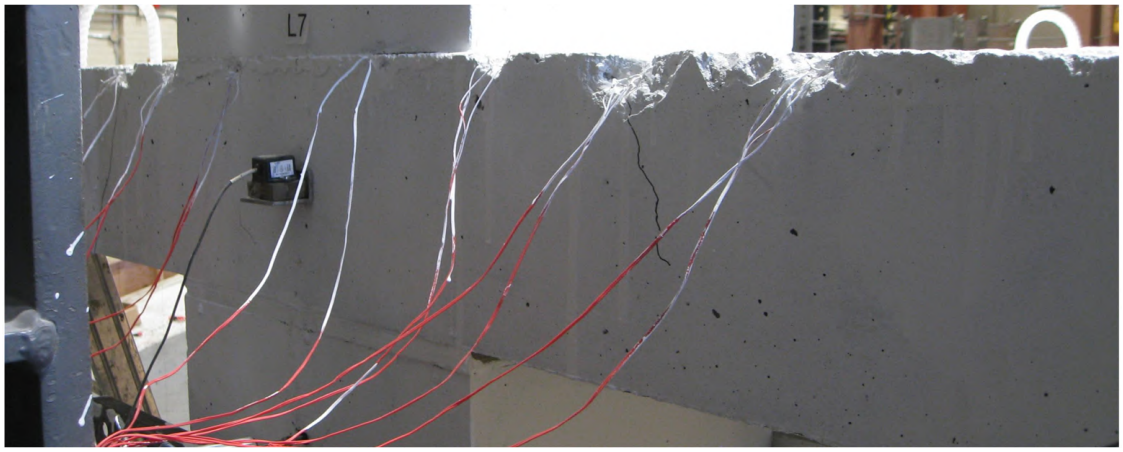

Figure 4.33: Specimen 3 free edge face cracks at V = 84.9 kN (west side)

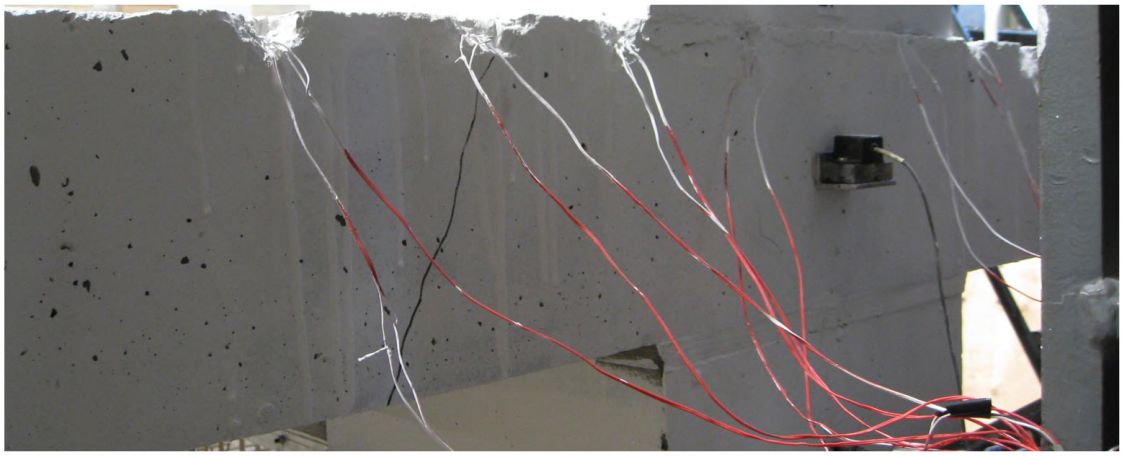

Figure 4.34: Specimen 3 free edge face cracks at V = 84.9 kN (east side)

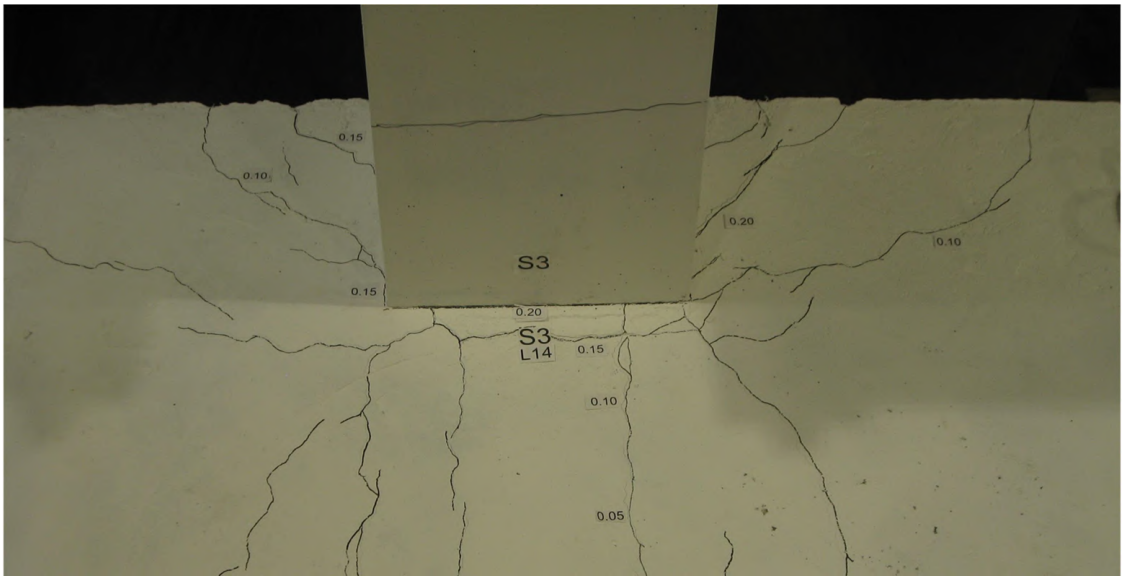

Figure 4.35: Specimen 3 slab cracks at V = 154.9 kN

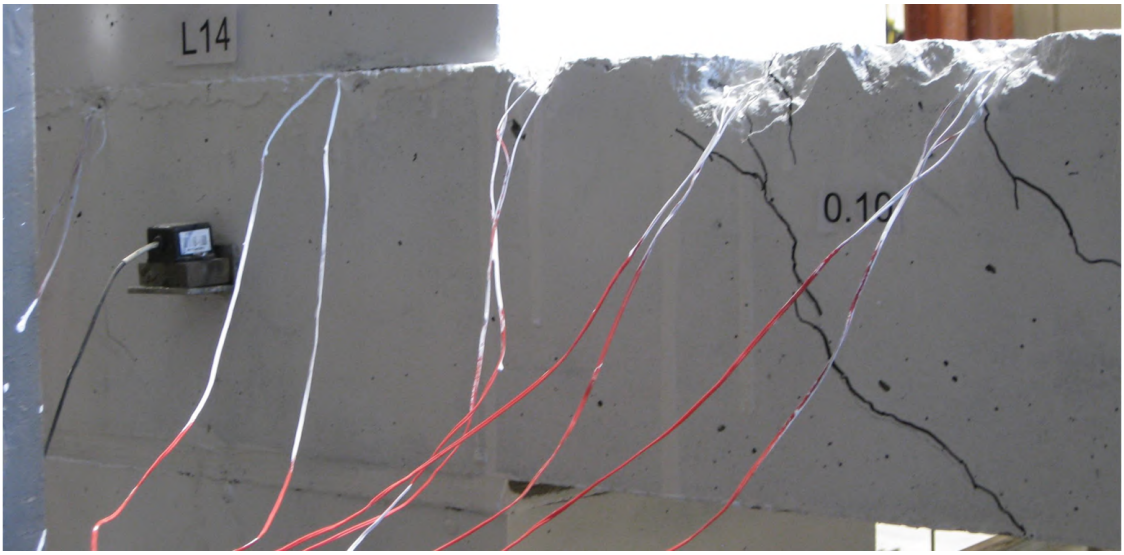

Figure 4.36: Specimen 3 free edge face cracks at V = 154.9 kN (west side)

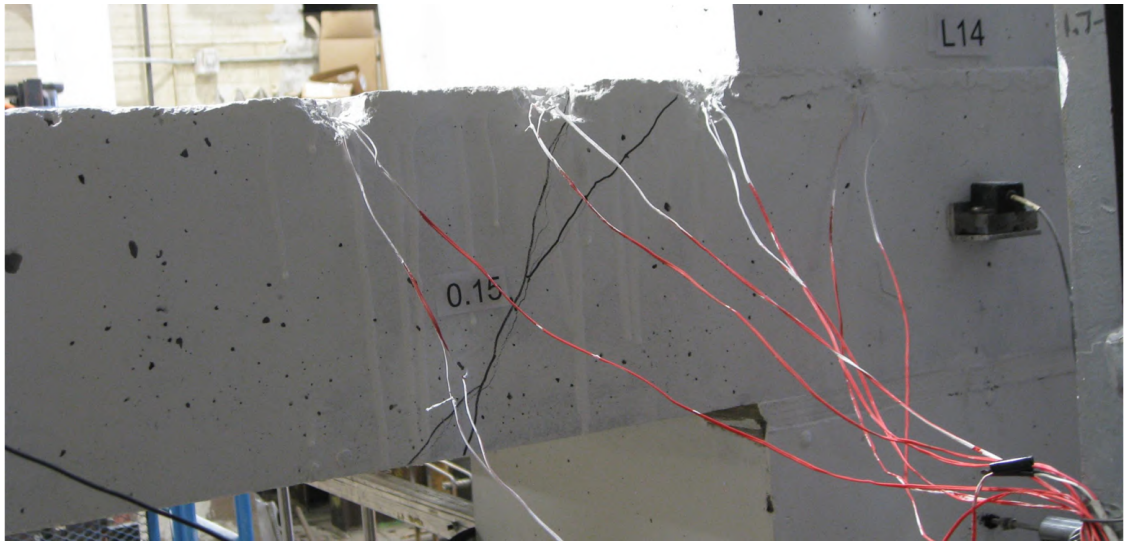

Figure 4.37: Specimen 3 free edge face cracks at V = 154.9 kN (east side)

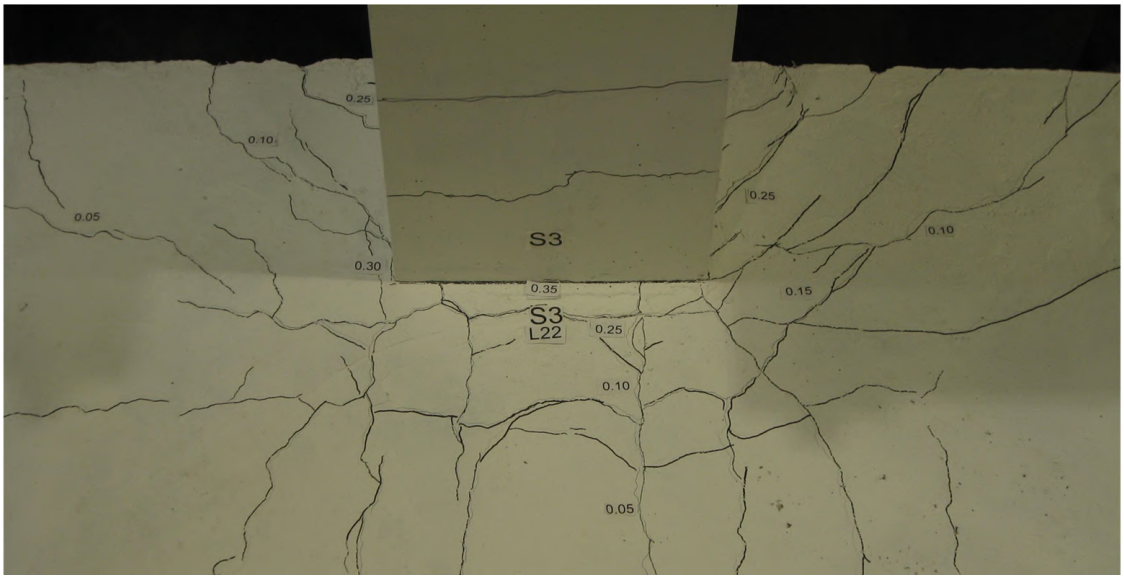

Figure 4.38: Specimen 3 slab cracks at V = 234.9 kN

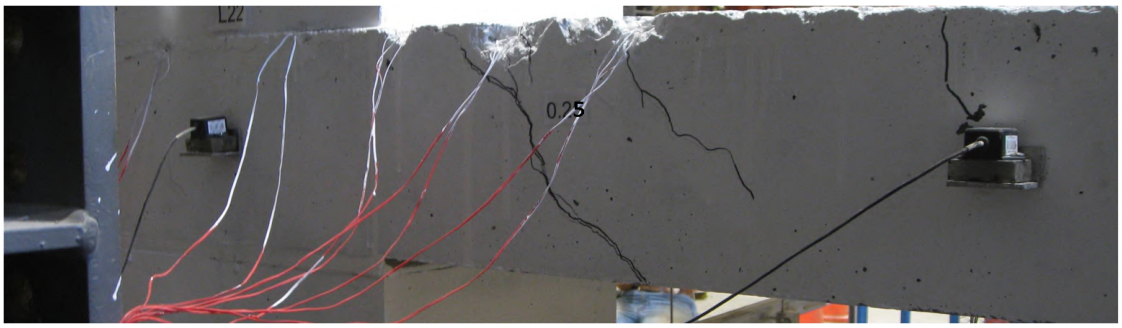

Figure 4.39: Specimen 3 free edge face cracks at V = 234.9 kN (west side)

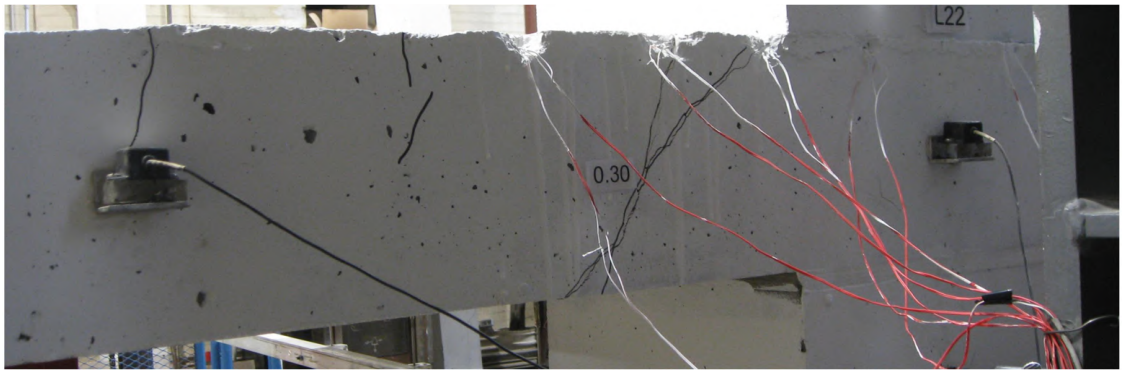

Figure 4.40: Specimen 3 free edge face cracks at V = 234.9 kN (east side)

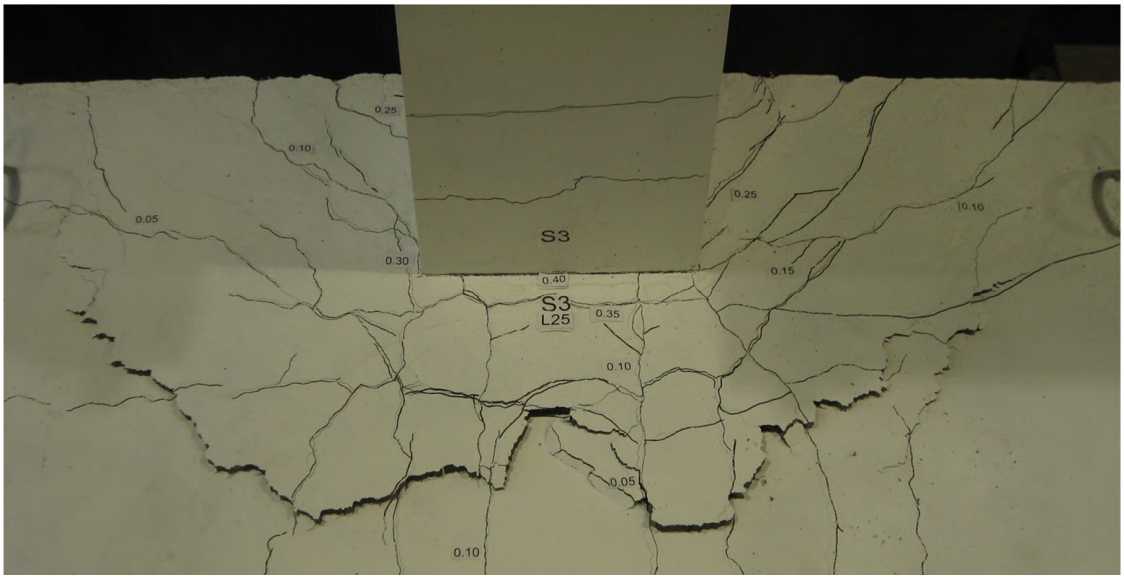

Figure 4.41: Specimen 3 at failure

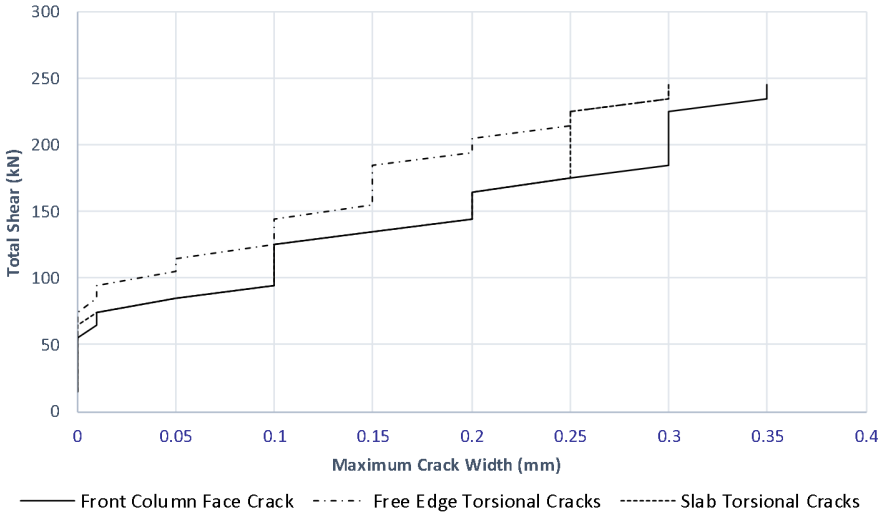

Figure 4.42: Load-maximum crack width response of Specimen 3

4.3.2 Reinforcement Strains

The strain data for the reinforcing bars in the band width b_b are presented at four critical stages: the formation of the first crack, 64.9 kN; the initial yielding of the bars at the face of the column, 154.9 kN; the yielding of bars F3 and F4, 229.9 kN; and at the maximum shear, 252.0 kN. The reinforcement strains measured along a line parallel to and passing through the column front face are shown in Figure 4.43 and those measured along the midline of the column are given in Figure 4.44.

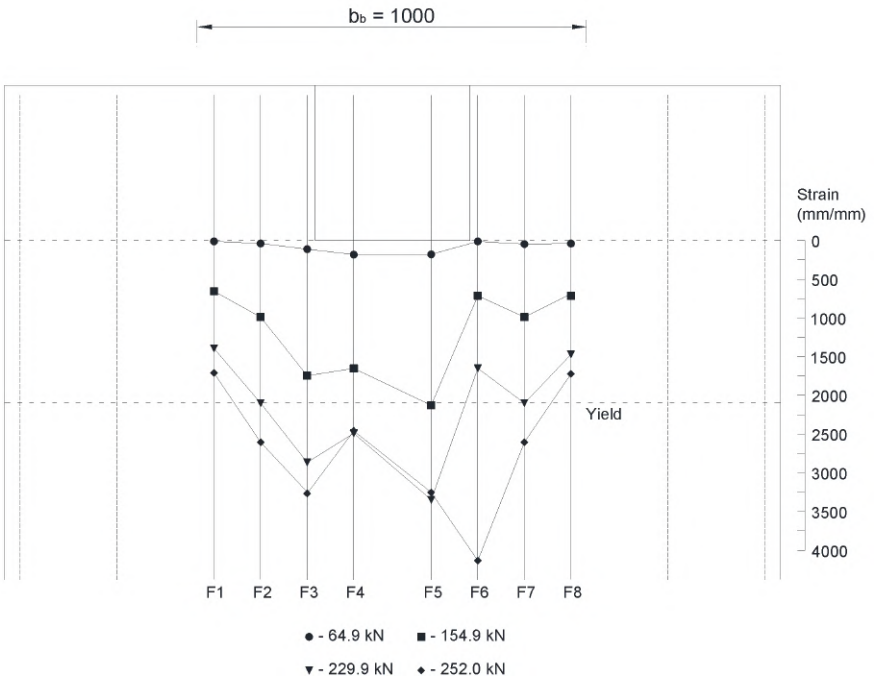

Figure 4.43: Reinforcement strains along the column face for Specimen 3 (units in mm)

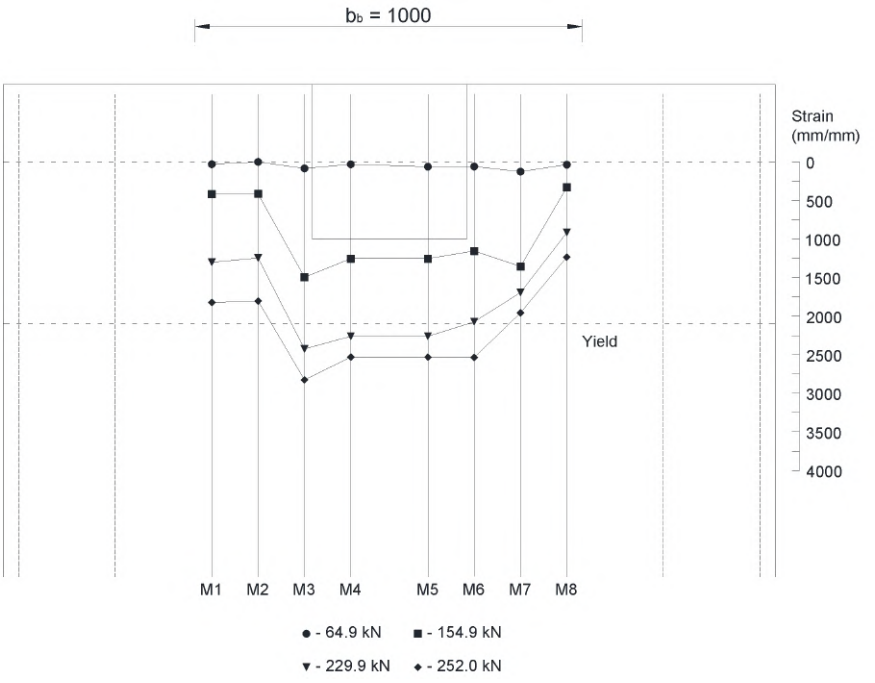

Figure 4.44: Reinforcement strains along the column midline for Specimen 3 (units in mm)

4.3.3 Slab Deflections and Rotations

The centerline deflections of the slab corresponding to the load stages discussed in Section 4.3.2 are provided in Figure 4.45 and Table 4.3. Additionally, the load-rotation responses of the column and the free edge of the slab are shown in Figure 4.45.

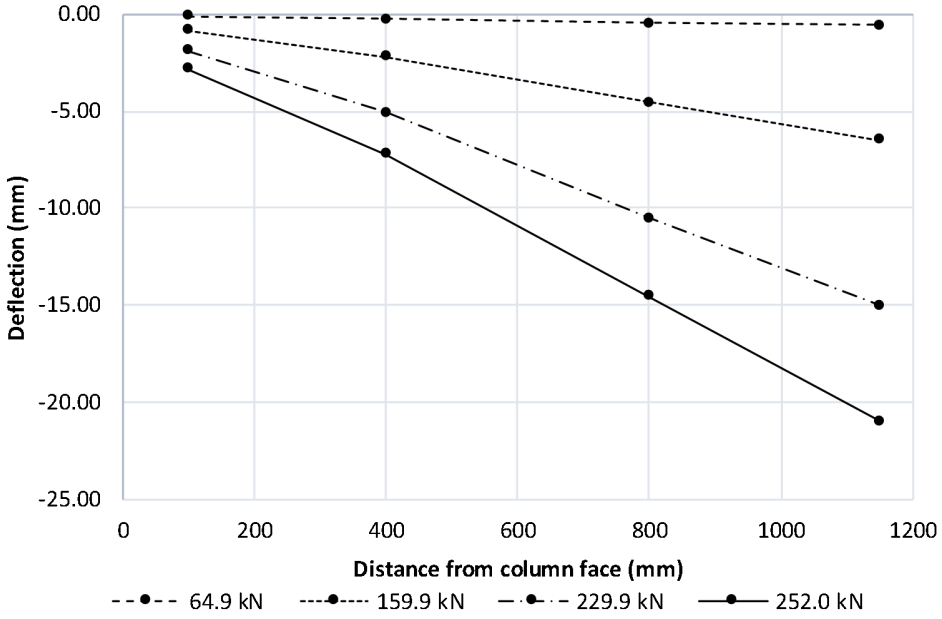

Figure 4.45: Slab deflections for Specimen 3

Table 4.3: Slab deflections for Specimen 3

	Deflection (mm)			
Distance from column face (mm)	V = 64.9 kN	V = 159.9 kN	V = 229.9 kN	V = 252.0 kN
100	0.1	0.8	1.9	2.8
400	0.3	2.2	5.1	7.2
800	0.5	4.5	10.5	14.5
1150	0.6	6.5	15.0	21.0

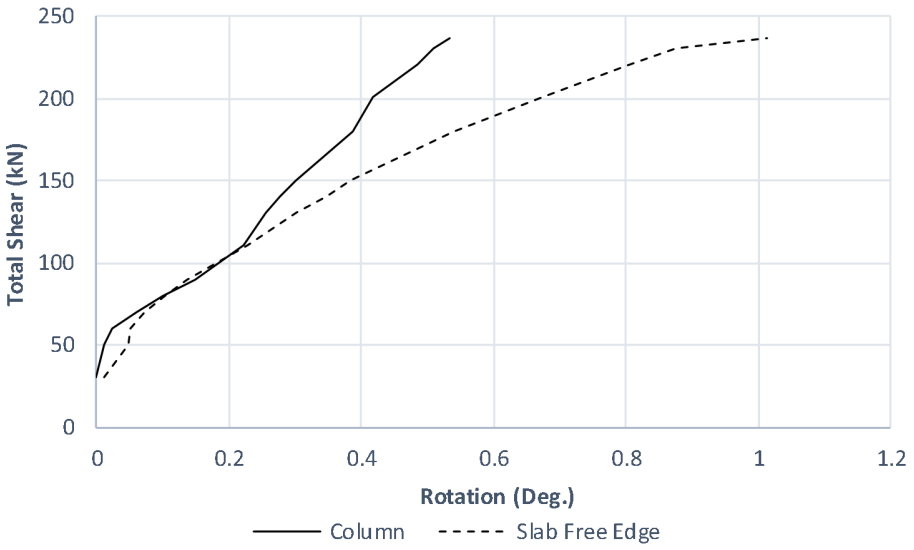

Figure 4.46: Column and slab free edge load-rotation responses for Specimen 3

4.4 Specimen 4 Results

The load-deflection response for Specimen 4 is presented in Figure 4.47. The connection behaved elastically until the formation of a crack along the front face of the column at 76.0 kN and a POI deflection of 0.23 mm. Initial yielding of the top tension reinforcement inside b_b occurred with bar F4 (see Figure 4.64 for bar labels) at 186.0 kN and a POI deflection of 3.28 mm. Yielding of reinforcement outside of the column was observed with bar F3 at 234.4 kN and a POI deflection of 5.6 mm. The connection failed in punching shear at 246.0 kN and a POI deflection of 6.55 mm.

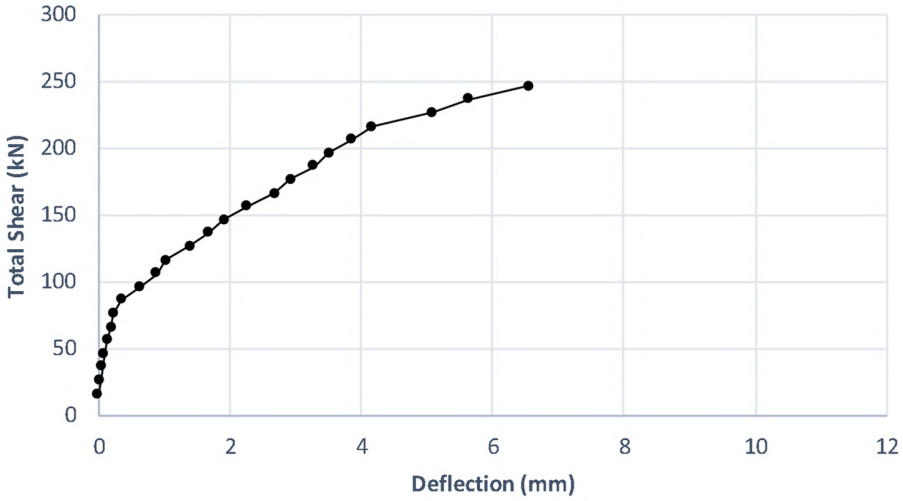

Figure 4.47: Load-deflection response of Specimen 4

4.4.1 Crack Progression

The first crack occurred across the front face of the column at a shear of 76.0 kN, see Figure 4.48. In the next load stage, at 86.0 kN, two slab torsional cracks initiated off the side faces of the column at 42 degree and 60 degree angles for the east and west sides, respectively, as shown in Figure 4.49. At 96.0 kN, two hairline cracks originating at the front face of the column and perpendicular to the free edge formed. As well, a hairline slab torsional crack off the west side formed, joining the middle of the side face of the column with the free edge (Figure 4.50). This load stage also produced the first free edge torsional cracks. These cracks originated at the top of the slab and descended towards the soffit at 78 degrees for the east side and 81 degrees for west side, see Figures 4.51 and 4.52.

At 126.0 kN, the front column face crack had opened to 0.15 mm and the slab torsional cracks had widened to 0.15 mm for the east side and 0.10 mm for the west side. Two additional hairline cracks perpendicular to the free edge had formed at the corners of the column. Furthermore, a new crack parallel to the free edge in front of the column developed bridging the perpendicular cracks formed at 96.0 kN. The free edge torsional cracks were unchanged relative to the load stage at 96.0 kN.

At 136.0 kN, two hairline slab torsional cracks formed on the east side parallel to the first slab torsional crack. As well, a second hairline crack parallel to the free edge in front of the column appeared, intersecting all four of the perpendicular cracks originating at the front column face, see Figure 4.53. Finally, one new free edge torsional crack on each side was observed as shown in Figures 4.54 and 4.55. Relative to 126.0 kN, no changes in the widths of the front column face, slab torsional, and free edge torsional cracks were

recorded.

At initial yielding of the top slab reinforcement in b_b with bar F4 at 186.0 kN, the front column face crack had opened to 0.20 mm and the slab torsional cracks had widened to 0.20 mm on both sides (Figure 4.56). The free edge torsional cracks had opened to 0.10 mm on the west side and were still hairline on the east, see Figures 4.57 and 4.58. At 196.0 kN, a new slab torsional crack formed on the west side close to the free edge and a new free edge torsional crack was observed on the east side. In the next load stage, at 206.0 kN, a third free edge torsional crack iniated on the west side. At 216.0 kN, a third crack parallel to and in front of the column was observed.

In the stage before punching shear failure at 245.0 kN, after the yielding of bar F8 at 227.0 kN, the front column face crack had opened to 0.30 mm and the slab torsional cracks had widened to maximum of 0.30 mm on both sides, presented in 4.59. The free edge torsional cracks on the free edge face had also opened to a maximum of 0.25 mm on both sides as shown in Figures 4.60 and 4.61.

In the final load stage, the specimen failed in punching shear. The post-punching crack pattern is given in Figure 4.62 and the load-maximum crack width response provided in Figure 4.63.

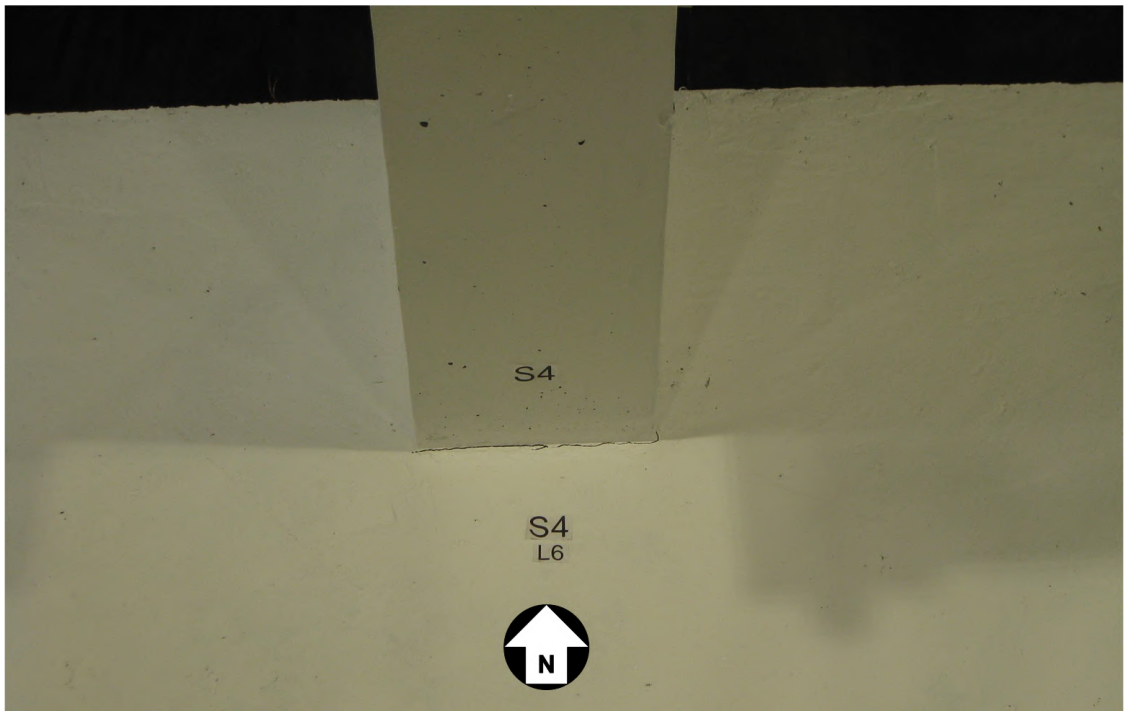

Figure 4.48: Specimen 4 slab cracks at V = 76.0 kN

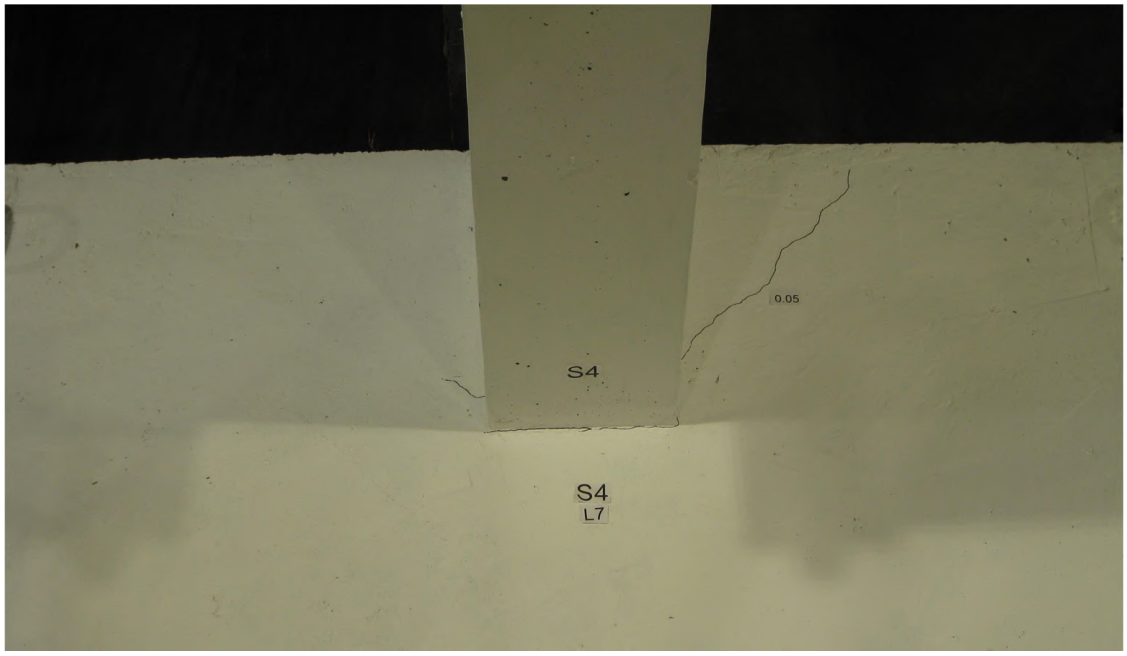

Figure 4.49: Specimen 4 slab cracks at V = 86.0 kN

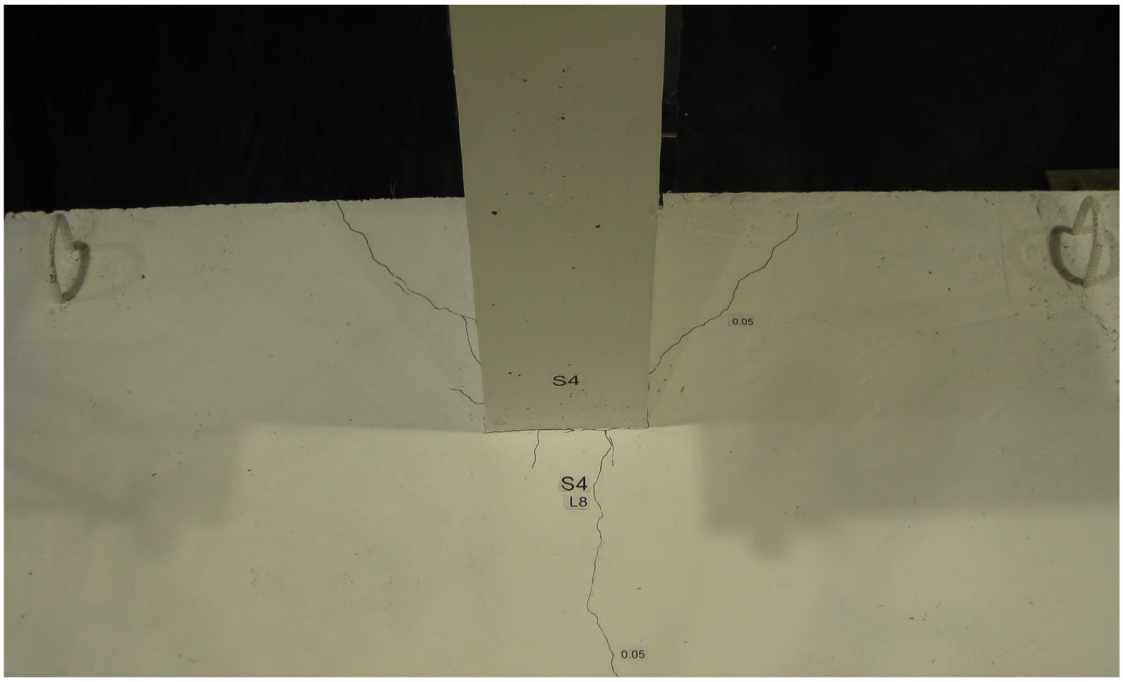

Figure 4.50: Specimen 4 slab cracks at V = 96.0 kN

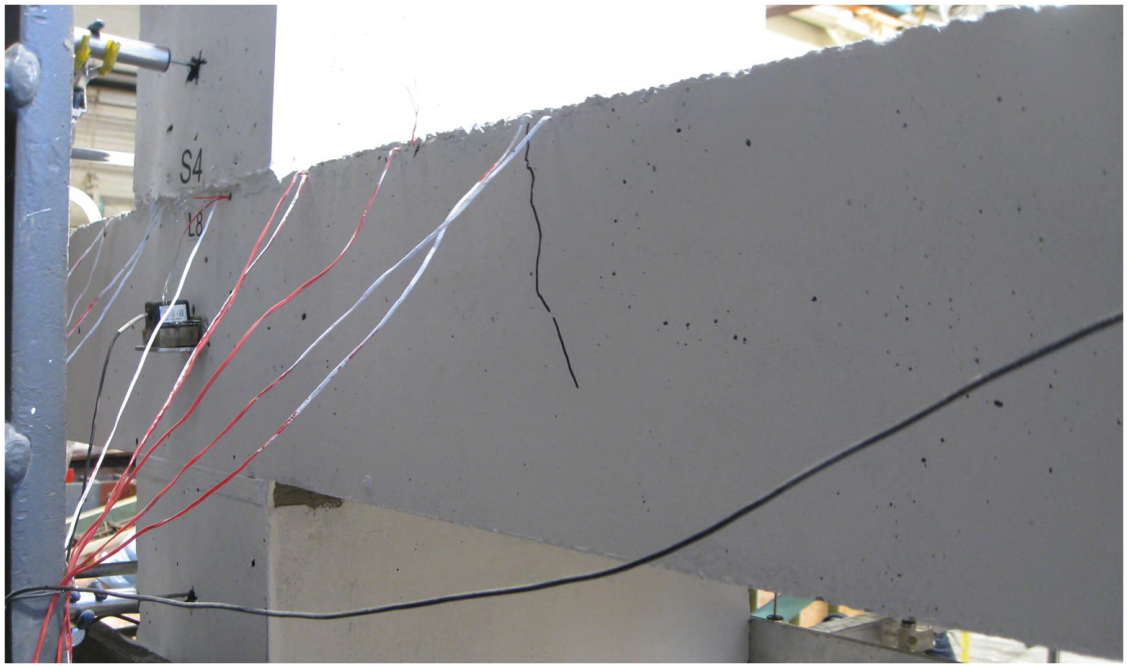

Figure 4.51: Specimen 4 free edge face cracks at V = 96.0 kN (west side)

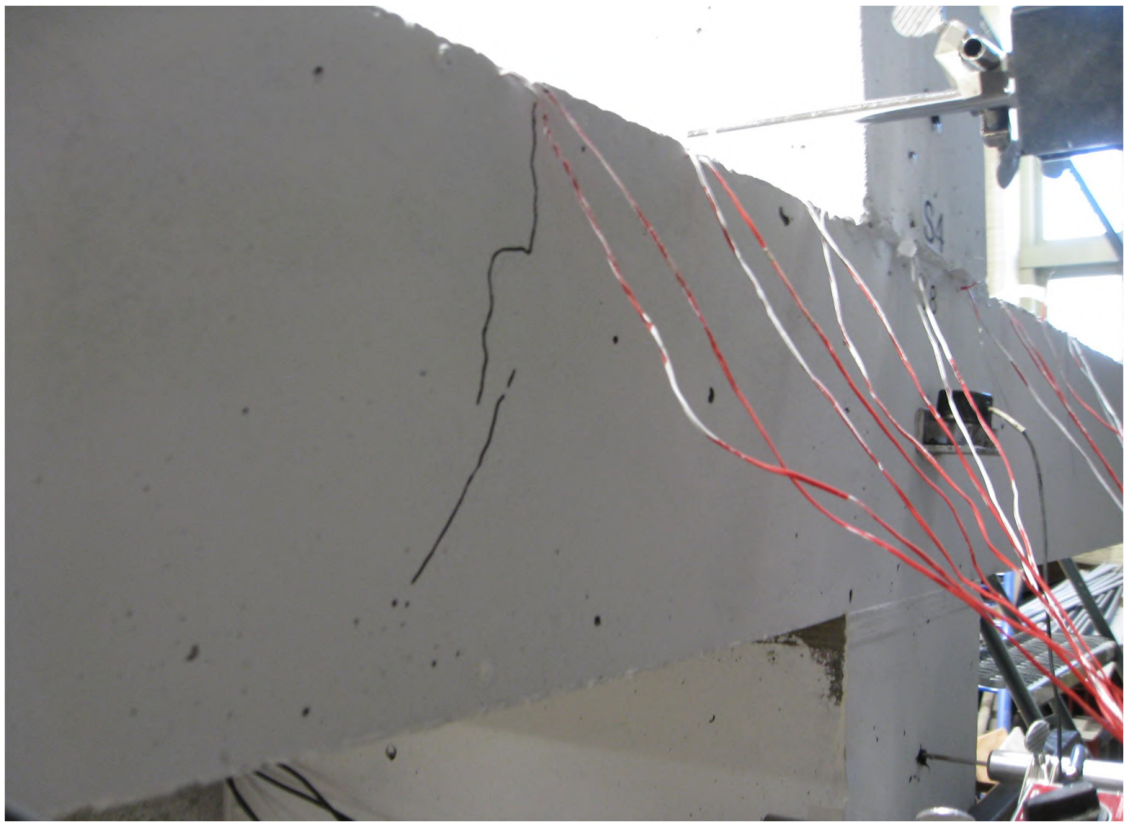

Figure 4.52: Specimen 4 free edge face cracks at V = 96.0 kN (east side)

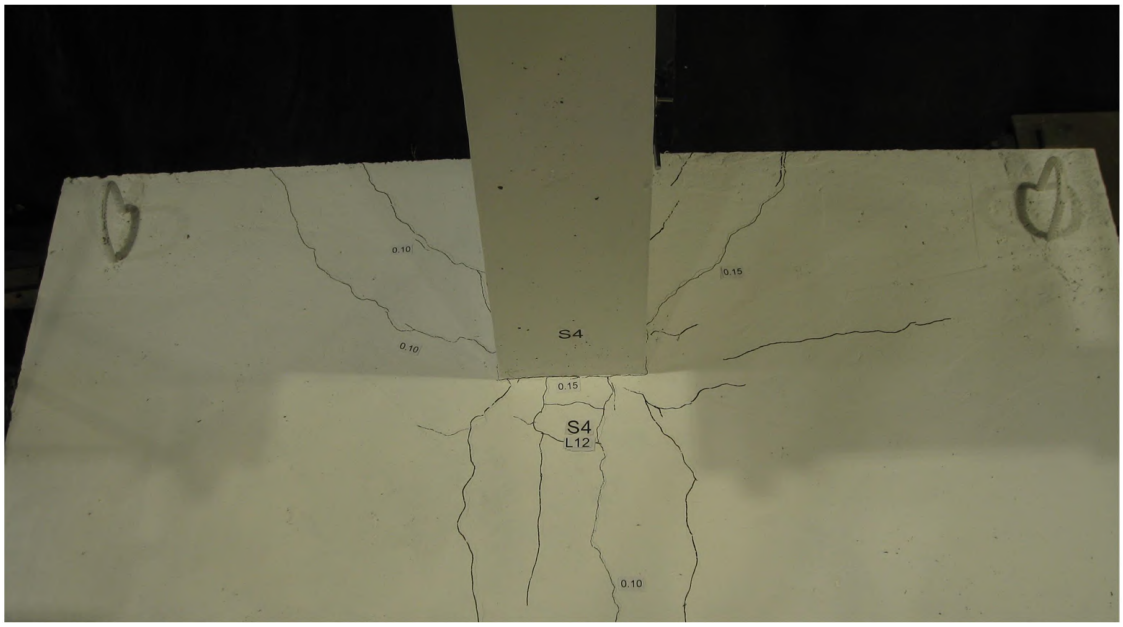

Figure 4.53: Specimen 4 slab cracks at V = 136.0 kN

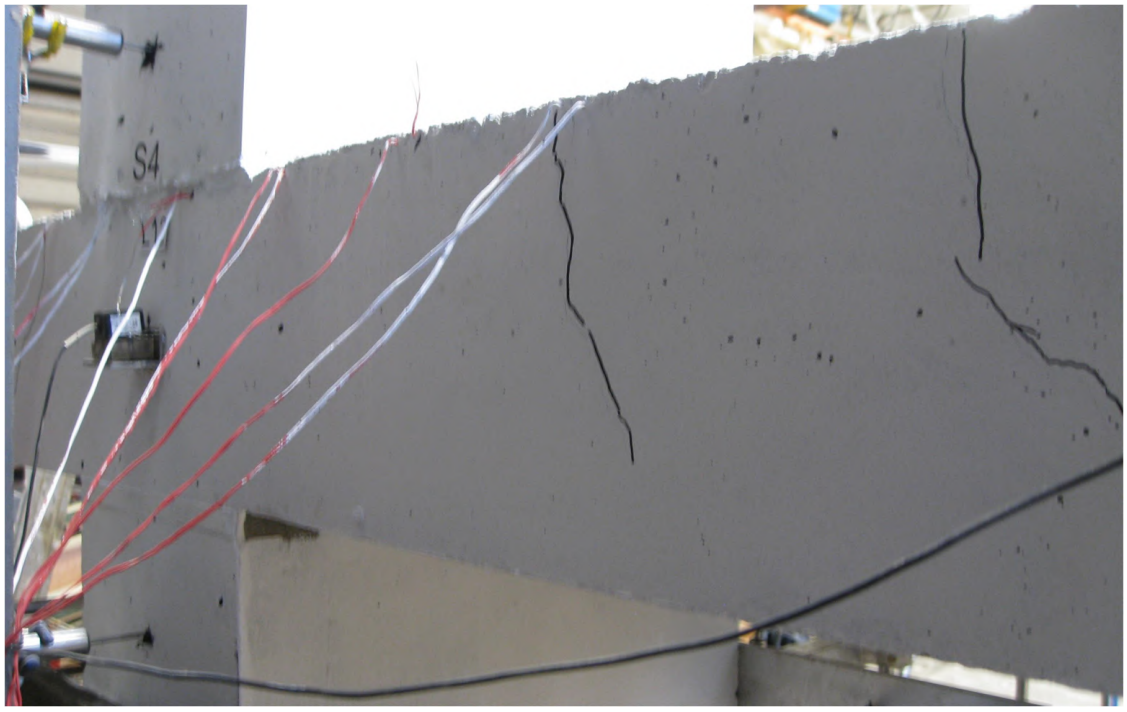

Figure 4.54: Specimen 4 free edge face cracks at V = 136.0 kN (west side)

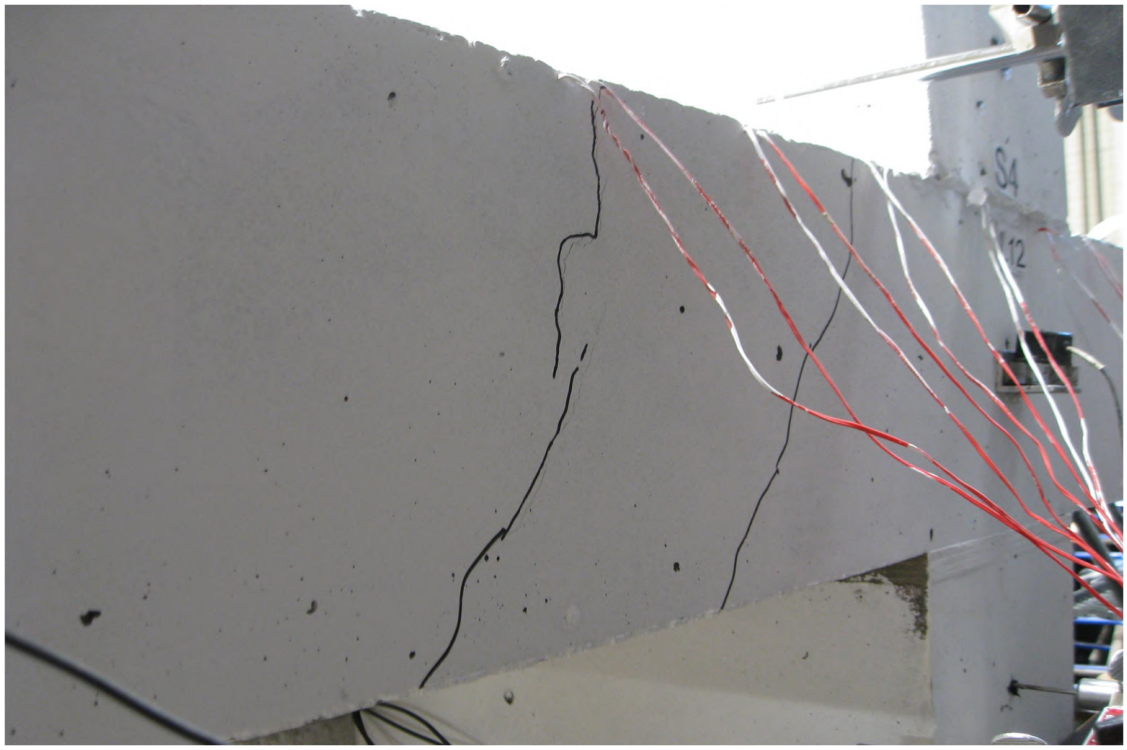

Figure 4.55: Specimen 4 free edge face cracks at V = 136.0 kN (east side)

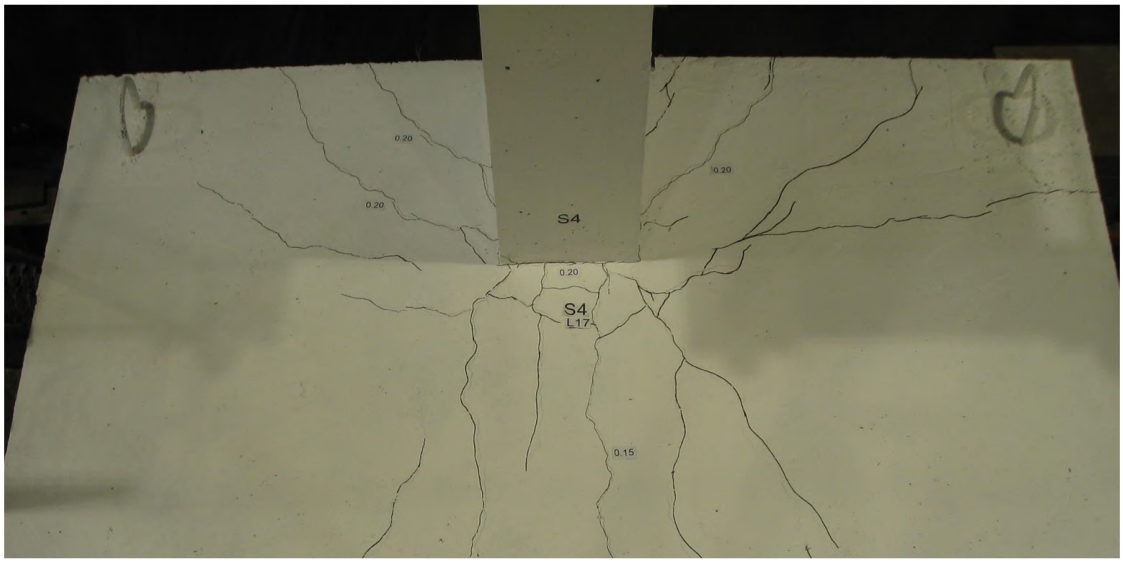

Figure 4.56: Specimen 4 slab cracks at V = 186.0 kN

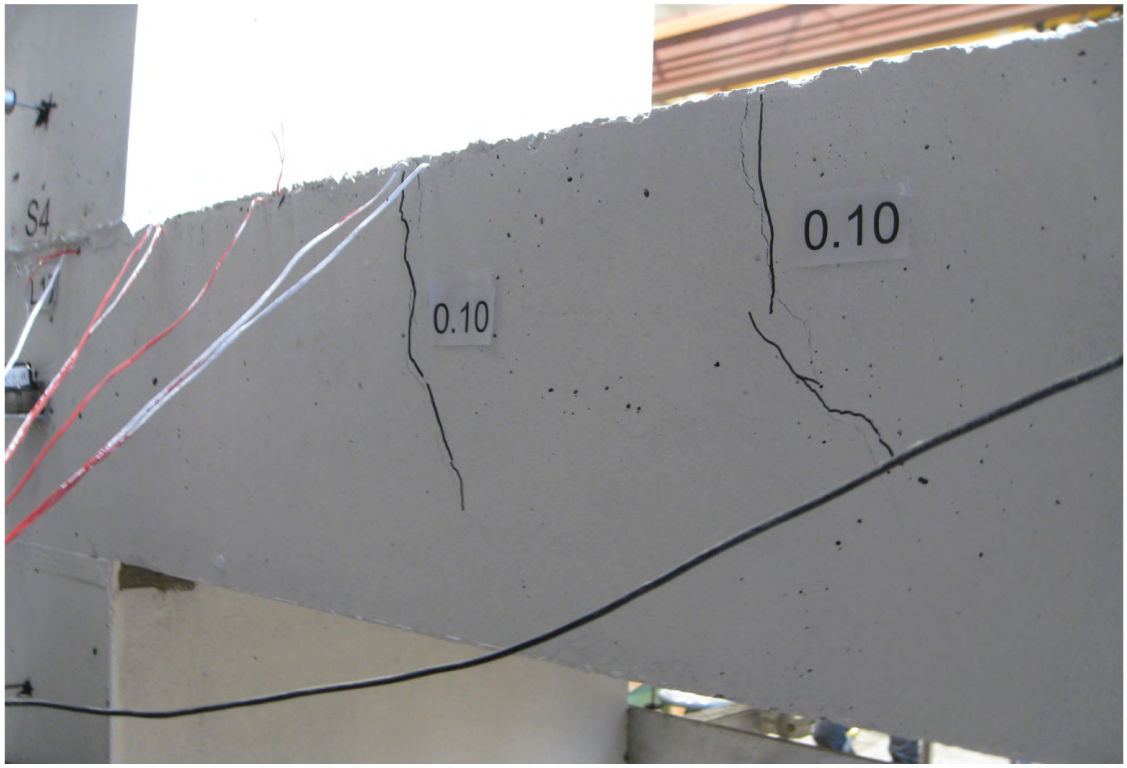

Figure 4.57: Specimen 4 free edge face cracks at V = 186.0 kN (west side)

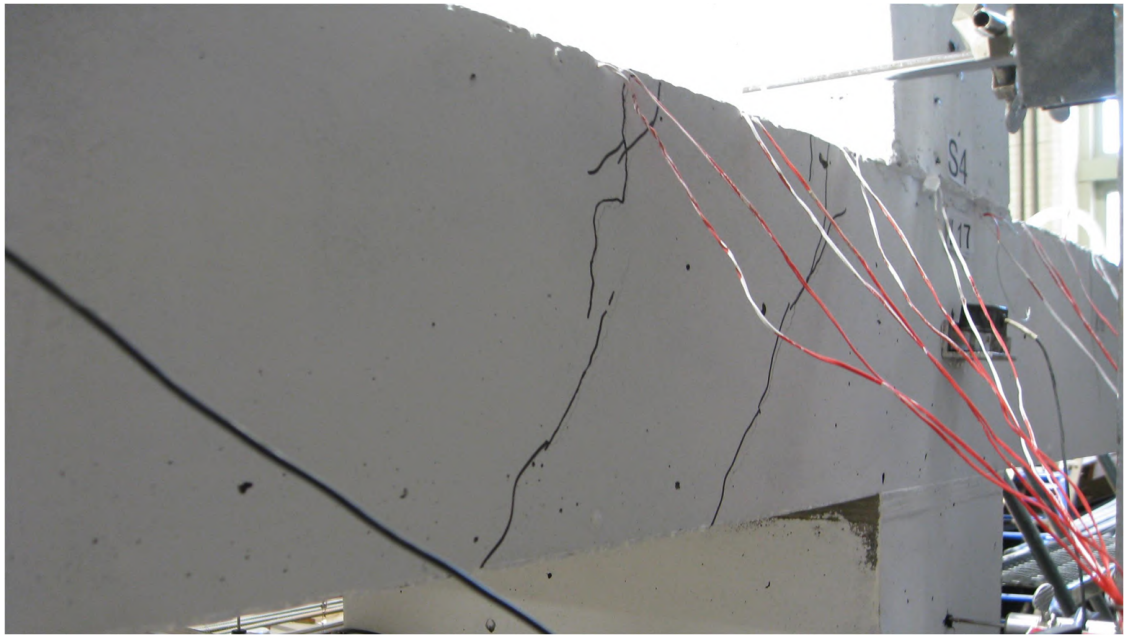

Figure 4.58: Specimen 4 free edge face cracks at V = 186.0 kN (east side)

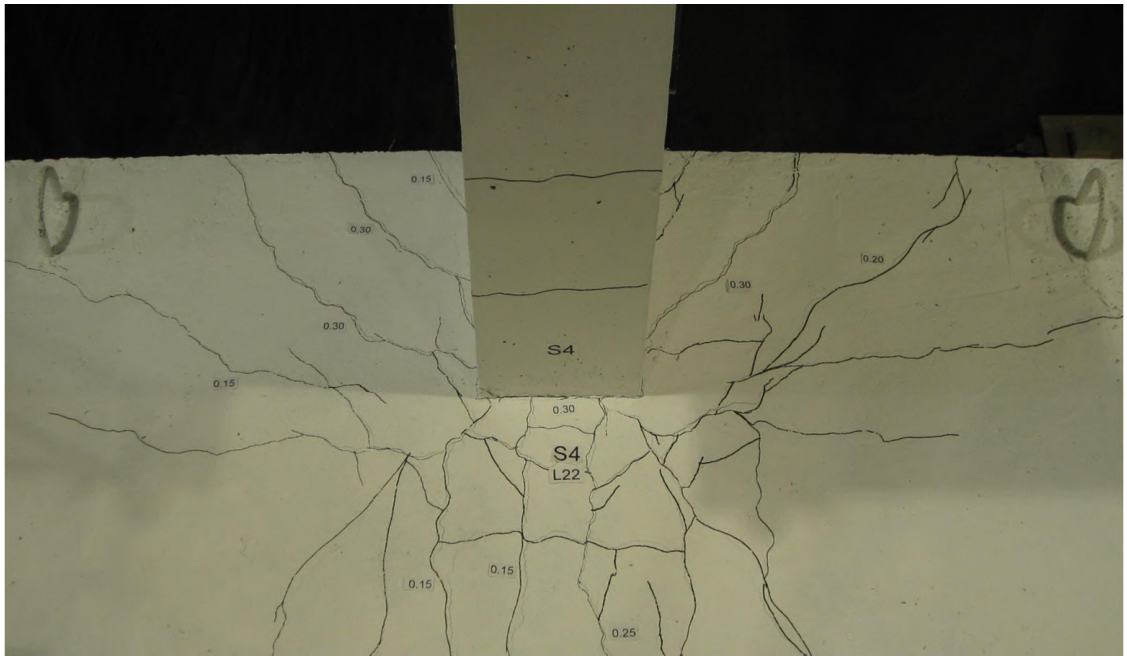

Figure 4.59: Specimen 4 slab cracks at V = 246.0 kN

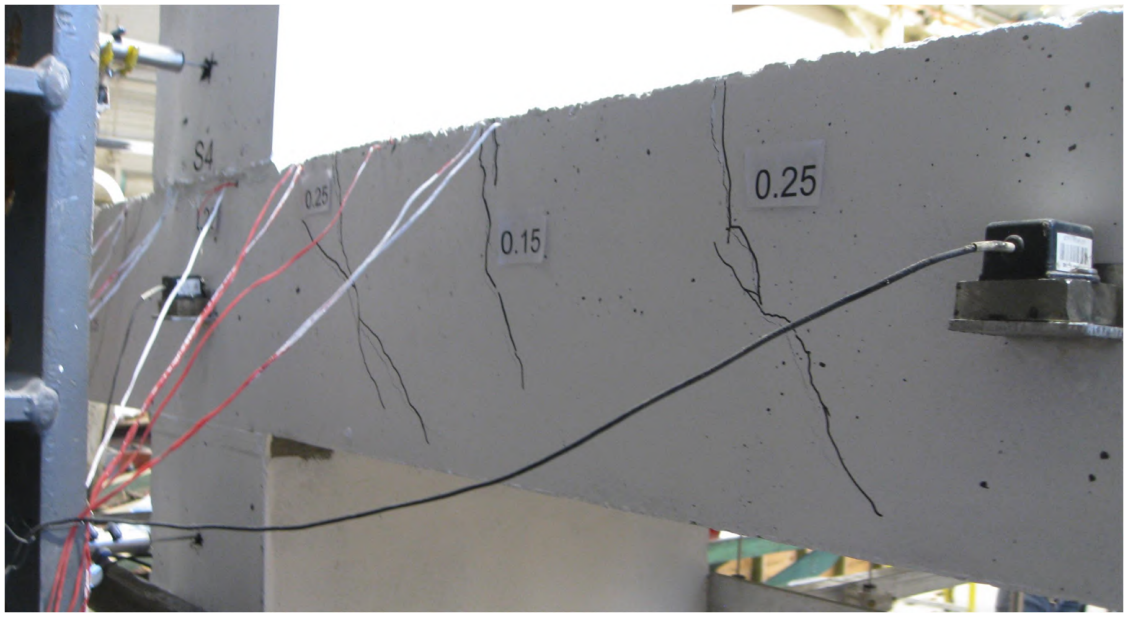

Figure 4.60: Specimen 4 free edge face cracks at V = 246.0 kN (west side)

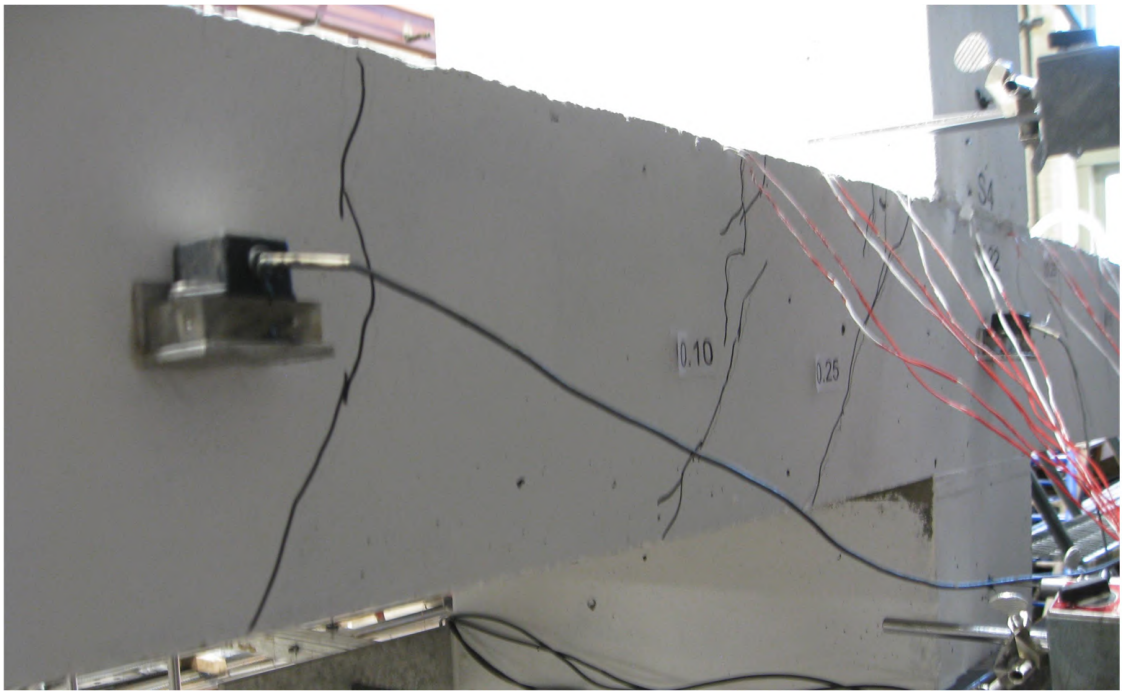

Figure 4.61: Specimen 4 free edge face cracks at V = 246.0 kN (east side)

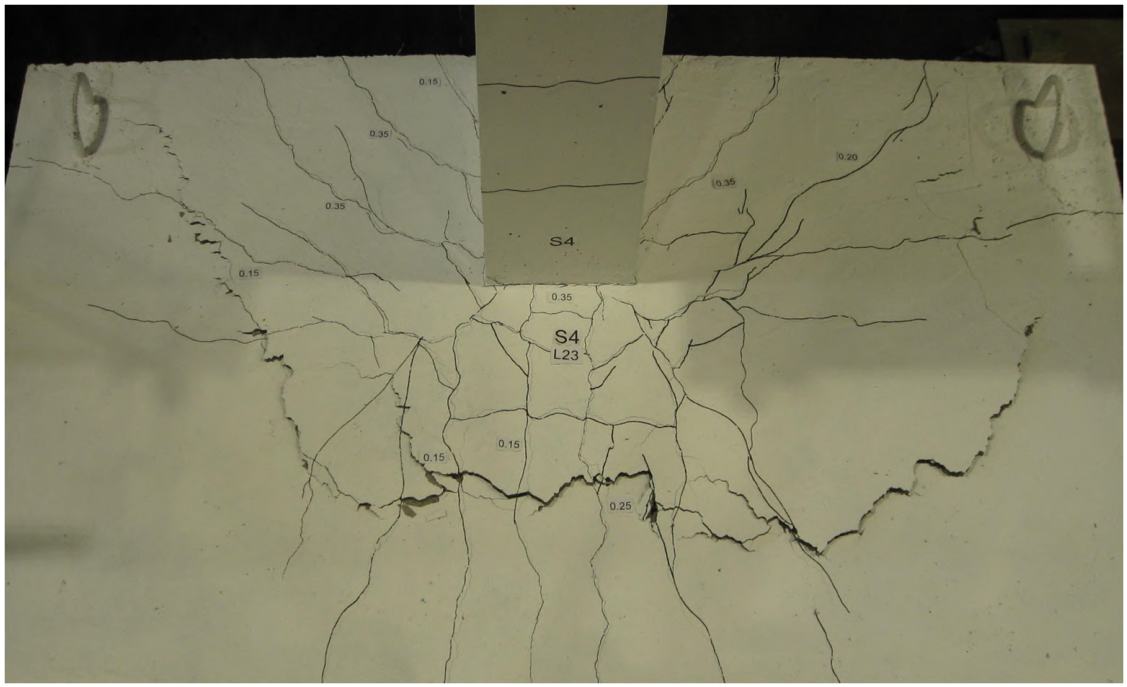

Figure 4.62: Specimen 4 at failure

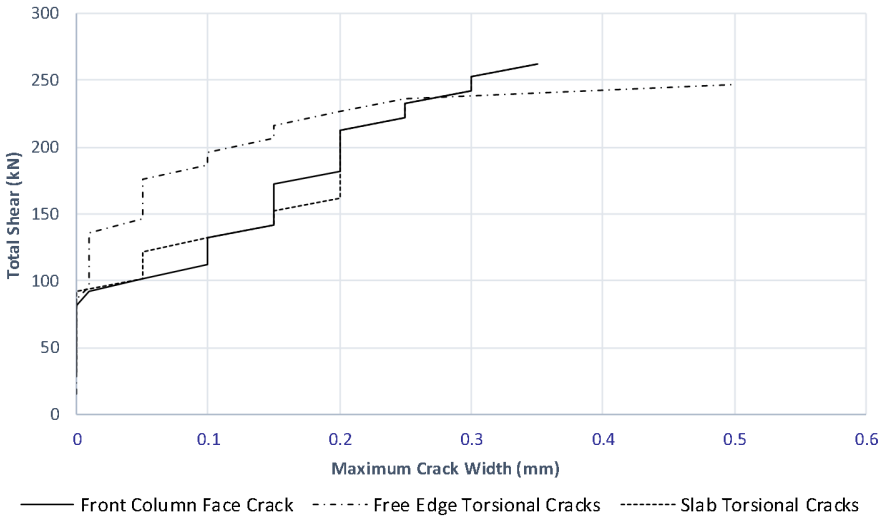

Figure 4.63: Load-maximum crack width response of Specimen 4

4.4.2 Reinforcement Strains

The reinforcement strains for the top tension reinforcement along a line parallel to and passing through the column face are shown in Figure 4.64. The reinforcement strains measured along a line parallel to and passing through the midline of the column are given in Figure 4.65. Four important load stages are presented: the formation of the first crack at 76.0 kN, the development of a second crack parallel to and in front of the column at 126.0 kN, yielding of bar F4 at 186.0 kN, and the load stage before failure at 246.0 kN.

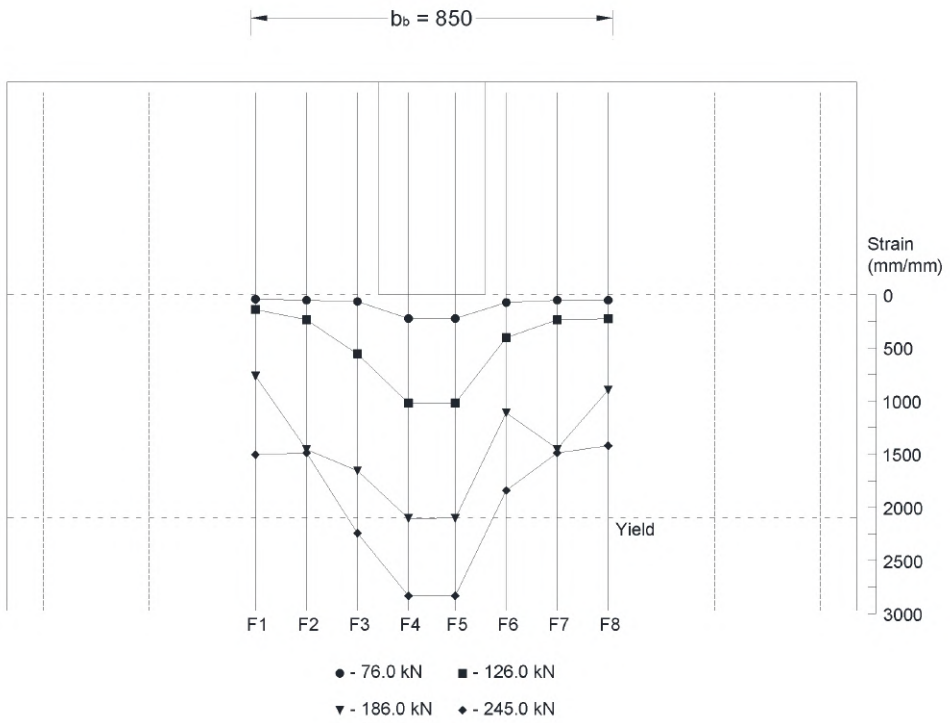

Figure 4.64: Reinforcement strains along the column face for Specimen 4 (units in mm)

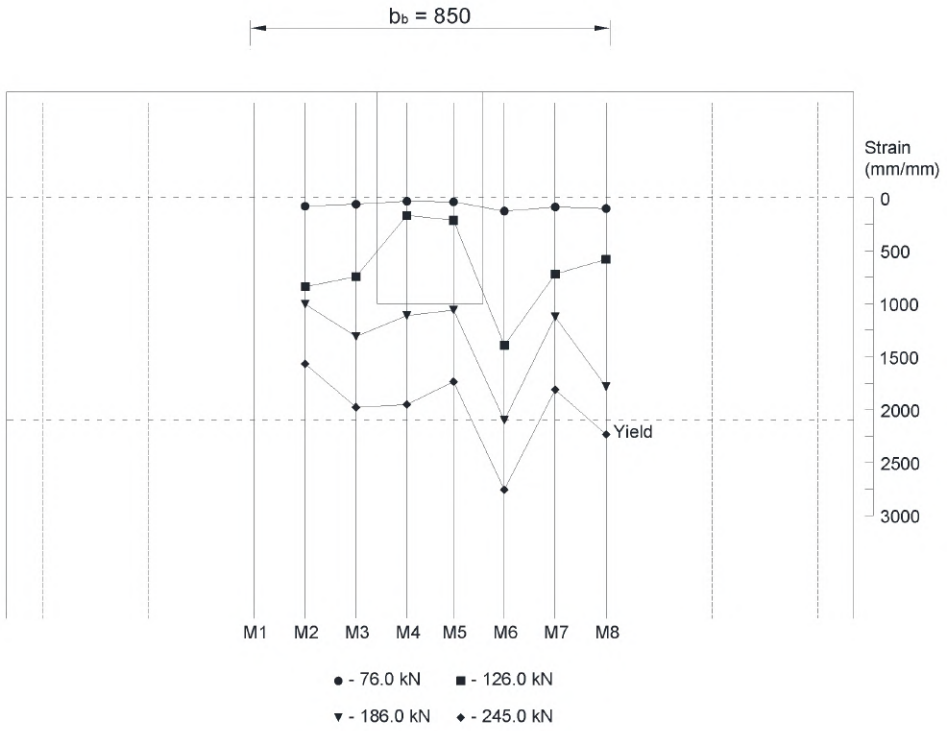

Figure 4.65: Reinforcement strains along the column midline for Specimen 4 (units in mm)

4.4.3 Slab Deflections and Rotations

The centerline deflections of the slab for the load stages described in Section 4.4.2 are given in Figure 4.66 and Table 4.4. Furthermore, the load-rotation responses of the column and the free edge of the slab are provided in Figure 4.67.

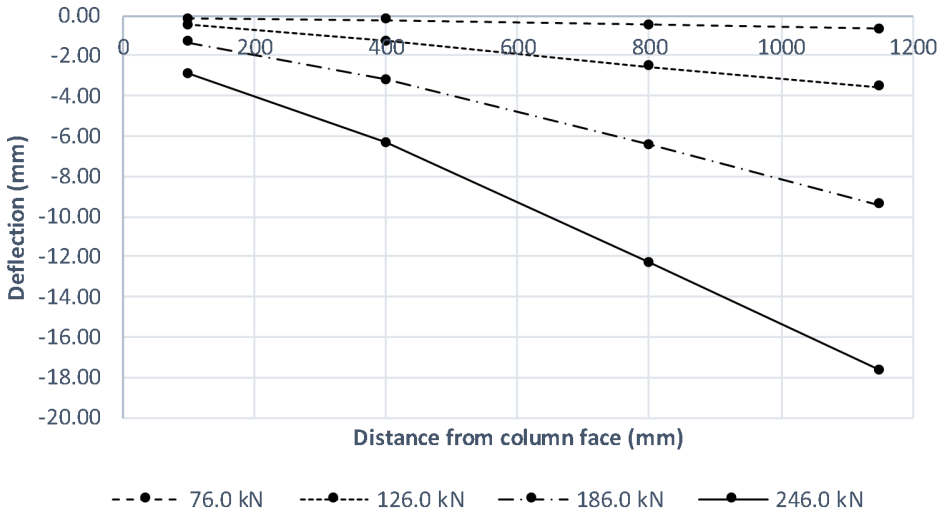

Figure 4.66: Slab deflections for Specimen 4

Table 4.4: Slab deflections for Specimen 4

	Deflection (mm)			
Distance from column face (mm)	V = 76.0 kN	V = 126.0 kN	V = 186.0 kN	V = 246.0 kN
100	0.2	0.5	1.3	2.9
400	0.2	1.3	3.2	6.3
800	0.5	2.5	6.5	12.3
1150	0.7	3.6	9.4	17.6

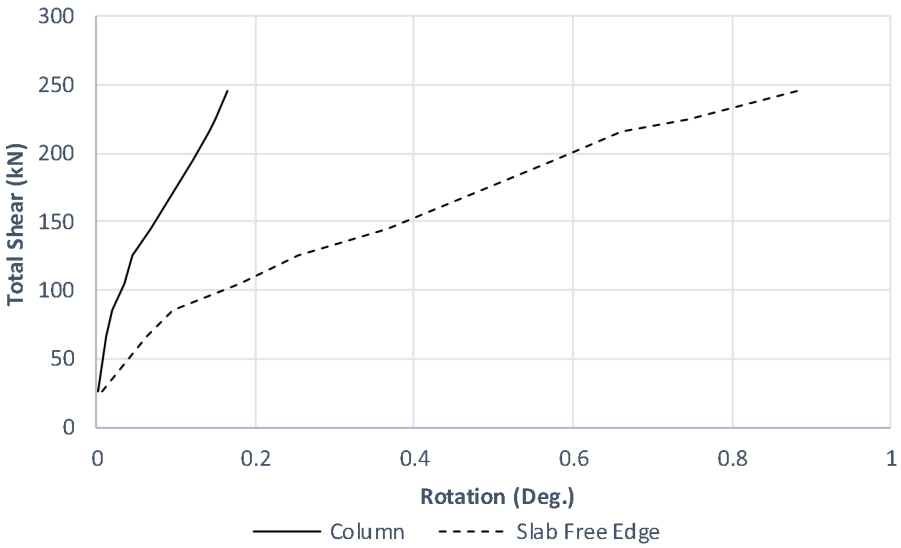

Figure 4.67: Column and slab free edge load-rotation responses for Specimen 4

5 Analysis and Comparison of Experimental Results

In this section, the experimental results are analyzed and compared with the CSA A23.3-14 and ACI 318-14 predicted flexural and shear responses. A method for determining the effectiveness of the top tension reinforcement in edge slab-column connections is then formulated.

An overview of the specimen design parameters is provided in Table 5.2 and a summary of the experimental results shown in Table 5.3. The specimens differed principally in the dimension of the column perpendicular to the free edge, c_1; the dimension of the column parallel to the free edge, c_2; the distance from the front column face to the free edge, c_3; and the number of top tension reinforcing bars perpendicular to the free edge, n_l, in the moment transfer band width, b_b.

Table 5.1: Summary of Specimen Design Parameters

Specimen	h	c_1 (mm)	c_2 (mm)	c_3 (mm)	d (mm)	b_0 (mm)	n_1 (# 15M)	b_b (mm)
1	200	250	500	250	160	1320	6	1100
2	200	250	500	400	160	1620	8	1100
3	200	400	400	400	160	1520	8	1000
4	200	500	250	500	160	1570	8	850

Table 5.2: Summary of Specimen Results

Specimen	Load at First Crack (kN)	Load at First Yield (kN)	Load at Failure (kN)	Failure Mode
1	63.6	122.1	171.4	Flexure
2	85.0	165.0	280.0	Flexure
3	64.9	154.9	252.0	Flexure-Punching
4	76.0	186.0	246.0	Flexure-Punching

5.1 Comparison of Code Predictions and Experimental Results

5.1.1 Flexure

At edge slab-column connections, CSA A23.3-14 and ACI 318-14 require that 100 % of the l_1 span moment at the front column face, M_{face}, be resisted by the slab in the moment transfer band width, $b_b = c_2 + 3h$ (Figure 5.1). Similar to the flexural design of beams and one-way slabs, the codes imply a uniform horizontal distribution of longitudinal strains across b_b. It follows that the horizontal arrangement of reinforcing bars in

width b_b should not affect the flexural response of the connection and that these bars will yield simultaneously at failure.

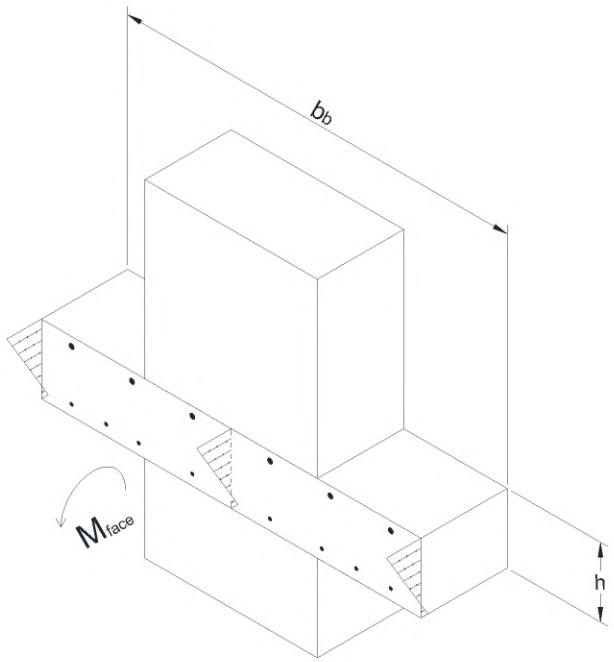

Figure 5.1: CSA A23.3-14 and ACI 318-14 flexural strength model for edge slab-column connections

The accuracy of the code provisions for the nominal flexural strength of the slab in the moment transfer band width, M_n, is analyzed in Table 5.3. The nominal flexural strength was calculated using Equation 5.1 for CSA A23.3-14 (2014) and Equation 5.2 for ACI 318-14 (2014), where α_1 is a factor in CSA A23.3-14 accounting for the shape of the compressive stress distribution as a function of the compressive strength, and d_1 is the effective depth to the top tension reinforcement perpendicular to the free edge.

$$M_n = A_s f_y \left(d_1 - \frac{A_s f_y}{\alpha_1 f'_c b_b} \right) \tag{5.1}$$

$$M_n = A_s f_y \left(d_1 - \frac{A_s f_y}{0.85 f'_c b_b} \right) \tag{5.2}$$

Table 5.3: Comparison of Experimental Results in Flexure with CSA A23.3-14 and ACI 318-14

	Experimental Results	Code Predicted Results		Comparison	
Specimen	M_{face} (kNm)	$M_{n\,CSA}$ (kNm)	$M_{n\,ACI}$ (kNm)	$M_{face}/M_{n\,CSA}$	$M_{cg}/M_{n\,ACI}$
1	64.7	81.1	81.3	0.79	0.80
2	112.5	106.8	107.0	1.05	1.05
3	101.5	106.2	106.7	0.96	0.95
4	98.2	105.0	105.6	0.94	0.93
			Average (Std. Dev.)	0.94 (0.09)	0.93 (0.09)

The codes predict that only Specimen 2 should have failed in flexure. This is accurate, as the flexural capacity of Specimen 2 was exceeded during testing with complete yielding of the top tension reinforcement in width b_b. The codes also correctly predict that Specimen 3 and 4 were unable to reach their respective flexural capacities, instead failing in punching shear. In this sense, the codes do not predict that any of the top tension reinforcement should have yielded in width b_b for these specimens; however, 6-15M and 4-15M of the 8-15M in width b_b yielded in Specimen 3 and 4, respectively. The codes predict with significantly less accuracy the flexural capacity of Specimen 1. This specimen failed in flexure, as demonstrated by the plateauing of its load-deflection curve in Figure 4.1, at a front column face moment 20 % less than predicted.

In addition, yielding of reinforcing bars in width b_b did not occur simultaneously. The first reinforcing bars to yield were those passing through the column, followed by the bars closest to the side column faces, see Figure 5.2.

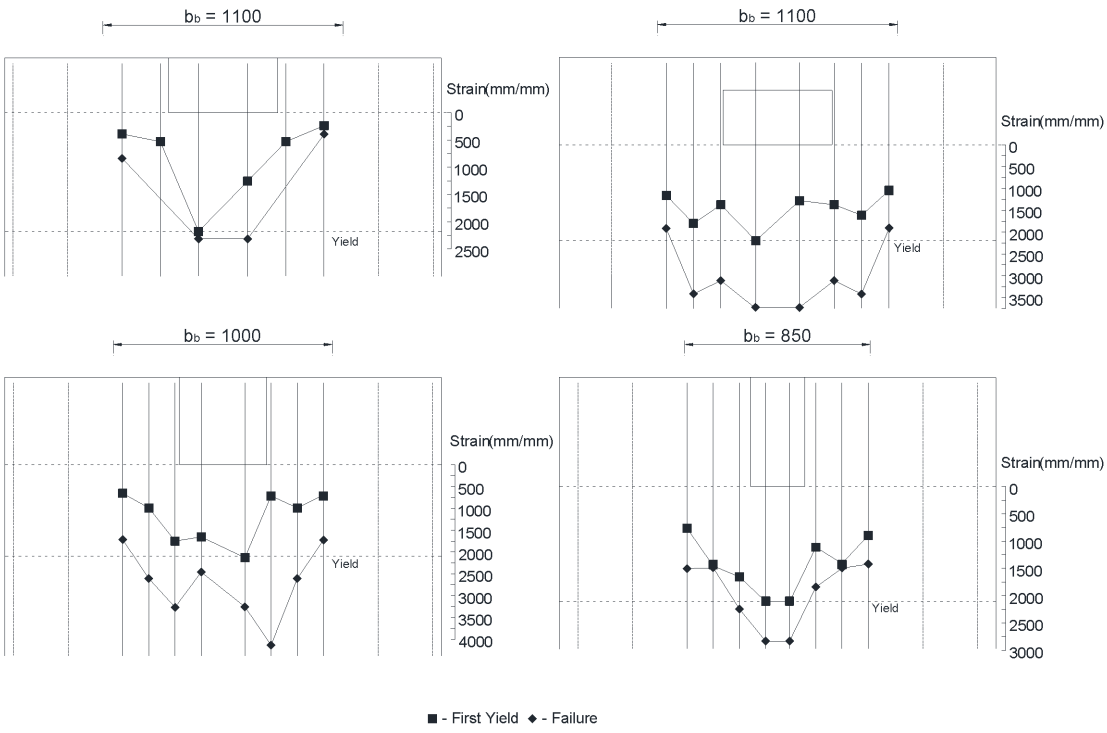

Figure 5.2: Summary of reinforcement strains at front column face at first yield and failure

Statistical analyses of the reinforcement stresses at shears of 100 kN, 150 kN, and at failure are provided in Tables 5.4, 5.5, and 5.6, respectively, where $\overline{\sigma}_{bar}$ is the average bar stress, $\overline{(\sigma_1 - \sigma_4)}$ is the average stress difference between the reinforcing bars inside the column and furthest away from the column centerline, $M_{\overline{\sigma}}$ is the predicted moment assuming that all reinforcing bars are at the average stress, and M_{c_2} is the moment contribution from the reinforcement inside the column. In the cases where reinforcement strains were missing, due to damaged strain gauges, the strain gauge at the same distance from the slab centerline on the opposite side of the column was used.

Table 5.4: Statistical Comparison of Reinforcement Strains at V = 100 kN

Specimen	$\overline{\sigma}_{bar}$ (Std. Dev.) (MPa)	$\overline{(\sigma_1 - \sigma_4)}$ (MPa)	$M_{\overline{\sigma}}$ (kNm)	M_{c_2} (kNm)	$M_{c_2}/\, M_{\overline{\sigma}}$	M_{face} (kNm)
1	149.6 (124.0)	267.6	29.6	20.6	0.69	40
2	122.2 (51.0)	113.3	32.2	11.4	0.36	40
3	132.7 (76.6)	134.6	34.9	15.3	0.44	40
4	75.3 (56.5)	139.3	19.9	11.1	0.55	40

Table 5.5: Statistical Comparison of Reinforcement Strains at V = 150 kN

Specimen	$\overline{\sigma}_{bar}$ (Std. Dev.) (MPa)	$\overline{(\sigma_1 - \sigma_4)}$ (MPa)	$M_{\overline{\sigma}}$ (kNm)	M_{c_2} (kNm)	$M_{c_2}/\, M_{\overline{\sigma}}$	M_{face} (kNm)
1	265.9 (158.8)	309.6	52.1	27.5	0.53	60
2	294.0 (65.9)	118.5	75.8	21.8	0.29	60
3	261.1 (101.2)	233.3	67.4	25.1	0.37	60
4	233.9 (78.5)	215.4	60.2	22.5	0.37	60

Table 5.6: Statistical Comparison of Reinforcement Strains at Failure

Specimen	$\overline{\sigma}_{bar}$ (Std. Dev.) (MPa)	$\overline{(\sigma_1 - \sigma_4)}$ (MPa)	$M_{\overline{\sigma}}$ (kNm)	M_{c_2} (kNm)	$M_{c_2}/\, M_{\overline{\sigma}}$	M_{face} (kNm)
1	292.7 (128.0)	258.2	57.0	27.4	0.48	62.8
2	412.2 (14.9)	33.9	104.6	25.6	0.27	105.6
3	401.3 (33.6)	77.7	101.4	26.8	0.30	94.8
4	350.8 (59.1)	129.2	88.5	26.7	0.34	92

Except for Specimen 1, the nonuniformity of the bar stresses, as quantified by the standard deviation and $\overline{(\sigma_1 - \sigma_4)}$, peaked and then decreased as M_{face} approached the nominal flexural strength of the specimen. Correspondingly, the ratio of the moment contribution of the reinforcement inside the column to the total computed moment, $M_{c_2}/\, M_{\overline{\sigma}}$, decreased with increasing load. According to CSA A23.3-14 and ACI 318-14, the moment contribution from these bars should remain constant and equal to the ratio of reinforcing bars inside the column to total bars in width b_b, that is, 0.33 for Specimen 1 and 0.25 for the other specimens. Lastly, the distribution of reinforcement stresses in Specimen 1 suggests that not all reinforcing bars in width $b_b = c_2 + 3h$ are effective. This is particularly evident when comparing the distribution of reinforcement stresses of Specimen 1 and 2, whose moment transfer band widths are the same, $b_b = 1100\, mm$. All of the top tension reinforcement in width b_b yielded in Specimen 2, whereas only 4 of the 6-15M bars in Specimen 1 yielded.

5.1.2 Shear

In CSA A23.3-14 and ACI 318-14, edge slab-column connections fail in punching shear when the maximum shear stress on the critical section, v_u, exceeds the shear strength of the concrete, v_n. Due to the presence

of unbalanced moments at edge slab-column connections, v_u is calculated as the sum of the direct shear stresses, $\frac{V_g}{b_o d}$, and the eccentric shear stresses at the front column face, $\frac{\gamma_v M_{cg} e_1}{J_1}$, as shown in Equation 5.3. This equation, and the calculation of variables γ_v, e_1, b_o, and J_1, are identical in both codes. The nominal shear strength of the connection, v_n, was computed using Equation 2.22 for CSA A23.3-14 and Equation 2.25 for ACI 318.14. Note that, despite the different coefficients used in the CSA A23.3-14 and ACI 318-14 equations, these codes predict the same nominal strength. The CSA A23.3-14 coefficients are higher due to the difference in ϕ factors, that is, $\phi_c = 0.65$ as opposed to $\phi = 0.75$ in ACI 318-14. The accuracy of the CSA A23.3-14 and ACI 318-14 provisions for punching shear was analyzed; the results of this analysis are provided in Table 5.7.

$$v_u = \frac{V_g}{b_0 d} + \frac{\gamma_v M_{cg} e_1}{J_1} \tag{5.3}$$

Table 5.7: Comparison of Experimental Results in Shear with CSA A23.3-14 and ACI 318-14

	Experimental Results			Code Predicted Results		Comparison	
Specimen	V_g (kN)	M_{cg} (kNm)	v_u (MPa)	$v_{n\,CSA}$ (MPa)	$v_{n\,ACI}$ (MPa)	$v_u/v_{n\,CSA}$	$v_u/v_{n\,ACI}$
1	452.0	65.1	1.47	2.14	2.14	0.69	0.69
2	554.7	129.93	2.05	2.14	2.14	0.96	0.96
3	532.6	119.5	2.10	2.19	2.19	0.96	0.96
4	550.1	131.2	2.26	2.19	2.19	1.03	1.03
				Average (Std. Dev.)		0.91 (0.13)	0.91 (0.13)

The CSA A23.3-14 and ACI 318-14 punching shear provisions predict the nominal strength of the connection with a high degree of accuracy. The difference between the experimental and code predicted results for Specimen 1 is due to its failure in flexure and not flexure-punching shear as with the other specimens. When Specimen 1 is not included in the calculation of the average ratio of the ultimate shear to the code predicted shear strength, the code averages increase to 0.98 with a standard deviation of 0.03.

In cases where the shear stress due to gravity loads is smaller than 75 % of the concrete shear strength, ACI 318-14 provision 8.4.2.3.4 allows for the reduction of γ_v to zero. In other words, the interaction between moment and shear is considered negligible and the connection is predicted to fail in flexure. As shown in Table 5.8, all specimens satisfied the condition of provision 8.4.2.3.4 at failure.

Table 5.8: Ratio of Applied Shear without Moment Transfer to ACI 318-14 Predicted Shear Strength

Specimen	V_g (kN)	$V_{n\,ACI}$ (kN)	$V_g/V_{n\,ACI}$
1	171.4	452.0	0.38
2	280.0	554.7	0.50
3	252.0	532.6	0.47
4	246.0	550.1	0.45

With ACI 318-14 provision 8.4.2.3.4 applied, the code predicts that all specimens should have failed in flexure, as shown in Table 5.9, where V_{flex} is the applied shear at the point of inflection causing flexural failure. As Specimen 2, 3, and 4 failed in punching shear after complete or partial yielding of the top tension reinforcement in b_b, the interaction of moment and shear is not negligible.

Table 5.9: Comparison of Experimental Results with No Moment Transfer in Shear

	Experimental Results	Code Predicted Results		Comparison		
Specimen	V_g (kN)	$V_{flex\,ACI}$ (kN)	$0.75V_{n\,ACI}$ (kN)	$V_g/V_{flex\,ACI}$	$V_g/0.75V_{n\,ACI}$	Failure Mode
1	171.4	202.7	339.0	0.85	0.38	Flexure
2	280.0	266.9	416.0	1.05	0.50	Flexure
3	252.0	265.4	399.5	0.95	0.47	Flexure-Shear
4	246.0	262.5	412.6	0.94	0.45	Flexure-Shear
		Average (Std. Dev.)		0.95 (0.07)		

5.2 Method for Determining the Flexural Strength of Edge Slab-Column Connections

A method is presented for determining the effectiveness of the top tension reinforcement in the transfer of moments in edge slab-column connections. Recall that the CSA A23.3-14 and ACI 318-14 codes require that 100 % of the unbalanced moment at the column front face be resisted by the top tension reinforcement in the band width $b_b = c_2 + 3h$. In this band width, the codes imply a uniform horizontal distribution of strains and that all reinforcing bars in width b_b will yield, independent of their position relative to the column center or the free edge. The reinforcement strain results of this experimental program, provided in

Figure **??** and 5.2, notably demonstrate two significant contradictions to the assumptions made in the code models:

1. The reinforcement strains are not uniform across b_b, rather they decrease with increasing distance from the column centerline.

2. Not all reinforcement in $b_b = c_2 + 3h$ yields despite failure in pure flexure.

These observations are additionally supported by the experimental program conducted at McGill University by Rughani (1983). Rughani's specimens featured edge slab-column connections with varying c_3 dimensions, that is, the distance from the front column face to the free edge. Only Specimen 2 failed in punching shear, while Specimen 3, 4, and 4a failed in pure flexure. As dimension c_3 decreased from Specimen 2 to 4a, the reinforcement strains outside of the column also decreased relative to the reinforcement strains inside the column.

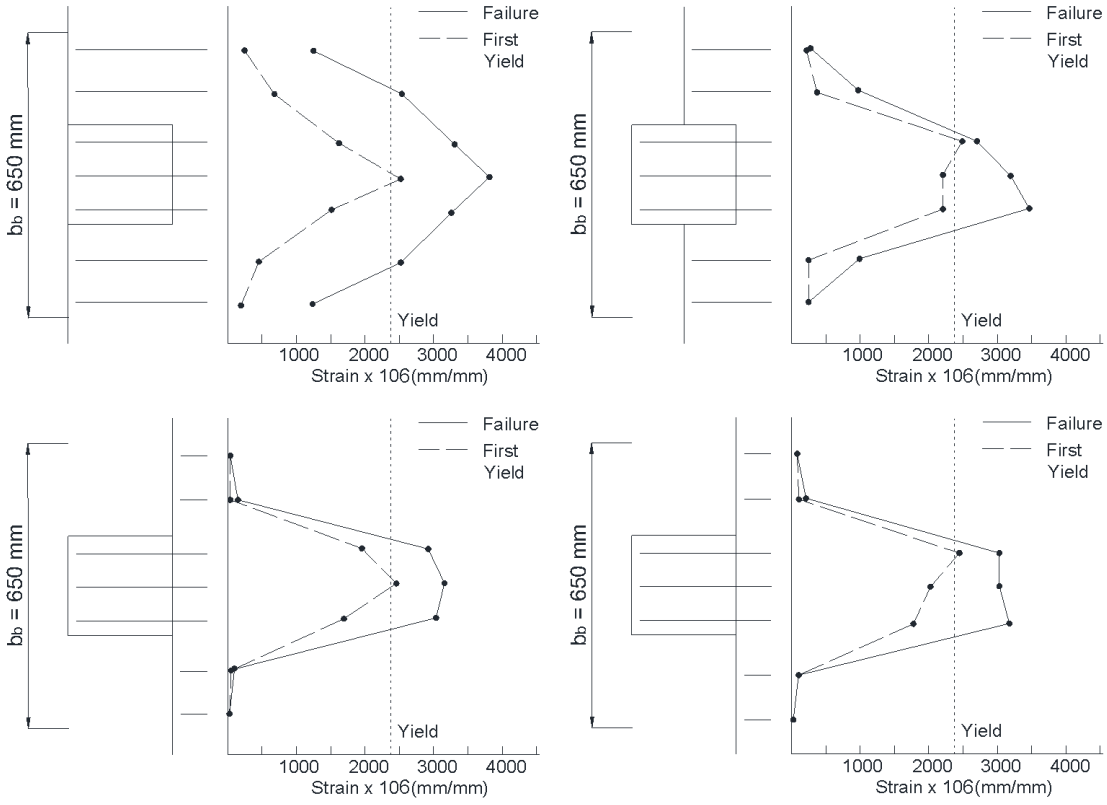

Figure 5.3: Strain results from Rughani's tests. Clockwise from top left: AR2, AR3, AR4A, AR4 (1983)

5.2.1 Proposed Method

A critical section for flexure for edge slab-column connections is proposed based on the formation of local yield lines, as shown in Figure 5.4. The angle, θ, of the yield lines adjacent to the column, or the torsional

yield lines, is a function of the orthogonal top tension reinforcement in the slab in the vicinity of the column (Kennedy and Goodchild, 2004). For design purposes, yield line analyses carried out by Regan (1981) and Moehle (1988) on edge slab-column connections indicate that the yield line angle, θ, may be conservatively taken as 45 degrees. As $tan45^\circ = 1$, the dimensions of the critical section for flexure may be defined solely by the column dimension parallel to the free edge, c_2, and the distance from the front column face to the free edge, c_3.

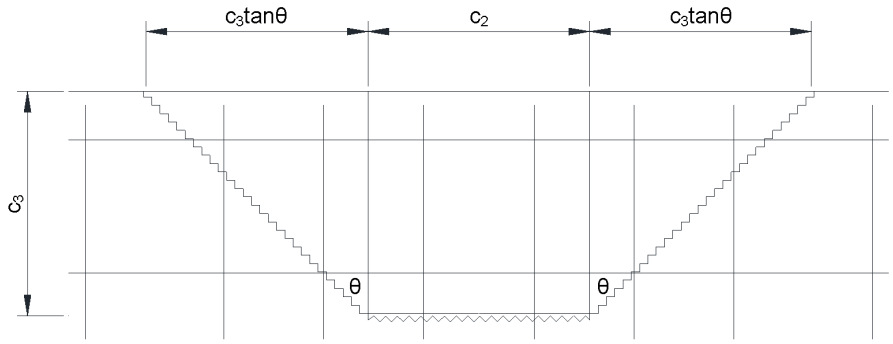

Figure 5.4: Proposed critical section for flexure

According to Yield Line Theory, reinforcing bars that intersect a yield line have reached the yield strain. However, due to the proximity of the free edge, intersection with the torsional yield line does not guarantee that a reinforcing bar will yield. Instead, it is recommended that a reinforcing bar be sufficiently embedded inside the critical section for flexure in order to yield. In cases where a reinforcing bar intersects the torsional yield line without an embedment length greater than or equal to its development length, these bars are only capable of developing a fraction of their yield stress. Provided that 50 % of the bar stress is transferred by anchorage of the hook and 50 % by straight bar bond, the effectiveness of a reinforcing bar can be described by Equation 5.4 (Alexander, 2017).

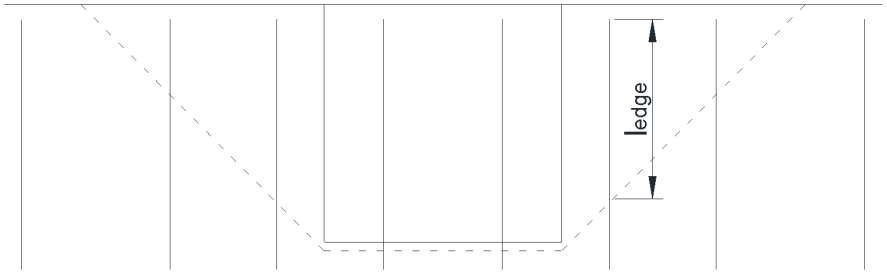

Figure 5.5: Embedment length in critical section for flexure

$$\eta_i = 0.5\left[1 + \left(\frac{l_{edge}}{l_{dh}}\right)\right] \leq 1.0 \tag{5.4}$$

The number of effective bars intersecting the yield line is then:

$$n_{bar\,eff} = \sum \eta_i \tag{5.5}$$

The nominal flexural strength of the connection may be determined with a sectional analysis of the slab. By modifying Equation 5.1 for the number of effective bars and the projected width enclosed by the torsional yield lines, $c_2 + 2c_3$, the nominal flexural resistance of the connection is given in Equation 5.6, where A_{bar} is the cross-sectional area of one bar.

$$M_n = n_{bar\,eff} A_{bar} f_y \left(d - \frac{n_{bar\,eff} A_{bar} f_y}{\alpha_1 f'_c (c_2 + 2c_3)}\right) \tag{5.6}$$

In Table 5.10, the predictions of the proposed method, M_{prop}, are compared with the CSA A23.3-14 and ACI 318-14 predictions, M_{codes}, and the flexural responses of the specimens of this experimental program and the specimens of Rughani's experimental program (1983), which are identified by the designation "AR."

Table 5.10: Comparison of CSA A23.3-14 and ACI 318-14 Model with Proposed Method

Specimen	c_1 (mm)	c_2 (mm)	c_3 (mm)	h (mm)	M_{codes} (kNm)	M_{prop} (kNm)	M_{face} (kNm)	$\frac{M_{face}}{M_{codes}}$	$\frac{M_{face}}{M_{prop}}$
1	250	500	250	200	81.1	68.3	64.7	0.80	0.95
2	250	500	400	200	106.5	104.4	112.5	1.06	1.08
3	400	400	400	200	106.2	104.1	101.5	0.96	0.97
4	500	250	500	200	104.7	107.4	98.2	0.94	0.91
AR2	300	300	300	175	81.8	76.1	80.6	0.98	1.06
AR3	300	300	150	175	95.0	66.0	65.6	0.69	0.99
AR4	300	300	0	175	80.9	34.4	42.2	0.52	1.23
AR4A	300	300	0	175	93.9	46.3	46.2	0.49	1.00
							Average (Std. Dev.)	0.80 (0.22)	1.02 (0.10)

The proposed method demonstrates better agreement between the predicted and experimental results than the approach used by the CSA A23.3-14 and ACI 318-14. This is especially evident when comparing the code predicted results with the revised method for cases where $\frac{c_3}{1.5h} < 1.0$, as in Specimen 1 of this

experimental program and Specimen AR3, AR4, and AR4A of Rughani's experimental program. For these aspect ratios, the code overpredicts the flexural capacity that would result in a premature failure in flexure. If the results of Specimen 2, 3, 4, and AR2 are not included in the calculation of the average and standard deviation, the code model average changes to 0.63 with a standard deviation of 0.59 and the revised method average changes to 1.04 with a standard deviation of 0.12. In cases where $\frac{c_3}{1.5h} \approx 1.0$, the codes and the revised method predict similar flexural resistances, as observed in Specimen 2, 3, 4, and AR2.

In cases where $\frac{c_3}{1.5h} > 1.0$, the codes tend to underpredict the flexural capacity of the connection, resulting in a predicted punching shear failure before failure in flexure. For example, Anggadjaja and Teng (2008) tested an edge slab-column connection featuring a column with dimensions $c_2 = 180\,mm$ and $c_3 = 900\,mm$. In order to ensure that the specimen failed in punching shear, the top tension reinforcement consisted of 13 mm diameter bars distributed over a 2500 mm band width. The codes predict a moment resistance of 57.0 kNm in width $c_2 + 3h$ and the revised method predicts a moment resistance of 85.8 kNm; the specimen failed in punching shear at a front column face moment of 81.0 kNm and shear of 245.0 kN.

By combining the results of Angagadjaja and Teng (2008) with the experimental results of this study and Rughani's study (1983), Figure 5.6 provides a comparison of the experimental front column face failure moment to the CSA A23.3-14 and ACI 318-14 predicted front column face failure moment. The dashed line represents the case where the experimental and the predicted front column face failure moments are the same.

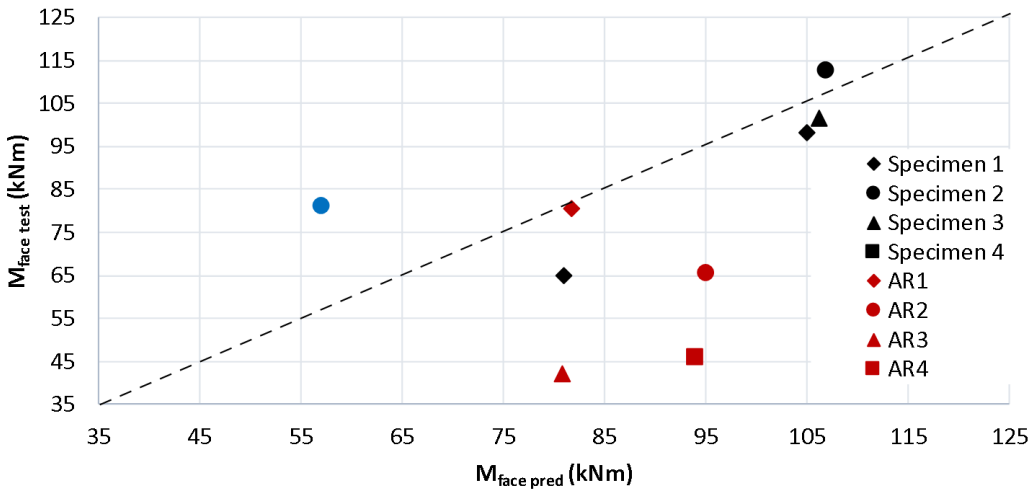

Figure 5.6: Comparison of the experimental front column face failure moment with the CSA A23.3-14 and ACI 318-14 predicted front column face failure moment

Figure 5.7 provides a comparison of the experimental front column face failure moment to the front

column face failure moment predicted by the proposed method. Using the proposed method, significantly better agreement is obtained between the experimental and predicted results, especially in the cases where $\frac{c_3}{1.5h} < 1.0$ and $\frac{c_3}{1.5h} > 1.0$.

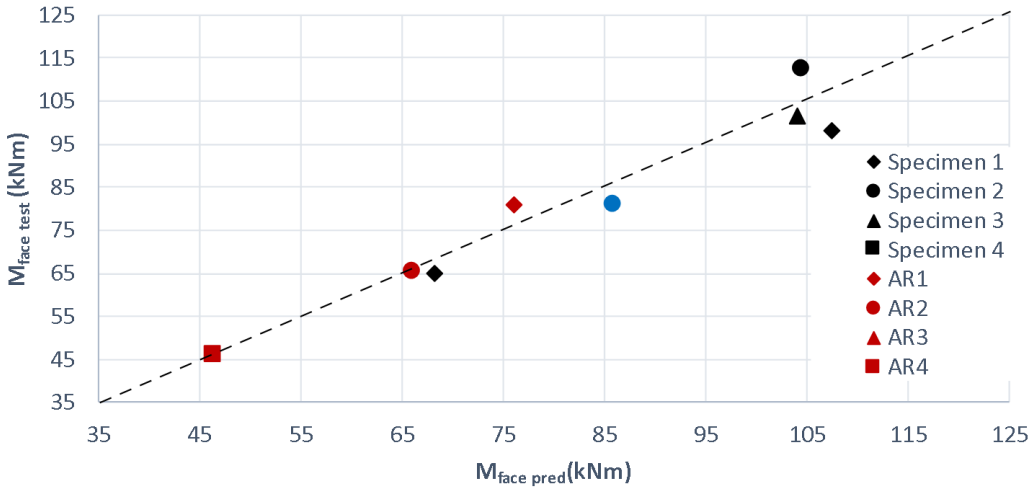

Figure 5.7: Comparison of the experimental front column face failure moment with the predicted front column face failure moment of the proposed method

5.2.2 Code Formulation

In this section, a formulation of the proposed method described in 5.2.1 is provided for consideration in the CSA A23.3 standard.

13.10.3 Exterior Columns

The reinforcement for the total factored negative moment transferred to exterior columns shall be placed within a band width equal to the column width plus c_3 on either side of the column, where c_3 is the distance from the free edge to the inner column face. The development of the negative moment reinforcement within this band width shall be accounted for by assuming that the critical section follows a 45 degree line from the corner of the column on the inside face to the free edge.

6 Conclusions

The following conclusions were formulated based on the experimental results and the analysis and comparison of these results:

1. The longitudinal strains of the top slab reinforcement perpendicular to the free edge were not uniformly distributed across width $b_b = c_2 + 3h$ during loading. Reinforcement strains were typically highest for those bars passing inside the column and tended to decrease with increasing distance from the column centerline.

2. Not all reinforcing bars inside width $b_b = c_2 + 3h$ were 100 % effective in resisting the negative moment at the front column face. For specimens where $\frac{c_3}{1.5h} < 1.0$, those bars farthest from the column centerline were unable to reach their yield strain despite failure of the connection in flexure.

3. For specimens with the same $c_2 + 3h$ band width, more bars were effective in the specimen with a larger c_3 dimension, that is the distance from the free edge to the front column face. The effectiveness of the top slab reinforcement in transferring negative moment should reflect the importance of this variable.

4. The effectiveness of the top slab reinforcement perpendicular to the free edge for transferring the negative moment to the column may be determined by considering the anchorage of the reinforcement inside a critical section for flexure bounded by the front column face and lines projecting at 45 degree angles from the corners of this face towards the free edge.

5. The post-cracking load-deflection response of the connection depended on the number of effective reinforcing bars. The column dimensions and presence of an overhang did not affect the load-deflection response.

6. The CSA A23.3-14 Standard and ACI 318-14 Code provisions for punching shear provided accurate predictions of the punching shear strength of the flat plate edge slab-column connections tested in this experimental program.

7. The ACI 318-14 Code provision 8.4.2.3.4 produced non-conservative predictions for the punching shear strength of the connection. It is recommended that the interaction between shear and moment at edge slab-column connections always be considered, regardless of the magnitude of the shear.

References

[1] Alexander, S. and Simmonds, S. (1991). Bond Model for Punching Strength of Slab-Column Connections. *IABSE, (62),* 709-714.

[2] Alexander, S. (2017). Shear and Moment Transfer at slab-column Connections. *ACI-fib International Symposium: Punching Shear Strength of Structural Concrete Slabs, (81),* 1-22.

[3] Anggadjaja, E. And Teng, S. (2008). Edge-Column Slab Connections under Gravity and Lateral Loading. *Journal of the American Concrete Institute, (105-S50)*, 541- 551.

[4] American Concrete Association. (1977). *Building Code Requirements for Reinforced Concrete and Commentary* (318-77).

[5] American Concrete Association. (1983). *Building Code Requirements for Reinforced Concrete and Commentary* (318-83).

[6] American Concrete Association. (2005). *Building Code Requirements for Reinforced Concrete and Commentary* (318-05).

[7] American Concrete Association. (2014). *Building Code Requirements for Reinforced Concrete and Commentary* (318-14).

[8] ASTM International. (2016). *Standard Specification for Deformed and Plain Carbon-Steel Bars for Concrete Reinforcement* (ASTM A615/A615M-16).

[9] Canadian Standards Association. (1994). *Design of Concrete Structures* (A23.3-94).

[10] Canadian Standards Association. (2009). *Billet-Steel Bars for Concrete Placement* (CSA G30.18-09).

[11] Canadian Standards Association. (2014). *Test methods and standard practices for concrete* (CSA A23.2-14).

[12] Canadian Standards Association. (2014). *Design of Concrete Structures* (A23.3-14).

[13] Di Stasio, J. and Van Buren, M.P. (1960). Transfer of Bending Moment Between Flat Plate Floor and Column. *Journal of the American Concrete Institut*e..

[14] Elstner, R. and Hognestad, E.. (1956). Shearing Strength of Reinforced Concrete Slabs. *Journal of the American Concrete Institute, (57-14),* 299-314.

[15] Hanson, N. and Hanson, J. (1968). Shear and Moment Transfer Between Concrete Slabs and Columns. *PCA Research and Development Laboratories, (10-1).*

[16] Hawkins, N.M. and Corley, W.G. (1971). Transfer of Unbalanced Moment and Shear from Flat Plates to Columns. *Journal of the American Concrete Institute, (30-7),* 147-176..

[17] Kinnunen, S. (1971). Tests on Concrete Slabs Supported on Columns at Free Edges. *National Swedish Building Research Summaries.*

[18] Moehle, J. (1988). Strength of Slab-Column Edge Connections. *Journal of the American Concrete Institute, (85-11), 89-98.*

[19] Muttoni, A. (2008). Punching Shear Strength of Reinforced Concrete Slabs withotu Transverse Reinforcement. *Journal of the American Concrete Institute, (105-42),* 440-450.

[20] Neth, V.W., de Paiva, H.A.R., and Long, A.E. (1981). Behavior of Models of a Reinforced Concrete Flat Plate Edge-Column Connection. *Journal of the American Concrete Institute, (78-24),* 269-275.

[21] Park, H. and Choi, K. (2006). Strength of Exterior Slab-Column Connections Subjected to Unbalanced Moments. *Engineering Structures, (29),* 1096-1114.

[22] Rangan, B. and Hall, A.S. (1983). Moment and Shear Transfer between Slab and Edge Column. *Journal of the American Concrete Institute, (80-18),* 183-191.

[23] Regan, P.E. (1981). Behaviour of Reinforced Concrete Flat Slabs. *Construction Industry and Information Association, (89).*

[24] Rha, C. et al. (2014) Gravity and Lateral Load-Carrying Capacities of Reinforced Concrete Flat Plate Systems. *Journal of the American Concrete Institute, (111-4),* 753-764.

[25] Rughani, A. (1983) *Behaviour of Exterior Column-Slab Connections* (Master's Thesis). McGill University, Montreal, Quebec.

[26] Sherif, A. (1996). *Behaviour of Reinforced Concrete Flat Slabs* (Doctoral Dissertation). University of Calgary, Calgary, Alberta. .

[27] Sherif, A. and Dilger, W. (2003). Critical review of Canadian Standards Association Standard CSA-A23.3-94 Provisions for Punching Shear Strength of Edge slab-column Connections. *Canadian Journal of Civil Engineering, (30),* 1069-1080.

[28] Simmonds, S. and Alexander, S. (1987). Truss Model for Edge slab-column Connections. *Journal of the American Concrete Institute, (84-32), 296-303.*

[29] Stamenkovic, A. and Chapman, J.C. (1974). Local Strength at Column Heads in Flat Slabs Subjected to Combined Vertical and Horizontal Loading. *Proceedings of the Institute of Civil Engineers, (57-4),* 773-776.

[30] Sudarsana, K. and Gardner, N. (2006). Punching Shear in Edge Column Slab Connections of Flat Plate Structures. *2nd Asian Concrete Federation Conference.*

[31] Taranath, B. (2010). *Reinforced Concrete Design of Tall Buildings.* Boca Raton, Florida: CRC Press.

[32] Zaghlool, E.R.F. (1971). *Strength and Behaviour of Comer and Edge Column-Slab Connections in Reinforced Concrete Flat Plates* (Doctoral dissertation), Department of Civil Engineering, University of Calgary, Alberta, Canada.